

Aims and Scope: The "Cell Journal (Yakhteh)" is a peer review and monthly English publication of Royan Institute of Iran. The aim of the journal is to disseminate information by publishing the most recent scientific research studies based on medical and developmental biology including cell therapy and regenerative medicine, stem cell biology reproductive medicine, medical genetics, immunology, oncology, clinical biochemistry, neuroscience, and tissue engineering. **Cell J**, has been certified by the Ministry of Culture and Islamic Guidance since 1999 and accredited as a scientific and research journal by HBI (Health and Biomedical Information) Journal Accreditation Commission since 2000 which is an open access journal. **This journal holds the membership of the Committee on Publication Ethics (COPE).**

1. Types of articles

The articles in the field of Cellular and Molecular can be considered for publications in **Cell J**. These articles are as below:

A. Original articles

Original articles are scientific reports of the original research studies. The article consists of English Abstract (structured), Introduction, Materials and Methods, Results, Discussion, Conclusion, Acknowledgements, Author's Contributions, and References (**Up to 40**).

B. Review articles

Review articles are the articles written by well experienced authors and those who have excellence in the related fields. The corresponding author of the review article must be one of the authors of at least three published articles appearing in the references. The review article consists of English Abstract (unstructured), Introduction, Conclusion, Author's Contributions, and References (**Up to 90**).

C. Systematic Reviews

Systematic reviews are a type of literature review that collect and critically analyzes multiple research studies or papers. The Systematic reviews consist of English Abstract (unstructured), Introduction, Materials and Methods, Results, Discussion, Conclusion, Acknowledgements, Author's Contributions, and References (**Up to 90**).

D. Short communications

Short communications are articles containing new findings. Submissions should be brief reports of ongoing researches. The short communication consists of English Abstract (unstructured), the body of the manuscript (should not hold heading or sub-heading), Acknowledgements, Author's Contributions, and References (**Up to 30**).

E. Case reports

Case reports are short discussions of a case or case series with unique features not previously described which make an important teaching point or scientific observation. They may describe novel techniques or use equipment, or new information on diseases of importance. It consists of English Abstracts (Unstructured), Introduction, Case Report, Discussion, Acknowledgements, Author's Contributions, and References (**Up to 30**).

F. Commentary

Commentaries are short articles containing a contemporary issue that is relevant to the journal's scope and also expressing a personal opinion or a new perspective about existing research on a particular topic. The Commentary consists of English Abstract (unstructured), the body of the manuscript (should not hold heading or subheading), Acknowledgements, Author's Contributions, and References (**Up to 30**).

G. Editorial

Editorials are articles should be written in relevant and new data of journals' filed by either the editor in chief or the editorial board.

H. Imaging in biology

Images in biology should focus on a single case with an interesting illustration such as a photograph, histological specimen or investigation. Color images are welcomed. The text should be brief and informative.

I. Letter to the editors

Letter to the editors are in response to previously published **Cell J** articles, and may also include interesting cases that do not meet the requirement of being truly exceptional, as well as other brief technical or clinical notes of general interest.

J. Debate

Debates are articles which show a discussion of the positive and negative view of the author concerning all aspect of the issue relevant to scientific research.

2. Submission process

It is recommended to see the guidelines for reporting different kinds of manuscripts. This guide explains how to prepare the manuscript for submission. Before submitting, we suggest authors to familiarize themselves with **Cell J** format and content by reading the journal via the website (www.celljournal.com). The corresponding author ensures that all authors are included in the author list and agree with its order, and they must be aware of the manuscript submission.

A. Author contributions statements

It is essential for authors to include a statement of responsibility in the manuscript that specifies all the authors' contributions. This participation must include: Conceptualization, Methodology, Software, Validation, Formal analysis, Investigation, Resources, Data Curation, Writing - Original Draft, Writing - Review & Editing, Visualization, Supervision, Project administration, and Funding acquisition. Authors who do not meet the above criteria should be acknowledged in the Acknowledgments section.

B. Cover letter and copyright

Each manuscript should be accompanied by a cover letter, signed by all authors specifying the following statement: "The manuscript has been seen and approved by all authors and is not under active consideration for publication. It has neither been accepted for publication nor published in another journal fully or partially (except in abstract form). **Also, no manuscript would be accepted in case it has been pre-printed or submitted to other websites.** I hereby assign the copyright of the enclosed manuscript to **Cell J**." The corresponding author must confirm the proof of the manuscript before online publishing. It is needed to suggest three peer reviewers in the field of their manuscript.

C. Manuscript preparation

Authors whose first language is not English encouraged to consult a native English speaker in order to confirm his manuscripts to American or British (not a mixture) English usage and grammar. It is necessary to mention that we will check the plagiarism of your manuscript by iThenticate Software. The manuscript should be prepared in accordance with the "International Committee of Medical Journal Editors (ICMJE)". Please send your manuscript in two formats word and PDF (including: title, name of all the authors with their degree, abstract, full text, references, tables and figures) and also send tables and figures separately in the site. The abstract and text pages should have consecutive line numbers in the left margin beginning with the title page and continuing through the last page of the written text. Each abbreviation must be defined in the abstract and text when they are mentioned for the first time. Avoid using abbreviation in the title. Please use the international and standard abbreviations and symbols

It should be added that an essential step toward the integration and linking of scientific information reported in published literature is using standardized nomenclature in all fields of science and medicine. Species names must be italicized (*e.g.*, *Homo sapiens*) and also the full genus and species written out in full, both in the title of the manuscript and at the first mention of an organism in a paper.

It is necessary to mention that genes, mutations, genotypes, and alleles must be indicated in italics. Please use the recommended name by consulting the appropriate genetic nomenclature database, *e.g.*, HUGO for human genes. In another words; if it is a human gene, you must write all the letters in capital and italic (*e.g.*, *OCT4*, *c-MYC*). If not, only write the first letter in capital and italic (*e.g.*, *Oct4*, *c-Myc*). **In addition, protein designations are the same as the gene symbol but are not italicized.**

Of note, Cell J will only consider publishing genetic association study papers that are novel and statistically robust. Authors are advised to adhere to the recommendations outlined in the STREGA statement (<http://www.strega-statement.org>). The following criteria must be met for all submissions:

1. Hardy-Weinberg Equilibrium (HWE) calculations must be carried out and reported along with the P-values if applicable [see Namipashaki et al. 2015 (Cell J, Vol 17, N 2, Pages: 187-192) for a discussion].
2. Linkage disequilibrium (LD) structure between SNPs (if multiple SNPs are reported) must be presented.
3. Appropriate multiple testing correction (if multiple independent SNPs are reported) must be included.

Submissions that fail to meet the above criteria will be rejected before being sent out for review.

Each of the following manuscript components should begin in the following sequence:

Authors' names and order of them must be carefully considered (full name(s), highest awarded academic degree(s), email(s), and institutional affiliation(s) of all the authors in English. Also, you must send mobile number and full postal address of the corresponding author).

Changes to Authorship such as addition, deletion or rearrangement of author names must be made only before the manuscript has been accepted in the case of approving by the journal editor. In this case, the corresponding author must explain the reason of changing and confirm them (which has been signed by all authors of the manuscript). If the manuscript has already been published in an online issue, an erratum is needed. Please contact us via info@celljournal.org in case of any changes (corrections, retractions, erratum, etc.).

Title is providing the full title of the research (do not use abbreviations in title).

Running title is providing a maximum of 7 words (no more than 50 characters).

Abstract must include Objective, Materials and Methods, Results, and Conclusion (no more than 300 words).

Keywords, three to five, must be supplied by the authors at the foot of the abstract chosen from the Medical Subject Heading (MeSH). Therefore; they must be specific and relevant to the paper.

The following components should be identified after the abstract:

Introduction: The Introduction should provide a brief background to the subject of the paper, explain the importance of the study, and state a precise study question or purpose.

Materials and Methods: It includes the exact methods or observations of experiments. If an apparatus is used, its manufacturer's name and address should be stipulated in parenthesis. If the method is established, give reference but if the method is new, give enough information so that another author can perform it. If a drug is used, its generic name, dose, and route of administration must be given. Standard units of measurements and chemical symbols of elements do not need to be defined.

Statistical analysis: Type of study and statistical methods should be mentioned and specified by any general computer program used.

Ethical considerations: Please state that informed consent was obtained from all human adult participants and from the parents or legal guardians of minors and include the name of the appropriate institutional review board that approved the project. It is necessary to indicate in the text that the maintenance and care of experimental animals complies with National Institutes of Health guidelines for the humane use of laboratory animals, or those of your Institute or agency.

Clinical trial registration: All of the Clinical Trials performing in Iran must be registered in Iranian Registry of Clinical Trials (www.irct.ir). The clinical trials performed abroad, could be considered for publication if they register in a registration site approved by WHO or www.clinicaltrials.gov. If you are reporting phase II or phase III randomized controlled trials, you must refer to the CONSORT Statement for recommendations to facilitate the complete and transparent reporting of trial findings. Reports that do not conform to the CONSORT guidelines may need to be revised before peer-reviewing.

Results: They must be presented in the form of text, tables, and figures. Take care that the text does not repeat data that are presented in tables and/or figures. Only emphasize and summarize the essential features of the main results. Tables and figures must be numbered consecutively as appeared in the text and should be organized in separate pages at the end of the manuscript while their location should be mentioned in the main text.

Tables and figures: If the result of your manuscript is too short, it is better to use the text instead of tables & figures. Tables should have a short descriptive heading above them and also any footnotes. Figure's caption should contain a brief title for the whole figure and continue with a short explanation of each part and also the symbols used (no more than 100 words). All figures must be prepared based on cell journal's guideline in color (no more than 6 Figures and Tables) and also in TIF format with 300 DPI resolution.

Of Note: Please put the tables & figures of the result in the results section not any other section of the manuscript.

Supplementary materials would be published on the online version of the journal. This material is important to the understanding and interpretation of the report and should not repeat material within the print article. The amount of supplementary material should be limited. Supplementary material should be original and not previously published and will undergo editorial and peer review with the main manuscript. Also, they must be cited in the manuscript text in parentheses, in a similar way as when citing a figure or a table. Provide a caption for each supplementary material submitted.

Discussion: It should emphasize the present findings and the variations or similarities with other researches done by other researchers. The detailed results should not be repeated in the discussion again. It must emphasize the new and important aspects of the study.

Conclusion: It emphasizes the new and important aspects of the study. All conclusions are justified by the results of the study.

Acknowledgements: This part includes a statement thanking those who contributed substantially with work relevant to the study but does not have authorship criteria. It includes those who provided technical help, writing assistance and name of departments that provided only general support. You must mention financial support in the study. Otherwise; write this sentence "There is no financial support in this study".

Conflict of interest: Any conflict of interest (financial or otherwise) and sources of financial support must be listed in the Acknowledgements. It includes providers of supplies and services from a commercial organization. Any commercial affiliation

must be disclosed, regardless of providing the funding or not.

Of Note: If you have already any patent related to the subject of your manuscript, or you are going to apply for such a patent, it must be mentioned in this part.

References: The references must be written based on the Vancouver style. Thus the references are cited numerically in the text and listed in the bibliography by the order of their appearance. The titles of journals must be abbreviated according to the style used in the list of Journals Indexed in PubMed. Write surname and initials of all authors when there are six or less. In the case of seven or more authors, the names of the first six authors followed by "et al." must be listed. You can download Endnote file for Journal references style: endnote file

The reference of information must be based on the following order:

Article:

Surname(s) and first letter of name & middle name(s) of author(s) .Manuscript title. Journal title (abbr).publication date (year); Volume & Issue: Page number.

Example: Manicardi GC, Bianchi PG, Pantano S, Azzoni P, Bizzaro D, Bianchi U, et al. Presence of endogenous nicks in DNA of ejaculated human spermatozoa and its relationship to chromomycin A3 accessibility. Biol Reprod. 1995; 52(4): 864-867.

Book:

Surname(s) and first letter of name & middle name(s) of author(s).Book title. Edition. Publication place: publisher name; publication date (year); Page number.

Example: Edelman CL, Mandel CL. Health promotion throughout the lifespan. 2nd ed. ST Louis: Mosby; 1998; 145-163.

Chapter of book:

Surname(s) and first letter of name & middle name(s) of author(s). Chapter title. In: Surname(s) and first letter of name & middle name(s) of editor(s), editors. Book title. Edition. Publication place: publisher name; publication date (year); Page number.

Example: Phillips SJ, Whisnant JP. Hypertension and stroke. In: Laragh JH, Brenner BM, editors. Hypertension: pathophysiology, diagnosis, and management. 2nd ed. New York: Raven Press; 1995; 465-478.

Abstract book:

Example: Amini rad O. The antioxidant effect of pomegranate juice on sperm parameters and fertility potential in mice. Cell J. 2008;10 Suppl 1:38.

Thesis:

Name of author. Thesis title. Degree. City name. University. Publication date (year).

Example: Eftekhari Yazdi P. Comparison of fragment removal and co-culture with Vero cell monolayers on development of human fragmented embryos. Presented for the Ph.D., Tehran. Tarbiyat Modarres University. 2004.

Internet references

Article:

Example: Jahanshahi A, Mirnajafi-Zadeh J, Javan M, Mohammad-Zadeh M, Rohani M. Effect of low-frequency stimulation on adenosine A1 and A2A receptors gene expression in dentate gyrus of perforant path kindled rats. Cell J. 2008; 10 (2): 87-92. Available from: <http://www.celljournal.org>. (20 Oct 2008).

Book:

Example: Anderson SC, Poulsen KB. Anderson's electronic atlas of hematology.[CD-ROM]. Philadelphia: Lippincott Williams & Wilkins; 2002.

D. Proofs are sent by email as PDF files and should be checked and returned within 72 hours of receipt. It is the authors' responsibility to check that all the text and data as contained in the page proofs are correct and suitable for publication. **We are requested to pay particular attention to author's names and affiliations as it is essential that these details be accurate when the article is published.**

E. Pay for publication: Publishing an article in **Cell J** requires Article Processing Charges (APC) that will be billed to the submitting author following the acceptance of an article for publication. For more information please see www.celljournal.org.

F. Ethics of scientific publication: Manuscripts that have been published elsewhere with the same intellectual material will

refer to duplicate publication. If authors have used their own previously published work or work that is currently under review, as the basis for a submitted manuscript, they are required to cite the previous work and indicate how their submitted manuscript offers novel contributions beyond those of the previous work. Research and publication misconduct is considered a serious breach of ethics.

The Journal systematically employs iThenticate, plagiarism detection and prevention software designed to ensure the originality of written work before publication. Plagiarism of text from a previously published manuscript by the same or another author is a serious publication offence. Some parts of text may be used, only where the source of the quoted material is clearly acknowledged.

3. General information

A. You can send your manuscript via online submission system which is available on our website. If the manuscript is not prepared according to the format of **Cell J**, it will be returned to authors.

B. The order of article appearance in the Journal is not demonstrating the scientific characters of the authors.

C. **Cell J** has authority to accept or reject the manuscript.

D. Corresponding authors should send the manuscripts via the Online Manuscript Submission System. All submissions will be evaluated by the associated editor in order to check scope and novelty. If the manuscript suits the journal criteria, the associated editor would select the single-blind peer-reviewers. The reviewers of the manuscript must not share information about the review with anyone without permission of the editors and authors. If three reviewers pass their judgments on the manuscript, it will be presented to the associated editor of **Cell J**. In the case of having a favorable judgment on the manuscript, reviewers' comments will be presented to the corresponding author (the identification of the reviewers will not be revealed). After receiving the revision, the associated editor would choose the final reviewer among the previous ones. The final decision will be taken by editor-in-chief based on the final reviewer's comments. The review process takes between 2 to 4 months in **Cell J**. The executive member of journal will contact the corresponding author directly within 3-4 weeks by email. If authors do not receive any reply from journal office after the specified time, they can contact the journal office. Finally, the executive manager will respond promptly to authors' request.

After receiving the acceptance letter, the abstract of the paper would be published electronically. The paper will be in a queue to be published in one Cell J. At last, the corresponding author should verify a proof copy of the paper in order to be published.

The Final Checklist

The authors must ensure that before submitting the manuscript for publication, they have to consider the following parts:

1. The first page of manuscript should contain title, name of the author/coauthors, their academic qualifications, designation & institutions they are affiliated with, mailing address for future correspondence, email address, phone, and fax number.
2. Text of manuscript and References prepared as stated in the "guide for authors" section.
3. Tables should be on a separate page. Figures must be sent in color and also in JPEG (Jpg) format.
4. Cover Letter should be uploaded with the signature of all authors.
5. An ethical committee letter should be inserted at the end of the cover letter.

The Editor-in-Chief: Ahmad Hosseini, Ph.D.

Cell Journal (Yakhteh)

P.O. Box: 16635-148, Iran

Tel/Fax: + 98-21-22510895

Emails: info@celljournal.org

journals@celljournal.org



IN THE NAME OF GOD



Gone But not Forgotten

In the memory of the late Director of Royan Institute,
Founder of Stem Cells Research in Iran and Chairman of
Cell Journal (Yakhteh). May he rest in peace.

Dr. Saeed Kazemi Ashtiani

OWNED:

Royan Institute, Iranian Academic Center for Education Culture and Research (ACECR)

CHAIRMAN:

Hamid Gourabi, Ph.D., (Professor, Royan Institute, Tehran, Iran)

EDITOR IN CHIEF:

Ahmad Hosseini, Ph.D., (Professor, Shahid Beheshti Medical University, Tehran, Iran)

SECTION EDITORS:

Saeid Abroun, Ph.D., Professor, Tarbiat Modares University, Tehran, Iran
Masoud Vosough, M.D., Ph.D., Associate Professor, Royan Institute, Iran
Hoda Madani, M.D., Ph.D., Royan Institute, Iran
Marzieh Ebrahimi, Ph.D., Professor, Royan Institute, Tehran, Iran
Sara Soudi, Ph.D., Associate Professor, Tarbiat Modares University, Tehran, Iran
Sharif Moradi, Ph.D., Assistant Professor, Royan Institute, Tehran, Iran
Sara Pahlavan, Ph.D., Assistant Professor, Royan Institute, Tehran, Iran
Sadaf Vahdat, Ph.D., Assistant Professor, Tarbiat Modares University, Tehran, Iran
Amir Amiri-Yekta, Ph.D., Assistant Professor, Royan Institute, Tehran, Iran
Afagh Alavi, Ph.D., Associate Professor, University of Social Welfare and Rehabilitation Sciences, Tehran, Iran
Seyed Javad Mirnajafi-Zadeh, Ph.D., Assistant Professor, Tarbiat Modares University, Tehran, Iran
Sahar Kiani, Ph.D., Associate Professor, Royan Institute, Tehran, Iran
Marjan Sabaghian, Ph.D., Associate Professor, Royan Institute, Tehran, Iran
Seyyed Abolghasem Ghadami, Ph.D., Alzahra University, Tehran, Iran
Mohammad Kazemi Ashtiani, Ph.D., Royan Institute, Tehran, Iran
Hamed Daemi, Ph.D., Assistant Professor, Royan Institute, Tehran, Iran
Fatemeh Hassani, Ph.D., Assistant Professor, Royan Institute, Tehran, Iran
Mahshid Bazrafkan, Ph.D., Assistant Professor, Avicenna Fertility Center, Karaj, Iran
Alireza Soltanian, Ph.D., Professor, University of Medical Sciences, Hamadan, Iran

EDITORIAL BOARDS:

Saeid Abroun, Ph.D., (Professor, Tarbiat Modares University, Tehran, Iran)
Kamran Alimoghadam, M.D., (Associate Professor, Tehran Medical University, Tehran, Iran)
Alireza Asgari, Ph.D., (Professor, Baghyatallah University, Tehran, Iran)
Mohammad Kazem Aghaee Mazaheri, D.D.S., (Assistant Professor, ACECR, Tehran, Iran)
Mohamadreza Baghaban Eslaminejad, Ph.D., (Professor, Royan Institute, Tehran, Iran)
Gila Behzadi, Ph.D., (Professor, Shahid Beheshti Medical University, Tehran, Iran)
Hossein Baharvand, Ph.D., (Professor, Royan Institute, Tehran, Iran)
Marzieh Ebrahimi, Ph.D., (Professor, Royan Institute, Tehran, Iran)
Mary Familiar, Ph.D., (Senior Lecturer, University of Melbourne, Melbourne, Australia)
Hamid Gourabi, Ph.D., (Professor, Royan Institute, Tehran, Iran)
Jurgen Hescheler, M.D., (Professor, Institute of Neurophysiology of University Zu Koln, Germany)
Ghasem Hosseini Salekdeh, Ph.D., (Professor, Agricultural Biotechnology Research Institute, Karaj, Iran)
Esmail Jabbari, Ph.D., (Associate Professor, University of South Carolina, Columbia, USA)
Suresh Jesuthasan, Ph.D., (Associate Professor, National University of Singapore, Singapore)
Bahram Kazemi, Ph.D., (Professor, Shahid Beheshti Medical University, Tehran, Iran)
Saadi Khochbin, Ph.D., (Professor, Inserm/Grenoble University, France)
Ali Khademhosseini, Ph.D., (Professor, Harvard Medical School, USA)
Kun Ping Lu, M.D., Ph.D., (Professor, Harvard Medical School, Boston, USA)
Navid Manuchehrabadi, Ph.D., (Angio Dynamics, Marlborough, USA)
Hosseinali Mehrani, Ph.D., (Professor, Baghyatallah University, Tehran, Iran)
Marcos Meseguer, Ph.D., (Clinical Embryology Laboratory IVI Valencia, Valencia, Spain)
Seyed Javad Mowla, Ph.D., (Professor, Tarbiat Modares University, Tehran, Iran)
Mohammad Hossein Nasr Esfahani, Ph.D., (Professor, Royan Institute, Tehran, Iran)
Toru Nakano, M.D., Ph.D., (Professor, Osaka University, Osaka, Japan)
Donald Newgreen, Ph.D., (Professor, Murdoch Children Research Institute, Melbourne, Australia)
Mojtaba Rezazadeh Valojerdi, Ph.D., (Professor, Tarbiat Modares University, Tehran, Iran)
Mohammad Hossein Sanati, Ph.D., (Associate Professor, National Institute for Genetic Engineering and Biotechnology, Tehran, Iran)
Eimei Sato, Ph.D., (Professor, Tohoku University, Sendai, Japan)
Andreas Serra, M.D., (Professor, University of Zurich, Zurich, Switzerland)
Abdolhossein Shahverdi, Ph.D., (Professor, Royan Institute, Tehran, Iran)

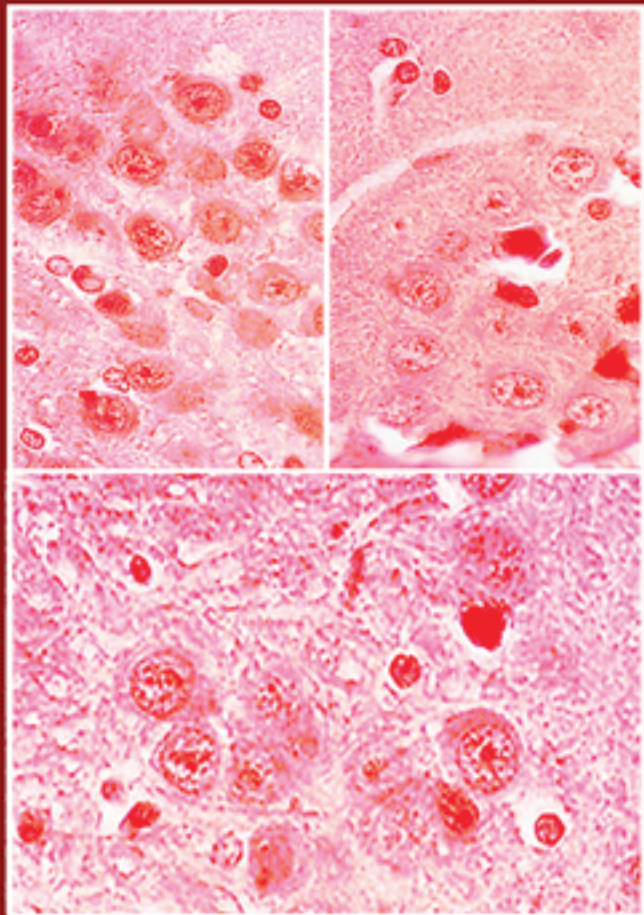
CELL JOURNAL

(Yakhteh)

Vol 25, No 11, November 2023, Serial Number: 118
Pages: 741-812

ISSN: 2228-5806
eISSN: 2228-5814

www.celljournal.org



A monthly publication of the Royan Institute

Michele Catherine Studer, Ph.D., (Institute of Biology Valrose, IBV University of Nice Sophia-Antipolis, France)
Peter Timashev, Ph.D., (Sechenov University, Moscow, Russia)
Daniela Toniolo, Ph.D., (Head, Unit of Common Disorders, San Raffaele Research Institute, Milano, Italy)
Christian van den Bos, Ph.D., Managing Director MARES Ltd, Greven, Germany
Catherine Verfaillie, Ph.D., (Professor, Katholie Universiteit Leuven, Leuven, Belgium)
Gianpaolo Zerbinì, M.D., Ph.D., (San Raffaele Scientific Institute, Italy)
Shubing Zhang, Ph.D., (Associate Professor, Central South University, China)
Daniele Zink, Ph.D., (Institute of Bioengineering and Nanotechnology, Agency for Science Technology & Science, Singapore)

EXECUTIVE MANAGER:

Farideh Malekzadeh, M.Sc., (Royan Institute, Tehran, Iran)

EXECUTIVE BOARDS:

Parvaneh Afsharian, Ph.D., (Royan Institute, Tehran, Iran)
Reza Azimi, B.Sc., (Royan Institute, Tehran, Iran)
Reza Omani-Samani, M.D., (Royan Institute, Tehran, Iran)
Elham Amirchaghmaghi, M.D., Ph.D., (Royan Institute, Tehran, Iran)
Leila Daliri, M.Sc., (Royan Institute, Tehran, Iran)
Mahdi Lottfipannah, M.Sc., (Royan Institute, Tehran, Iran)
Faezeh Shekari, Ph.D., (Royan Institute, Tehran, Iran)

ENGLISH EDITORS:

Mitra Amiri Khabooshan, Ph.D., (Monash University, Victoria, Australia)
Sima Binaafar, M. Sc., (Royan Institute, Tehran, Iran)
Saman Eghtesad, Ph.D., (Royan Institute, Tehran, Iran)
Jane Elizabeth Ferrie, Ph.D., (University College of London, London, UK)
Vahid Ezzatizadeh, Ph.D., (Royan Institute, Tehran, Iran)
Farnaz Shapouri, Ph.D., (Memphasys Limited, NSW, Australia)
Kim Vagharfard, M.Sc., (Royan Institute, Tehran, Iran)
Maryam Vatani, M.Sc., (University of Calgary, Canada)

GRAPHIST:

Laleh Mirza Ali Shirvani, B.Sc., (Royan Institute, Tehran, Iran)

PUBLISHED & SPONSORED BY:

Publication of Royan Institute (ACECR)

Indexed in:

1. Thomson Reuters (ISI)
2. PubMed
3. PubMed Central (PMC)
4. National Library Medicine (NLM)
5. Biosis Preview
6. Index Medicus for the Eastern Mediterranean Region (IMEMR)
7. Regional Information Center for Sciences and Technology (RICEST)
8. Index Copernicus International
9. Cambridge Scientific Abstract (CSA)
10. EMBASE
11. Scopus
12. Cinahl Database
13. Google Scholar
14. Chemical Abstract Service (CAS)
15. Proquest
16. Directory of Open Access Journals (DOAJ)
17. Open Academic Journals Index (OAJI)
18. Directory of Research Journals Indexing (DRJI)
19. Scientific Information Database (SID)
20. Iranmedex
21. Islamic World Science Citation Center (ISC)
22. Magiran
23. Science Library Index
24. Biological Abstracts
25. Essential Science Indicators
26. EuroPub

ACECR

Copyright and license information:

The **Cell Journal**^(Yakhteh) is an open access journal which means the articles are freely available online for any individual author to download and use the providing address. The journal is licensed under a Creative Commons Attribution-Non Commercial 3.0 Unported License which allows the author(s) to hold the copyright without restrictions that is permitting unrestricted non-commercial use, distribution, and reproduction in any medium provided the original work is properly cited.

Editorial Office Address (Dr. Ahmad Hosseini):

Royan Institute, P.O.Box: 16635-148,
Tehran, Iran
Tel & Fax: (+9821)22510895
Website: www.celljournal.org
Emails: info@celljournal.org
journals@celljournal.org

Printing Company:

Naghsh e Johar Co.
No. 103, Fajr alley, Tehranpars Street,
Tehran, Iran.



CONTENTS

Original Articles

● **Melatonin Protects Mouse Type A Spermatogonial Stem Cells against Oxidative Stress via The Mitochondrial Thioredoxin System**

Somayeh Heidarizadi, Zahra Rashidi, Cyrus Jalili, Kamran Mansouri, Iraj Rashidi, Behzad Mahaki, Mohammadreza Gholami 741

● **Osteoblastic Differentiation of Stem Cells from Human Exfoliated Deciduous Teeth by Probiotic Hydroxyapatite**

Sabereh Nouri, Rasoul Roghanian, Giti Emtiazi, Oguzhan Gunduz, Rasoul Shafiei 753

● **Adipose Tissue-Derived Mesenchymal Stem Cells Alter Metabolites of Brain Cholesterol Homeostasis in An Alzheimer's Model**

Mehrnaz Karimi Darabi, Zahra Nazeri, Arash Rafeinia, Seyedeh Pardis Pezeshki, Alireza Kheirollah, Yaghoob Farbood, Maryam Adelipour, Shirin Azizidoost, Maryam Cheraghzadeh 764

● **Spinal Cord Injury Affects Gene Expression of Transmembrane Proteins in Tissue and Release of Extracellular Vesicle in Blood: In Silico and In Vivo Analysis**

Yasmin Mirzaalikhan, Nasim Eslami, Amin Izadi, Faezeh Shekari, Sahar Kiani 772

● **Association of MGLL Intronic C>T Single Nucleotide Polymorphism (rs782440) with Borderline Personality Disorder: A Case-Control Study**

Nazanin Hatami Bavarsad, Leila Jahangard, Masood Saidijam, Seyed Asaad Karimi, Ali Reza Soltanian, Elahe Shahriari, Saeid Afshar, Abdolrahman Sarihi 783

● **The Effect of Mesenchymal Stem Cells Derived-Conditioned Media in Combination with Oral Anti-Androgenic Drugs on Male Pattern Baldness: An Animal Study**

Majid Kamali-Dolat Abadi, Gholamhossein Yousefi, Farzaneh Dehghani, Ali Akbar Alizadeh, Abolfazl Jangholi, Mohammad Amin Moadab, Maryam Naseh, Shima Parsa, Golara Nasiri, Negar Azarpira, Mehdi Dianatpour 790

● **Annexin A7 and Its Related Protein Suppressor of Death Domains Regulates Migration and Proliferation of Hca-P Cells**

Shaoqing Wang, Qingyang Bai, Xiuwen Yu, Feng Gao, Yurong Sun, Xianyan Wang 801


Case Report

● **Royan Institute First Attempts: Autotransplantation of Vitrified Human Ovarian Tissue in Cancer Patients**

Naeimeh Sadat Abtahi, Bitah Ebrahimi, Firouzeh Ghaffari, Rouhollah Fathi, Mojtaba Rezazadeh Valojerdi, Abolfazl Mehdizadehkashi, Sepideh Khodaverdi, Azar Yahyaei, Maziar Faridi 809

● **Front page of Cell Journal_(Yakhteh): Figure 5, Page: 769**

Melatonin Protects Mouse Type A Spermatogonial Stem Cells against Oxidative Stress via The Mitochondrial Thioredoxin System

Somayeh Heidarizadi, Ph.D.¹, Zahra Rashidi, Ph.D.^{1,2}, Cyrus Jalili, Ph.D.^{1,3}, Kamran Mansouri, Ph.D.³, Iraj Rashidi, Ph.D.¹, Behzad Mahaki, Ph.D.⁴, Mohammadreza Gholami, Ph.D.^{5*} 

1. Faculty of Medicine, Kermanshah University of Medical Sciences, Kermanshah, Iran

2. Fertility and Infertility Research Centre, Health Technology Institute, Kermanshah University of Medical Sciences, Kermanshah, Iran

3. Medical Biology Research Centre, Health Technology Institute, Kermanshah University of Medical Sciences, Kermanshah, Iran

4. Department of Biostatistics, School of Health, Kermanshah University of Medical Sciences, Kermanshah, Iran

5. Medical Technology Research Centre, Institute of Health Technology, Kermanshah University of Medical Sciences, Kermanshah, Iran

Abstract

Objective: Mitochondrial oxidative stress is an important factor in infertility. The mitochondrial thioredoxin system plays an important role in this condition. N-acetyl-5-methoxy tryptamine (melatonin) plays a role in reducing oxidative stress and apoptosis in spermatogonial stem cells (SSCs). In this study, we explore the probable protective effects of melatonin on the mitochondrial thioredoxin system [thioredoxin 2 (Trx2)/Txnip] in SSCs under oxidative stress.

Materials and Methods: In this experimental study, SSCs were co-cultured two-dimensionally (2D) with Sertoli cells in DMEM culture medium that contained 10% fetal bovine serum (FBS), 1% antibiotics, and 10 ng/ml glial cell-derived neurotrophic factor (GDNF) for 30 days. The cultured cells were subsequently divided into four groups: control; melatonin (250 μ M, 24 hours); melatonin (250 μ M, 24 hours)+hydrogen peroxide (H_2O_2 , 50 μ M, 24 hours); and H_2O_2 (50 μ M, 24 hours). Intracellular reactive oxygen species (ROS) production was determined by flow cytometry. Malondialdehyde (MDA) levels were measured by Fluorometry. The expressions of apoptotic and antioxidant genes and nuclear factor erythroid 2-related factor 2 (Nrf2), Trx2, and nicotinamide nucleotide transhydrogenase (NNT) proteins were determined by quantitative real-time polymerase chain reaction (qRT-PCR) and Western blot. Adenosine triphosphate (ATP) levels were measured by fluorometry.

Results: Melatonin reduced H_2O_2 -induced ROS levels and apoptosis in the SSCs. Melatonin also increased mRNA expression of *Nrf2*, *Trx2*, *NNT*, Sirtuin 3 (*Sirt3*), and decreased mRNA expression of *Txnip*, and increased protein expressions of Nrf2, Trx2, NNT thereby increasing activity of the mitochondrial thioredoxin system. In addition, melatonin increased ATP levels.

Conclusion: Melatonin increased *Trx2* expression through the *Nrf2* pathway. This study suggests that melatonin may protect SSCs from oxidative stress in diseases related to infertility.

Keywords: Melatonin, Oxidative Stress, Spermatogonia

Citation: Heidarizadi S, Rashidi Z, Jalili C, Mansouri K, Rashidi I, Mahaki B, Gholami M. Melatonin protects mouse type a spermatogonial stem cells against oxidative stress via the mitochondrial thioredoxin system. Cell J. 2023; 25(11): 741-752. doi: 10.22074/CELLJ.2023.2003766.1316

This open-access article has been published under the terms of the Creative Commons Attribution Non-Commercial 3.0 (CC BY-NC 3.0).

Introduction

Mitochondria play a key role in fertility. The primary biological reactions inside mitochondria are oxidative metabolism, energy production, and free radical production (1). This organelle also participates in the regulation of cell death, a function that appears to be directly related to reactive oxygen species (ROS) production (2). Mitochondria are the main source of intracellular superoxide anions (O_2^-) and hydrogen peroxide (H_2O_2); issues in the mitochondrial electron transport chain can lead to ROS production, mitochondrial dysfunction, and cell death (3).

Mitochondrial oxidative stress is one of the important factors in infertility. Nearly half of all infertility cases are caused partly or entirely by male factors. It has been reported that about 30-80% of infertile men have high levels of ROS in their semen (4). Conditions such as smoking, varicocele, chronic stress, genital tract infections, gonadotropins, and hyperthermia induce oxidative stress and increase ROS levels. Also, a damaged mitochondrial respiratory chain and severe lack of adenosine triphosphate (ATP) often cause ROS production in the mitochondria and increase conditions for the development of pathological diseases (5).

Received: 01/June/2023, Revised: 03/August/2023, Accepted: 07/August/2023

*Corresponding Address: P.O.Box: 6714869914, Medical Technology Research Centre, Institute of Health Technology, Kermanshah University of Medical Sciences, Kermanshah, Iran

Email: mr.gholami@kums.ac.ir



Royan Institute
Cell Journal (Yakhteh)

Although normal levels of ROS are necessary to maintain the physiological state of stem cells, high levels of ROS can cause chromosomal abnormalities, mitochondrial DNA damage, and disturbances in stem cell differentiation (6). Spermatogonial stem cells (SSCs) are a group of cells positioned in the basement membrane of seminiferous tubules, which constitute only 0.03% of all testis cells. However, the continuation of spermatogenesis throughout life depends on the proper regulation of SSC self-renewal and differentiation processes. SSCs are sensitive to the overproduction of ROS (7).

Antioxidant molecules that can inhibit oxidative stress by restoring the balance between ROS and antioxidants have long been an interesting subject of research. However, the increase in ROS levels is not always the result of a lack of antioxidant defence, and other cases should be considered. It has recently been shown that an increase in ROS can be caused by “reductive stress” due to over-accumulation of reductant. Therefore, additional amounts of antioxidants do not seem to be beneficial (8, 9). N-acetyl-5-methoxy tryptamine (melatonin) is a small biological molecule secreted from the pineal gland and other organs, including the retina and testis (10). It is commonly found in nature (11). The results of our previous studies show that melatonin, an exogenous antioxidant agent, reduces apoptosis and oxidative stress in SSCs (10, 12, 13). The protective effects of melatonin include reduction of oxidative stress, apoptosis and inflammation, and regulation of mitochondrial function and sex hormones. It also indirectly reduces oxidative stress by regulating antioxidant enzymes, downregulating prooxidant enzymes, and regulating mitochondrial homeostasis as the main source of ROS production. Melatonin treatment (50 μM H_2O_2 and 2500 ng/L melatonin) is associated with regulation of the NF- κB /iNOS and nuclear factor erythroid 2-related factor 2 (Nrf2)/HO-1 signalling pathways (14). Treatment with melatonin reduces the severity of testicular tissue damage in animal models of hyperlipidaemia, testicular torsion, varicocele, and toxicity caused by chemotherapy drugs or environmental toxins (15, 16). The glutathione and thioredoxin-dependent pathways are two thiol-dependent peroxidation pathways that can remove H_2O_2 in the mitochondrial matrix. Both pathways depend on the regeneration of the oxidised disulfide form of an intermediate [e.g., glutathione disulfide (GSSG) or the cys-cys disulfide form] by a reductase. In both of the thiol-dependent pathways, reductase prefers to use NADPH rather than NADH. The main source of NADPH is the integral enzyme nicotinamide nucleotide transhydrogenase (NNT), which is positioned in the inner membrane of mitochondria.

The mitochondrial thioredoxin system consists of thioredoxin 2 (Trx2), thioredoxin reductase (TrxR2) and thioredoxin-dependent peroxidase. Since Trx2 can reduce disulfide bonds, overexpression of Trx can result in increased mitochondrial membrane potential and ATP synthesis. Trx2 deficiency leads to a release of cytochrome C from mitochondria and the activation of caspases 3 and 9.

Thus, Trx2 protects cells against mitochondrial oxidative stress and ROS-induced apoptosis (17). NNT is a rich source of NADPH that is required for the glutathione and thioredoxin antioxidant system (18). Evidence shows that melatonin increases the nuclear transcription of Nrf2 (19). The increase in Nrf2 is associated with an increase in the cellular levels of thioredoxin and TrxR2 (11, 20). From a clinical point of view, biomarkers that reflect the level of oxidative stress will be useful for clinicians to evaluate pathological features of various diseases and drug efficacies (21). Melatonin is an antioxidant that can affect the mitochondrial pathway of oxidative stress and maintain cell homeostasis by activating the thioredoxin system, which is a line of defence against oxidative stress. Here, we investigate the effects of melatonin on mitochondrial oxidative stress and its potential to reduce oxidative stress in type A SSCs. The main aim of this study is to determine the effects of melatonin on the mitochondrial thioredoxin system in mouse type A SSCs under oxidative stress conditions, as a future therapeutic solution for infertility.

Materials and Methods

The Ethics Committee of Kermanshah University of Medical Sciences, Kermanshah, Iran approved the animal experiments in this research (IR.KUMS.MED.REC.1400.083). Testes were obtained from 80, six-day-old male neonatal BALB/c mice for testicular cell isolation. The animals were kept under standard controlled conditions of a 12-hour light/12-hour dark cycle, room temperature of $20 \pm 2^\circ\text{C}$, and fed with concentrated food for mice and sufficient water. The male and female mice were placed in a cage and allowed to mate. The pregnant mice were subsequently placed in a separate cage until the birth of the pups. The birth date of the pups was considered to be day zero.

Isolation and purification of spermatogonial stem cells

Testes from the six-day-old mice were used to culture highly proliferative cells according to a two-step enzymatic digestion process for tissue digestion (22). The testicular tissues were placed in 2 ml of DMEM culture medium (DMEM/F-12; Life Technologies, Auckland, New Zealand) that contained 1 mg/ml collagenase IV (Sigma, USA) and 0.05 mg/ml DNase I (DNase I, RNase-free 500 U.1u/ μl -MO5401; Sinaclon, Iran), and incubated at 37°C and 5% CO_2 for 15 minutes, followed by centrifugation for 5 minutes at 1200 RPM.

In the second stage of the enzymatic digestion process, 0.25% trypsin (Sigma, USA) and 0.05 mg/ml DNase I were added to the cell plate to purify the spermatogonial cells from fibroblasts, myoglobins, and other impurities. Following isolation of these cells, trypsin activity was stopped by the addition of 10-20% fetal bovine serum (FBS, Gibco, EU-approved, South America) and the cell suspension was filtered through a 70 μm nylon mesh. The solution was then transferred to a flask and placed in an incubator at 37°C for 30 minutes. Subsequently, the

suspended spermatogonial stem cells were separated from the cells that were deposited on the bottom of the flask. The SSCs were co-cultured two-dimensionally (2D) with Sertoli cells in DMEM culture medium that contained 10% FBS (Gibco, EU-approved, South America) and 1% Pen/Strp (100 mg/ml streptomycin, 100 U/ml penicillin, Gibco, USA), and 10 ng/ml glial cell-derived neurotrophic factor (GDNF, Sigma, USA) for 30 days. The SSCs were incubated at 37°C and 5% CO₂ in a humidified atmosphere. The number of viable cells were then determined by the MTT assay. The SSCs were cultured in laminin-coated culture dishes and then sorted and purified by magnetic activated cell sorting (MACS) according to the Invitrogen protocol for MACS (22).

Preparation of a Sertoli cell feeder layer

A layer of Sertoli cells was used as a protective, feeding layer for the SSCs. A mouse Sertoli cell line (NCBI code: C513) was purchased from Pasteur Institute (Tehran, Iran). The Sertoli cells were cultured in a T-25 flask that contained DMEM supplemented with 10% FBS and 1% antibiotics (100 mg/ml streptomycin, 100 U/ml penicillin). Mitotic division of the progenitor cells was stopped by the addition of 10 µg/ml of mitomycin C (Sigma, USA) to the culture medium that contained the serum and the flask was allowed to incubate for two hours at 37°C (22). This medium was subsequently removed and the Sertoli cells were washed 2-3 times with PBS. After isolation and purification, the SSCs were co-cultured with Sertoli cells as a feeder layer (2D culture system). The culture medium consisted of 10% FBS and 10 ng/ml GDNF. The co-culture of SSCs and Sertoli cells was incubated at 37°C and 5% CO₂ in a humidified atmosphere for 30 days to enable the SSCs to form colonies.

Cell viability

The MTT assay was used to assess the cell cytotoxicity of melatonin (Sigma, USA, M5250-1G) and determine optimum concentrations of melatonin and H₂O₂ (Neutron Pharmaceutical Co., Iran) for SSC viability (23). To perform this assay, 4×10⁴ cells were placed in each well of a 96-well plate and treated with different concentrations of melatonin (100, 250, 500, 1000, 1500 µM) for 24 hours. The viability of the cultured cells was measured after incubation with 0.5 mg/ml of MTT (Thermo Fisher Scientific, USA). For this measurement, 100 µl of the medium that contained 0.5 mg/ml MTT was added to each well and the plates were incubated in the dark at 37°C for three to four hours. Then, the supernatant was discarded and the resultant formazan crystal was dissolved in 100 µl of dimethyl sulfoxide (DMSO, Sigma, USA). Optical density (OD) of the samples was read at 570 nm with an ELISA reader. In order to evaluate the SSCs viability after oxidative stress, the cells were treated with two different concentrations of H₂O₂ (50 and 100 µM) and the viability of the cultured cells was measured by the MTT assay. We investigated the effects of melatonin under oxidative stress conditions by simultaneously exposing the cells

to different concentrations of melatonin (100, 250, 500, 1000, 1500 µM) and 50 µM of H₂O₂ for 24 hours. The cells in the control group did not receive any treatment. Then, four groups of SSCs were examined: control, melatonin (250 µM), melatonin (250 µM)+H₂O₂ (50 µM), and H₂O₂ (50 µM).

Reactive oxygen species

The effect of the protective concentration of melatonin (250 µM) on ROS production in SSCs under oxidative stress conditions (H₂O₂ 50 µM) was measured by using 2'-7'-Dichlorodihydrofluorescein (DCFH-DA, Sigma, St. Louis, MO, USA, D6883) and a flow cytometer according to the manufacturer's instructions (24). For this measurement, three groups of SSCs were treated separately with either 250 µM of melatonin, 250 µM of melatonin plus 50 µM of H₂O₂, or 50 µM of H₂O₂. The cells in the control group did not receive any treatment. After 24 hours, the cells were washed with PBS. After resuspension in PBS, the cells were incubated with 1 µM of DCFH-DA dye at 37°C for 30 minutes. The green fluorescence of DCFH-DA in the FL-1 channel was read at 500-530 nm by a flow cytometer. The fluorescence intensity was determined by measuring 10 000 cells per group and examining the average fluorescence intensity in the resultant flow cytometry histograms. The data were statistically analysed with FlowJo software (Flowjo 7.6.1, BD Biosciences, USA).

Malondialdehyde

Lipid peroxidation was calculated by measuring malondialdehyde (MDA) with Fluorometry according to the manufacturer's instructions (Kiazist, KMDA-96, Iran) (25). For this measurement, 50 µl of the homogenate of each sample that contained SSCs treated with a certain concentration of melatonin and H₂O₂ was mixed with 250 µl of the solution that contained 20% trichloroacetic acid and 100 µl of 0.6% thiobarbituric acid. The mixture was heated in a boiling water bath for at least 20 minutes. The samples were allowed to cool before they were centrifuged at 5000 RPM for five minutes to remove the impurities. Then, 200 µl of the supernatant from each sample was transferred to a 96-well plate and the absorbance was read compared to a blank (200 µl of water) at 535 nm by a spectrophotometer (Bio-Tek, Winooski, VT, USA). The amount of MDA produced was determined from a standard curve of 1,1,3,3-tetraethoxypropane (TEP). For this purpose, a 1 mM TEP solution was mixed with 50 ml of 1% sulphuric acid and incubated for one hour. Based on the stock concentration, TEP dilutions of 100, 50, 25, 12.5, and 0.63 nmol/ml were prepared and subjected to the same preparation processes performed on the samples. Absorbance of the standard samples was read at 535 nm and plotted against the standard MDA concentration in order to ascertain a standard MDA curve and determine the line formula. The concentration of the samples was then calculated from the slope of the standard curve.

Adenosine triphosphate

Fluorometry was used to determine the effects of 250 μM of melatonin on ATP levels in SSCs under oxidative stress conditions. The three groups of treated SSCs (250 μM of melatonin; 250 μM of melatonin+50 μM of H_2O_2 ; and 50 μM of H_2O_2) and the untreated control group were assessed. After 24 hours, the cell deposits were collected and analysed with a Colorimetric/Fluorometric ATP Assay Kit (catalogue number MAK190, Sigma). ATP levels were measured according to a previously published protocol (26).

Quantitative real-time polymerase chain reaction

The expressions of the apoptotic genes [Bcl-2 associated X-protein (*Bax*), Fas cell surface death receptor (*Fas*), B-cell lymphoma 2 (*Bcl2*)] and antioxidant genes [*Nrf2*, *Trx2*, *Txnip*, *NNT*, Sirtuin 3 (*Sirt3*)] were determined by quantitative real-time polymerase chain reaction (qRT-PCR). For this purpose, the three groups of SSCs were treated with either 250 μM of melatonin, 250 μM of melatonin plus 50 μM of H_2O_2 , or 50 μM of H_2O_2 for 24 hours at 37°C. The cells in the control group did not receive any treatment. RNA extraction was then performed using a Total RNA Extraction Kit (Pars Tous, Iran) (27) according to the manufacturer's instructions. We determined the concentration and quality of the extracted RNA by measuring light absorbance with a NanoDrop spectrophotometer (Pishro Pajooesh, Iran). Next, 1 μg of RNA, 1 μl of 10x reaction buffer that contained MgCl_2 , and 0.5 μl of DNase I that contained 1 unit of the enzyme without RNase were placed in an RNase-free microtube and incubated at 37°C for 30 minutes, followed by the addition of 1 μl of 50 mM EDTA. The product was allowed to incubate at 65°C for 10 minutes. The resultant RNA was used for cDNA synthesis and assessed with an Easy cDNA Synthesis Kit (Pars Tous, Iran, cat: A101162) according to the manufacturer's instructions.

Gene expressions were determined by qRT-PCR with a RunMei Q2000 PCR machine Hunan Runmei Gene Technology Company, Ltd (RunMei, China) and a 2X SYBR Green Real-Time PCR Master Mixmix (+ROX) kit (Pars Tous, Iran, cat: C101022) using SYBR green dye. The reactions were carried out in 50 cycles per gene in a volume of 12.5 μl .

The results were interpreted by comparing $\Delta\Delta\text{Ct}$ using RunMei QC3 software and the general $2^{-\Delta\Delta\text{Ct}}$ formula with *Gapdh* as the calibrator. The *Nrf2*, *Trx2*, *Txnip*, *NNT*, *Sirt3*, *Bax*, *Bcl2*, *Fas*, and *Gapdh* gene sequences were extracted from <http://www.ncbi.nlm.nih.gov>. Forward and reverse primers were designed using Primer express (version 3.05) software (Table S1, See Supplementary Online Information at www.celljournal.org).

Western blot

Western blot was used to investigate the effect of melatonin on the expressions of the antioxidant proteins

Nrf2, *Trx2*, and *NNT* in the four assessed groups of SSCs (28). The SSCs were treated in different groups as previously mentioned. After 24 hours, the cells were collected and placed in 200 μl of DMEM and kept in a -80°C freezer until Western blot analysis. A total of 300 μl of each sample of the treated cells was homogenised in lysis buffer (137 mM NaCl, 20 mM Tris HCl, pH=7.4, 5% sodium dodecyl sulfate (SDS), 10% glycerol, 1 mM phenylmethylsulfonyl fluoride (PMSF), 10 $\mu\text{g}/\text{ml}$ aprotinin, 1 $\mu\text{g}/\text{ml}$ leupeptin, 0.5 mM Sodium vanadate) using a SpeedMill PLUS homogeniser (Analytik Jena, Germany). The resultant suspension was centrifuged at 2500 RPM for two minutes, and the supernatant was collected and stored in a -80°C freezer until use. The amount of protein in the tissue homogenate was determined by the Bradford assay. For SDS-Polyacrylamide gel electrophoresis, 20 μg of protein from each sample was placed on 8% polyacrylamide gel and subjected to electrophoresis. The proteins were electrotransferred to polyvinylidene difluoride (PVDF) membranes and then blocked with 5% nonfat dry milk and 0.1% Tween-20 in TBS for one hour at room temperature. After blocking, the paper was incubated with the primary antibodies for *Trx-2* (1:1000; F-10:sc-133201, Santa Cruz Biotechnology, Inc.), *Nrf2* (1:1000; D1Z9C XP #12721, Cell Signalling Technology), *NNT* (1:1000; B-3:sc-390236, Santa Cruz Biotechnology, Inc.), *Gapdh* (1:1000; D16H11 XP #5174, Cell Signalling), and β -actin (1:1000; C4:sc-47778, Santa Cruz Biotechnology, Inc.) as the internal control gene for 16 to 18 hours. Another incubation was then performed for the secondary antibody (1:2000; mouse anti-rabbit IgG-HRP; sc-2357) in PBS for one hour. An ECL kit (Amersham Pharmacia Biotech, Inc., Piscataway, NJ, USA) was then used according to the manufacturer's instructions to reveal the proteins. Finally, light-sensitive papers were scanned with a JS 2000 scanner (Wuhan BonninTechnology Ltd, China) and the band density was determined.

Statistical analysis

All data in this paper are written as mean \pm SD for at least three independent replicates. The data were analysed with one-way ANOVA and Tukey's post hoc test with GraphPad Prism software (version 7, Dotmatics, USA). For quantitative variables, the normality of distributions was checked by the Kolmogorov-Smirnov test. $P < 0.05$ was considered to be statistically significant.

Results

Viability of the isolated spermatogonial stem cells

Mouse SSCs were isolated by a two-step enzymatic

digestion with collagenase IV, DNase I, and trypsin and purified with anti-Thy-I antibody by MACS. Trypan blue staining as measurement of cell viability showed that over 90% of the cells were viable.

Spermatogonial stem cell colony formation

The SSCs cultured on a feeder layer of Sertoli cells were round or oval with large nuclei and small cytoplasm. These cells started to form colonies at the end of the first week of culture. Large numbers of large colonies formed after 20 days (Fig.1).

Effect of N-acetyl-5-methoxy tryptamine (melatonin) on cell viability under oxidative stress conditions

The results of the MTT assay showed no significant difference in viability between the control group and the SSCs treated with different concentrations of melatonin (100, 250, 500, 1000, and 1500 μM) for 24 hours. However, the cells that were treated with lower concentrations of melatonin (100, 250, and 500 μM) had higher viability than those treated at higher concentrations (1000 and 1500 μM). The cells that were treated with H_2O_2 (50 and 100 μM) showed significantly lower viability than the control group ($P < 0.001$). The MTT assay results showed that the protective effect of melatonin on the cells under

oxidative stress conditions was greater at 250 μM , which was a significant difference compared to the H_2O_2 group. Therefore, 250 μM was chosen as the optimal dose in this study.

Effect of N-acetyl-5-methoxy tryptamine (melatonin) on reactive oxygen species levels under oxidative stress conditions

Flow cytometry data showed that H_2O_2 resulted in higher DCF fluorescence compared to the control group with a mean fluorescence intensity of (228 MFI compared to 105 MFI). Treatment with melatonin significantly ($P < 0.001$) reduced the impact of H_2O_2 (151 MFI versus 228 MFI) (Fig.2).

Effect of N-acetyl-5-methoxy tryptamine (melatonin) on malondialdehyde levels under oxidative stress conditions

Fluorometry results showed that exposure to 50 μM of H_2O_2 for 24 hours significantly ($P < 0.001$) increased lipid peroxidation levels in the SSCs (MDA level) compared to the control group. Co-treatment with 250 μM of melatonin significantly reduced MDA levels, and returned them to normal in the control group (Fig.3).

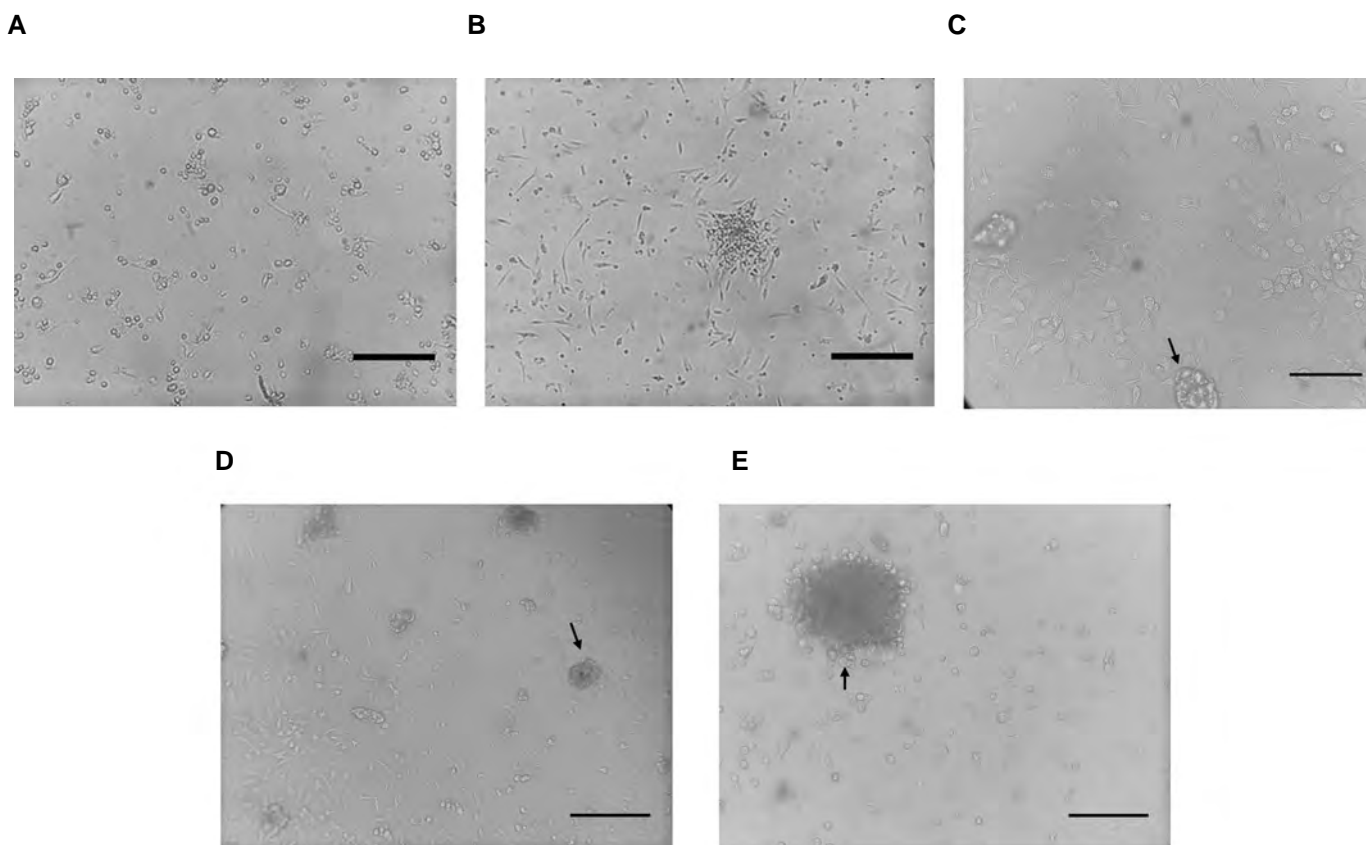
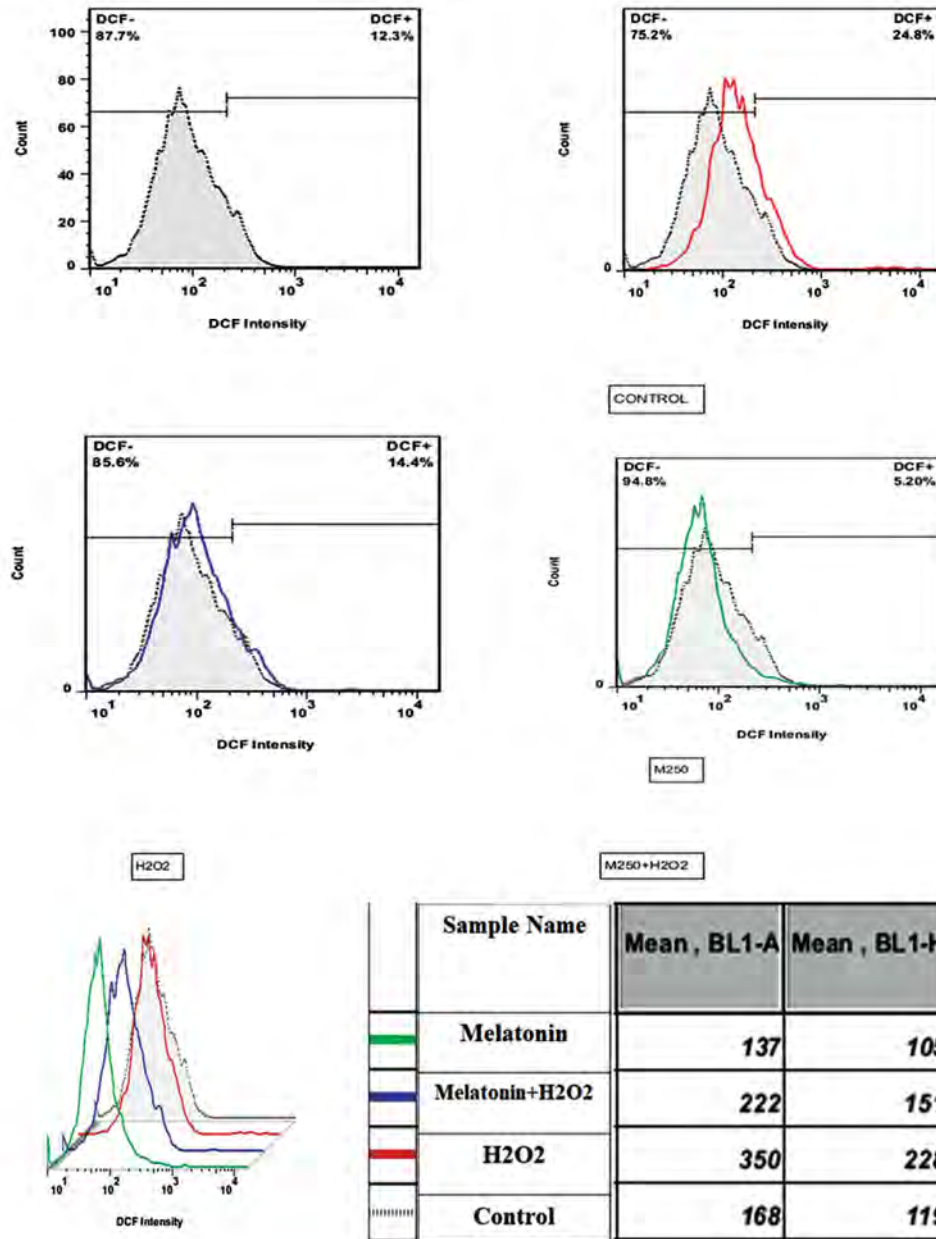


Fig.1: Spermatogonial stem cells (SSCs) culture and morphology. **A.** Mouse type A SSCs after enzymatic digestion with trypsin-EDTA (10x magnification). **B.** Sertoli cell morphology (10x magnification). **C-E.** Arrows indicate SSCs colony after 20 days of co-culture with a feeder layer of Sertoli cells in a 2D culture system (40x magnification, scale bar: 100 μm).

A



B

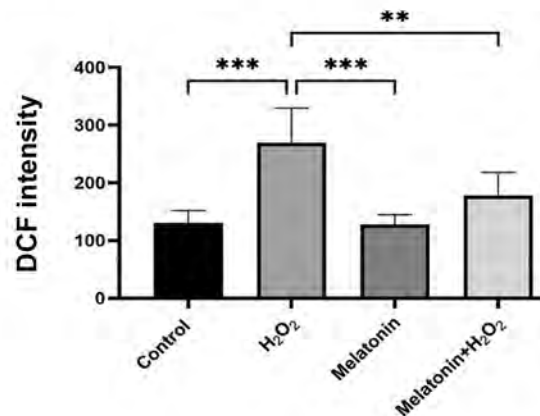


Fig.2: Protective effects of melatonin on ROS production induced by H₂O₂ in SSCs. **A.** Representative flow cytometry histograms show intracellular ROS levels measured by DCF fluorescence. **B.** The quantitative data are shown as mean ± SD. The SSCs were treated separately with 250 μM of melatonin, 250 μM of melatonin plus 50 μM of H₂O₂, or 50 μM of H₂O₂ for 24 hours. The cells in the control group did not receive any treatment. ROS; Reactive oxygen species, SSCs; Spermatogonial stem cells, DCF; Dichlorofluorescein, **, P<0.01, and ***, P<0.001.

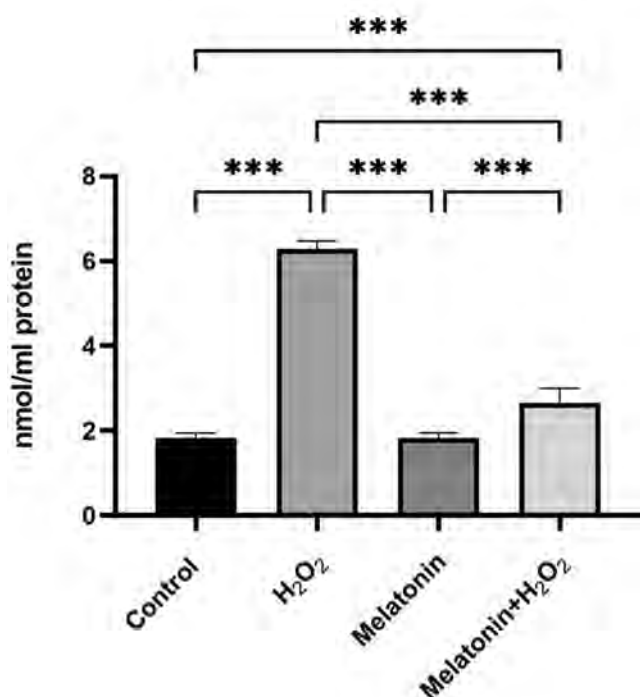


Fig.3: Protective effects of melatonin on MDA levels under oxidative stress conditions. SSCs were treated with either 250 μ M of melatonin, 250 μ M of melatonin plus 50 μ M of H₂O₂, or 50 μ M of H₂O₂ for 24 hours. The cells in the control group did not receive any treatment. Data are shown as mean \pm SD. MDA; Malondialdehyde, SSCs; Spermatogonial stem cells, and ***; P<0.001.

Effects of N-acetyl-5-methoxy tryptamine (melatonin) on adenosine triphosphate levels under oxidative stress conditions

Fluorometry results showed that 24 hours of exposure to melatonin significantly increased (P<0.001) ATP levels in the SSCs (1.2 nmol/ μ g protein) compared to the control group (1 nmol/ μ g protein). Exposure to H₂O₂ decreased the ATP levels, whereas melatonin caused an increase in ATP under oxidative stress (Fig.4).

Effect of N-acetyl-5-methoxy tryptamine (melatonin) on apoptotic gene expression under oxidative stress conditions

Exposure to H₂O₂ significantly increased the expressions of the apoptotic genes *Bax* and *Fas* in the SSCs. Melatonin significantly reduced the expressions of these genes (P<0.001) and restored them to the level of the untreated control group. Treatment with melatonin also increased *Bcl2* expression, which was significantly lower in the H₂O₂-treated group compared to the control group (P<0.001, Fig.5).

Effects of N-acetyl-5-methoxy tryptamine (melatonin) on the expression of antioxidant genes under oxidative stress conditions

Exposure to H₂O₂ significantly increased expressions

of *Nrf2* and its downstream genes in the mitochondrial thioredoxin system (*Trx2*, *NNT*, and *Sirt3*; P<0.001). Treatment with melatonin caused a greater increase in expressions of these genes. The cells also showed significantly lower expression of *Txnip*, an inhibitor of *Trx2*, in the presence of melatonin (Fig.5).

Effect of N-acetyl-5-methoxy tryptamine (melatonin) on the expression of Nrf2, Trx2, and NNT proteins under oxidative stress conditions

The results showed that oxidative stress conditions (H₂O₂, 50 μ M) increased expression of the antioxidant pathway proteins *Trx2*, *Nrf2*, and *NNT* (Fig.6). Melatonin, an exogenous antioxidant, significantly increased the expressions of these proteins under oxidative stress conditions (P<0.001). Western blot results also showed that 24 hours incubation of SSCs with 250 μ M of melatonin increased the expressions of *Nrf2*, *TRX2*, and *NNT* compared to the control group; this effect was greater under oxidative stress conditions. Western blot results showed that melatonin increased *NNT* protein expression in both oxidative stress (1.63 \pm 0.09) and normal (1.44 \pm 0.07) conditions compared to the control group (1.00 \pm 0.05). However, there was no significant difference in *NNT* protein expression observed between the H₂O₂ and melatonin plus H₂O₂ groups during oxidative stress.

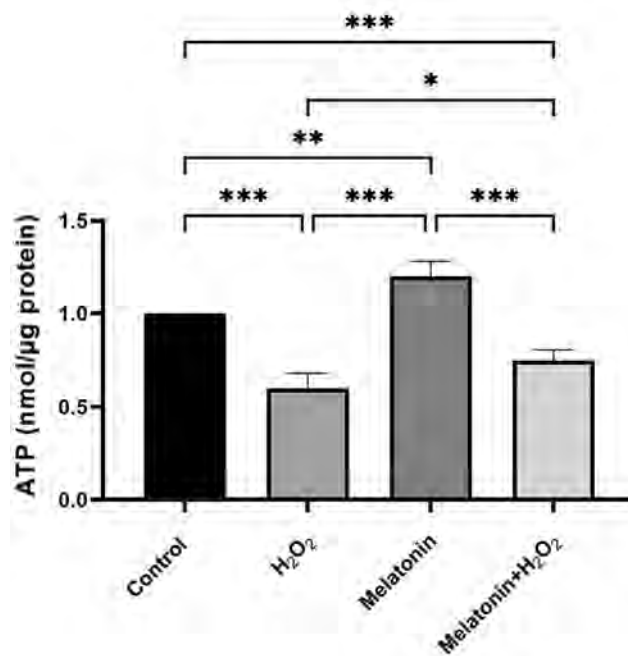


Fig.4: Protective effects of melatonin on ATP levels in oxidative stress conditions. SSCs were treated with either 250 μ M of melatonin, 250 μ M of melatonin plus 50 μ M of H₂O₂, or 50 μ M of H₂O₂ for 24 hours. The cells in the control group did not receive any treatment. Data are shown as mean \pm SD. ATP; Adenosine triphosphate, SSCs; Spermatogonial stem cells, *, P<0.05, **, P<0.01, and ***, P<0.001.

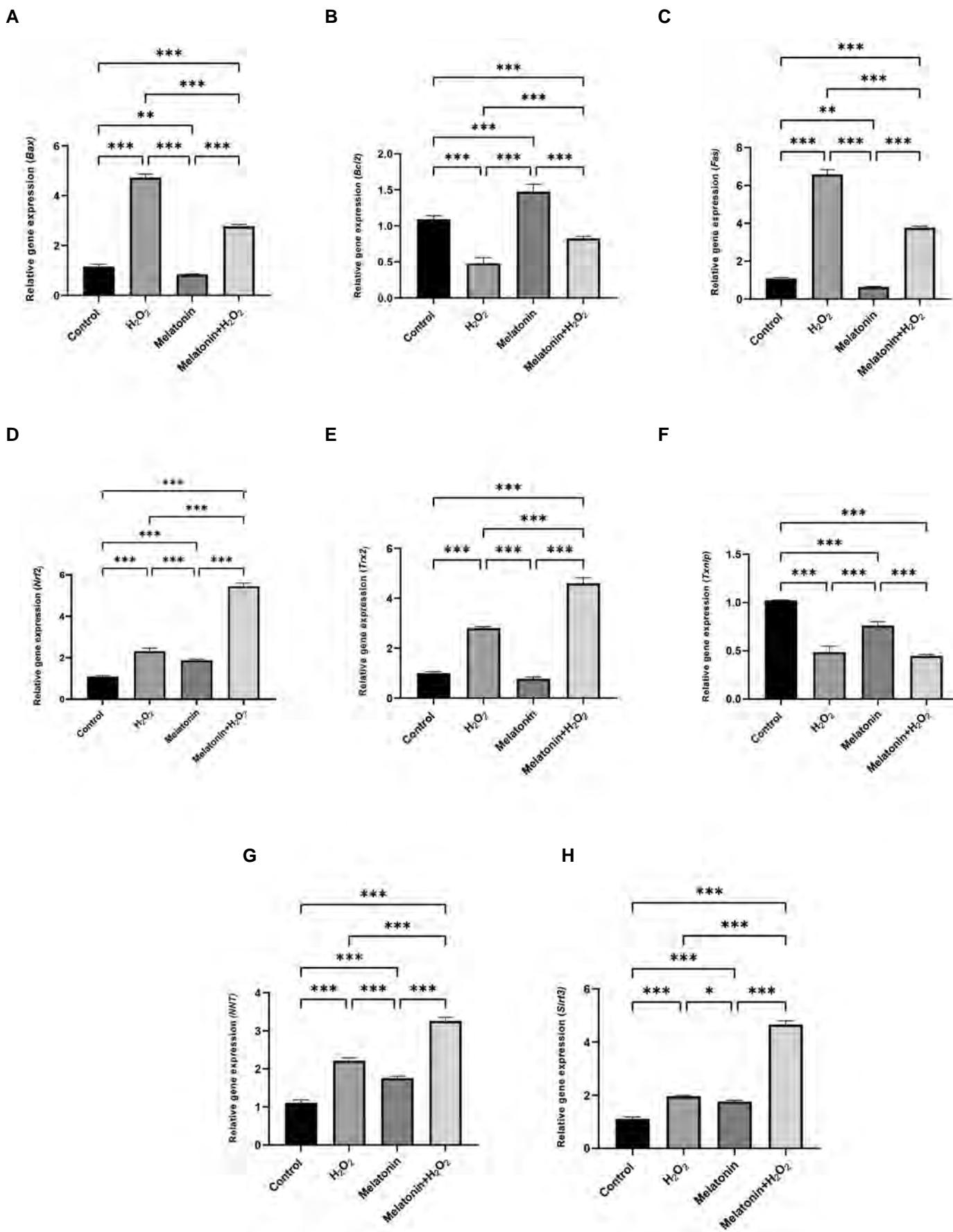


Fig.5: Effects of melatonin and H₂O₂ on apoptotic and antioxidant gene expressions. qRT-PCR analysis for **A.** *Bax*, **B.** *Bcl-2*, **C.** *Fas*, **D.** *Nrf2*, **E.** *Trx2*, **F.** *Txnip*, **G.** *NNT*, and **H.** *Sirt3* after exposure of cells with either 250 μM of melatonin, 250 μM of melatonin plus 50 μM of H₂O₂, or 50 μM of H₂O₂ for 24 hours. The cells in the control group did not receive any treatment. mRNA expression was normalised using *Gapdh* mRNA as an internal standard. Data are shown as mean ± SD. qRT-PCR; Quantitative real-time polymerase chain reaction, *; P<0.05, **; P<0.01, and ***; P<0.001.

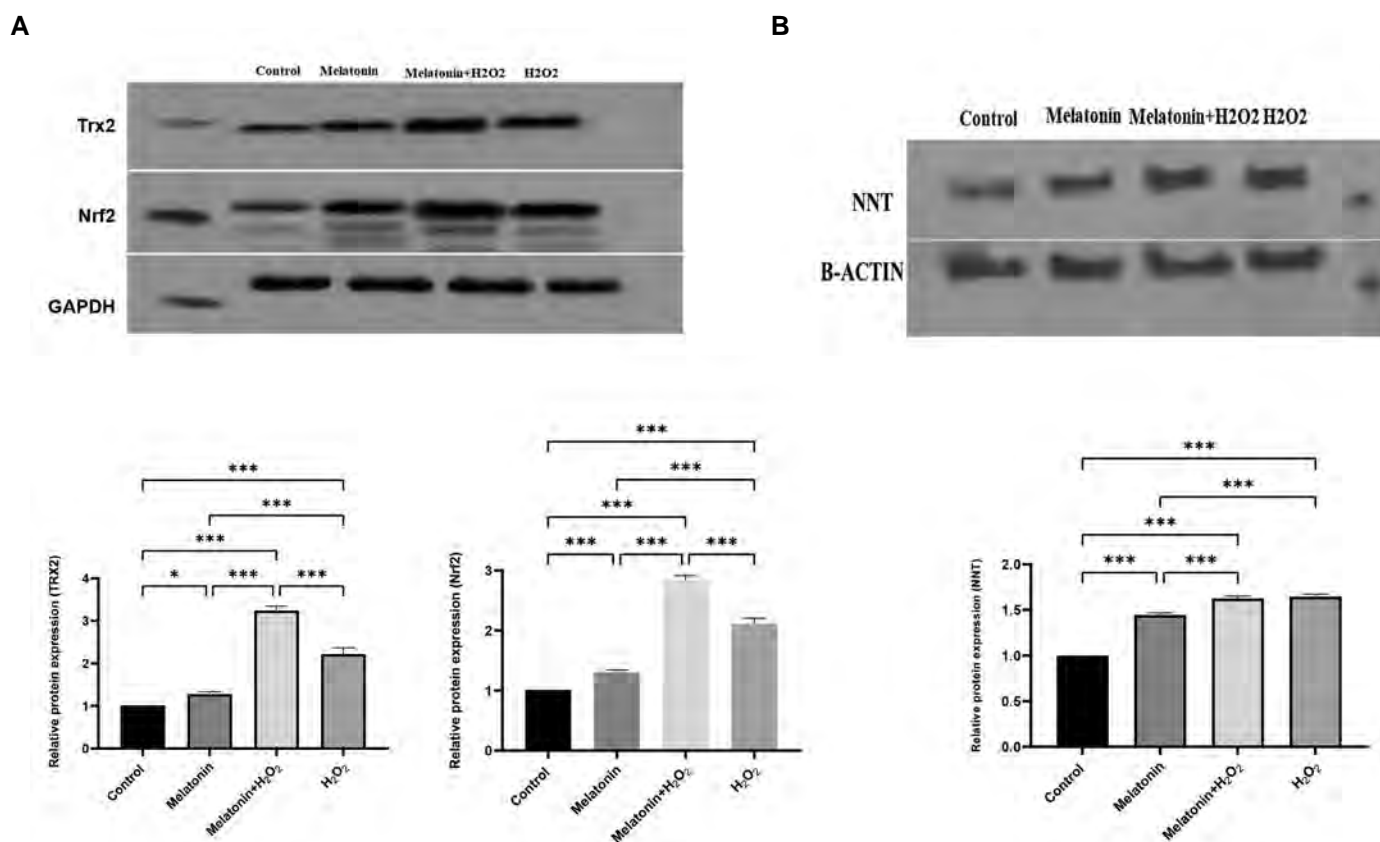


Fig.6: The effects of melatonin and H₂O₂ on the expressions of antioxidant proteins of the thioredoxin system. Western blot analysis for: **A.** Nrf2 and Trx2, and **B.** NNT after exposure of cells to either 250 μ M of melatonin, 250 μ M of melatonin plus 50 μ M of H₂O₂, or 50 μ M of H₂O₂ for 24 hours. The cells in the control group did not receive any treatment. Data are shown as mean \pm SD. *, P<0.05 and ***, P<0.001.

Discussion

This study investigated the effects of melatonin and its associated mitochondrial pathways on mouse type A SSCs under oxidative stress conditions. The results suggest that melatonin can reduce H₂O₂-induced ROS production and apoptosis in SSCs by activating the mitochondrial thioredoxin system. It can also increase protein and mRNA expression of *Nrf2* under oxidative stress conditions, which is expected to increase antioxidant activity of the mitochondrial thioredoxin system. According to the results, melatonin can mitigate the damaging effects of H₂O₂-induced ROS by increasing both gene and protein expressions of *Trx2* and decreasing gene expression of *Txnip* (Trx2 inhibitor), in addition to increasing gene and protein expressions of *NNT* and gene expression of *Sirt3*. Melatonin increases the amount of energy available to the cells by elevating ATP levels.

The effects of melatonin on SSCs have been examined in multiple studies. Li et al. (29) reported that melatonin increased the expression of superoxide dismutase (SOD) and regulated busulfan-induced ROS production. They observed that melatonin also increased *Sirt1* expression, which is involved in the deacetylation of *p53*; lower concentrations of deacetylated *p53* enhance the resistance of SSCs to apoptosis. There is evidence that melatonin can reduce bisphenol A-induced lipid peroxidation in

mouse testes, restore mitochondrial marker enzymes, and improve the activity of enzymatic and non-enzymatic mitochondrial antioxidants (30). Treatment with melatonin reduces the severity of testicular tissue damage in animal models of hyperlipidaemia, testicular torsion, varicocele, and toxicity caused by chemotherapy drugs or environmental toxins (15, 16). Jou et al. (31) showed that melatonin significantly inhibited ROS production under normal conditions and during the initial stages of H₂O₂-induced oxidative stress. They concluded that melatonin prevents ROS from depolarizing the mitochondrial membrane and opening mitochondrial membrane pores, which prevents the release of cytochrome C. Melatonin also suppresses palmitic acid-induced apoptosis by regulating the expressions of apoptosis-related proteins, including *Bcl2*, *Bax*, *C-caspase 3*, and *C-caspase 12* in type-B SSCs (32). In our study, we observed an association of melatonin with favourable changes in the expressions of apoptotic genes (decreased *Bax* and *Fas*, and increased *Bcl2*), a decrease in ROS and MDA levels, and an increase in activity of the thioredoxin antioxidant system under oxidative stress conditions. According to He et al. (33), Nrf2 suppresses the basal expression of *Txnip* in heart cells, which is important because *Txnip* induces ROS production and apoptosis by inhibiting *Trx*. Nrf2 also inhibits *Txnip* by binding to its promoter to prevent transcription, which increases thioredoxin activity.

Similarly, we found that melatonin treatment increased both gene and protein expressions of *Nrf2* under oxidative stress, and led to increased gene and protein expression of *Trx2* and reduced expression of *Txnip*. This suggests that melatonin, as an antioxidant, contributes to more effective ROS removal by increasing *Nrf2* and its downstream pathway, namely the thioredoxin system.

Zhou et al. (34) reported that the decrease in cellular ROS in melatonin-pretreated microglia was due to the inhibition of ROS production rather than the direct removal of ROS. According to this study, melatonin inhibits NADPH oxidase activation in amyloid-beta-activated microglia but has no apparent inhibitory effect on activated NADPH oxidase. This study provided evidence that melatonin can disrupt the NADPH oxidase accumulation in amyloid-beta-activated microglia and inhibit ROS production in a dose-dependent manner. However, melatonin's ability to directly inhibit superoxide was not significant at 100 μM and only notable at 250 μM . In our study, the best antioxidant effects of melatonin were observed at the 250 μM dose. However, no significant difference was observed between the 100 μM and 250 μM doses of melatonin under normal cellular conditions. Hence, it is suggested that the desired doses should be measured at 2-, 6-, and 12-hour intervals. Pretreatment with melatonin should be investigated in future studies. Florido et al. (26) reported that 0.5 and 1 mM doses of melatonin caused apoptosis by driving mitochondrial reverse electron transport to induce ROS production in head and neck squamous cell carcinoma cell lines. This finding indicated that high doses of melatonin could induce ROS.

Therefore, it is possible that 250 μM of melatonin could act as an important transcription factor for expression of phase II antioxidant enzymes. These enzymes comprise a group of vital proteins that carry out the detoxification process by increasing hydrophilicity and increasing excretion of xenobiotics through increasing *Nrf2* expression. The Keap1 protein is an important factor for *Nrf2* function and its transfer into the nucleus. *Nrf2* activating agents such as melatonin can affect this factor, and should be investigated in future studies on the Keap1 protein. Yu et al. (35) assessed the effects of melatonin on the thioredoxin system during myocardial ischemia-reperfusion (MI/R) injuries. They found that melatonin treatment reduced myocardial apoptosis; significantly increased Notch1/Hes1/Akt signalling pathway activity; improved the activity of the intracellular thioredoxin system by increasing Notch1, N1ICD, Hes1, and p-Akt activities; and decreased *Txnip* expression. Therefore, they concluded that melatonin reduces the activity of the thioredoxin system by decreasing the expression of *Txnip* through the Notch1/Hes1/Akt signalling pathway in a membrane receptor-dependent manner. We investigated the protective effects of melatonin on Trx/*Txnip* after induction of oxidative stress. Our results showed that melatonin changed the expression levels of Trx and *Txnip*. Trx expression significantly increased at the mRNA and protein levels in the groups treated with melatonin alone

and under oxidative stress conditions; on the other hand, it caused a decrease in *Txnip* expression at the mRNA level. Inhibition of *Nrf2*, an inhibitor of *Txnip*, is proposed to increase *Txnip* expression to some extent. Hence, the effect of melatonin on *Txnip* expression at the protein level and its function, and the effect of inhibition of *Nrf2* by trigonelline should be studied. It is also possible that melatonin directly increases Trx activity, which can be related to the regeneration of the oxidised form of Trx by melatonin, or that melatonin may directly inhibit *Txnip* or Trx activity. More studies that assess the effect of melatonin on *Txnip* and *Trx2* at the protein and activity levels are suggested.

One of the limitations of this study was the unavailability of a *Trx2* activity assay kit and 3D culture system for SSCs. Along with combining SSCs with Sertoli cells in a 2D environment, embedding SSCs in a 3D culture system can also provide a structure that imitates the complex structure found in living testes. Multiple studies have shown that *NNT* is a physiological source of NADPH in mitochondria (36, 37). Silencing of small interfering RNA of *NNT* in PC12 cells decreases cellular NADPH levels, thereby changing the cell's redox state by decreasing the GSH/GSSG ratio and increasing H_2O_2 levels, which leads to increased redox potential and disruption of electron flow to redox components, and ultimately results in mitochondrial dysfunction (37). We observed that, in the H_2O_2 group, expression of *NNT* increased to provide the amount of NADPH required by the mitochondrial redox system to overcome the oxidative stress conditions. In addition, melatonin contributed to more effective ROS removal by increasing *NNT* expression.

Sirt3 is a member of the Sirtuin family that is primarily positioned in the mitochondria, and protects the tissue against oxidative stress-related conditions such as MI/R. It has been shown that melatonin has positive effects on repairing the damage caused by MI/R. Zhai et al. (38) reported that MI/R injury significantly decreased myocardial *Sirt3* expression and activity. Treatment with melatonin regulated *Sirt3* expression and activity, thereby leading to decreased SOD-2 acetylation. They noted that melatonin increased *Bcl2* expression and decreased the expressions of *Bax* and *Caspase 3* after MI/R. However, the cardioprotective effects of melatonin were largely restricted by the selective *Sirt3* inhibitor (3-TYP), which indicates that *Sirt3* plays an essential role in mediating the protective effects of melatonin. This suggests that melatonin alleviates MI/R injury by reducing oxidative stress and apoptosis through activation of the *Sirt3* signalling pathway. We also observed that melatonin led to increased *Sirt3* expression and ATP levels in SSCs under oxidative stress conditions. Jiang et al. (39) reported that while *Nrf2* does not affect the quantity of mitochondrial antioxidant enzymes, it regulates NADPH by controlling gene expression in PPP, which is the main source of cytoplasmic NADPH. In this way, it indirectly increases mitochondrial NADPH to activate the *Trx2* system, and thus mobilises the mitochondrial thioredoxin system for

better H₂O₂ removal. In a study by Rao et al. (40), it was noted that NNT is a key enzyme in the mitochondrial inner membrane that regulates the NADPH required by thiol-dependent peroxidase systems of mitochondria. These researchers observed significant impairment in mitochondrial function in response to angiotensin II (Ang II), which was associated with increased superoxide and H₂O₂ levels. They reported an increase in NNT expression and activity in response to the mitochondrial dysfunction and oxidative stress associated with Ang II treatment. In their study, decreased NNT activity led to significantly increased mitochondrial ROS production and reduced glutathione peroxidase and glutathione reductase activity, which they linked to a reduced NADPH/NADP⁺ ratio, as well as impaired ATP production. We observed elevated *NNT* gene and protein expressions in response to the increased H₂O₂ level. Our results showed that melatonin, as an exogenous antioxidant, increased both gene and protein expressions of *NNT* under oxidative stress conditions, and helped supply the necessary amount of NADPH needed by the thioredoxin system for effective ROS removal. Therefore, our results showed that melatonin may be considered a natural antioxidant to reduce oxidative stress and its action pathways in SSCs. However, additional studies are needed to assess the effects of melatonin on SSCs and oxidative stress pathways, especially the glutathione peroxidase pathway. More research on the effects of melatonin on redoxosome and its role in diseases such as male infertility is needed.

Conclusion

The results of this study show that melatonin is a strong antioxidant that can affect the mitochondrial antioxidant system by increasing *Nrf2* expression at the gene and protein levels. Melatonin can induce the Trx2 system and the Trx/Txnip pathway, elevate expression of *NNT* at the gene and protein levels, and increase the amount of energy available to the cell by increasing ATP levels. Melatonin increases mRNA expression of *Sirt3* and decreases mRNA expression of *Txnip*, thereby enhancing the activity of the mitochondrial thioredoxin system. It seems that melatonin can play an effective role in reducing oxidative stress in SSCs under pathological conditions by activating the cytoplasmic and mitochondrial antioxidant pathways (Nrf2, Trx2); therefore, it can be used in the future as an effective antioxidant in the clinic and for infertility treatments.

Acknowledgements

The present study was supported by Kermanshah University of Medical Sciences, Kermanshah, Iran. The authors report no potential conflict of interest.

Authors' Contributions

M.Gh., S.H., Z.R.; Project administration, Conceptualization, and Methodology. M.Gh., S.H., Z.R., K.M., B.M.; Collected spermatogonial stem cells, Conducted the experiments, and Data analysis. Z.R.,

S.H., M.Gh., K.M., I.R., C.J.; Consulted in qRT-PCR and Western blot analyses. All authors read and approved the final manuscript.

References

- Rajender S, Rahul P, Mahdi AA. Mitochondria, spermatogenesis and male infertility. *Mitochondrion*. 2010; 10(5): 419-428.
- Orrenius S, Gogvadze V, Zhivotovsky B. Mitochondrial oxidative stress: implications for cell death. *Annu Rev Pharmacol Toxicol*. 2007; 47: 143-183.
- Martín M, Macías M, Escames G, León J, Acuña-Castroviejo D. Melatonin but not vitamins C and E maintains glutathione homeostasis in t-butyl hydroperoxide-induced mitochondrial oxidative stress. *FASEB J*. 2000; 14(12): 1677-1679.
- Barati E, Nikzad H, Karimian M. Oxidative stress and male infertility: current knowledge of pathophysiology and role of antioxidant therapy in disease management. *Cell Mol Life Sci*. 2020; 77(1): 93-113.
- Asadi N, Bahmani M, Kheradmand A, Rafeian-Kopaei M. The impact of oxidative stress on testicular function and the role of antioxidants in improving it: a review. *J Clin Diagn Res*. 2017; 11(5): IE01-IE05.
- Shaban S, El-Husseny MWA, Abushouk AI, Salem AMA, Mamdouh M, Abdel-Daim MM. Effects of antioxidant supplements on the survival and differentiation of stem cells. *Oxid Med Cell Longev*. 2017; 2017: 5032102.
- Aponte PM, van Bragt MP, de Rooij DG, van Pelt AM. Spermatogonial stem cells: characteristics and experimental possibilities. *APMIS*. 2005; 113(11-12): 727-742.
- Caroppo E, Dattilo M. Sperm redox biology challenges the role of antioxidants as a treatment for male factor infertility. *F&S Reviews*. 2022; 3(1): 90-104.
- Sadeghi N, Boissonneault G, Tavalae M, Nasr-Esfahani MH. Oxidative versus reductive stress: a delicate balance for sperm integrity. *Syst Biol Reprod Med*. 2023; 69(1): 20-31.
- Gholami M, Saki G, Hemadi M, Khodadadi A, Mohammadi-Asl J. Melatonin improves spermatogonial stem cells transplantation efficiency in azoospermic mice. *Iran J Basic Med Sci*. 2014; 17(2): 93-99.
- Reiter RJ, Tan DX, Rosales-Corral S, Galano A, Jou MJ, Acuna-Castroviejo D. Melatonin mitigates mitochondrial meltdown: interactions with SIRT3. *Int J Mol Sci*. 2018; 19(8): 2439.
- Gholami M, Saki G, Hemadi M, Khodadadi A, Mohammad-di-Asl J. Effect of melatonin on the expression of apoptotic genes in vitrified-thawed spermatogonia stem cells type A of 6-day-old mice. *Iran J Basic Med Sci*. 2013; 16(8): 906-909.
- Gholami MR, Saki G, Hemadi M, Khodadadi A, Mohammadi-Asl J. Supplementation vitrified-thawed media with melatonin do not protect immature mouse testicular tissue from vitrified-thawed induced injury. *Asian J Anim Vet Adv*. 2012; 7(10): 940-949.
- Guo Y, Sun J, Li T, Zhang Q, Bu S, Wang Q, et al. Melatonin ameliorates restraint stress-induced oxidative stress and apoptosis in testicular cells via NF-κB/iNOS and Nrf2/ HO-1 signaling pathway. *Sci Rep*. 2017; 7(1): 9599.
- Zhang K, Lv Z, Jia X, Huang D. Melatonin prevents testicular damage in hyperlipidaemic mice. *Andrologia*. 2012; 44(4): 230-236.
- Lee KM, Lee IC, Kim SH, Moon C, Park SH, Shin DH, et al. Melatonin attenuates doxorubicin-induced testicular toxicity in rats. *Andrologia*. 2012; 44 Suppl 1: 796-803.
- Munro D, Banh S, Sotiri E, Tamanna N, Treberg JR. The thioredoxin and glutathione-dependent H₂O₂ consumption pathways in muscle mitochondria: involvement in H₂O₂ metabolism and consequence to H₂O₂ efflux assays. *Free Radic Biol Med*. 2016; 96: 334-346.
- Roucher-Boulez F, Mallet-Motak D, Samara-Boustani D, Jilani H, Ladjouze A, Souchon PF, et al. NNT mutations: a cause of primary adrenal insufficiency, oxidative stress and extra-adrenal defects. *Eur J Endocrinol*. 2016; 175(1): 73-84.
- Ahmadi Z, Ashrafizadeh M. Melatonin as a potential modulator of Nrf2. *Fundam Clin Pharmacol*. 2020; 34(1): 11-19.
- Morris G, Walker AJ, Walder K, Berk M, Marx W, Carvalho AF, et al. Increasing Nrf2 activity as a treatment approach in neuropsychiatry. *Mol Neurobiol*. 2021; 58(5): 2158-2182.
- Yoshikawa T, Naito Y. What is oxidative stress? *JMAJ*. 2002; 45(7): 271-276.
- Veisi M, Mansouri K, Assadollahi V, Jalili C, Pirnia A, Salahshoor MR, et al. Evaluation of co-cultured spermatogonial stem cells en-

- capsulated in alginate hydrogel with Sertoli cells and their transplantation into azoospermic mice. *Zygote*. 2022; 30(3): 344-351.
23. Karimi E, Abbasi S, Abbasi N. Thymol polymeric nanoparticle synthesis and its effects on the toxicity of high glucose on OEC cells: involvement of growth factors and integrin-linked kinase. *Drug Des Devel Ther*. 2019; 13: 2513-2532.
 24. Rhee SG, Chang TS, Jeong W, Kang D. Methods for detection and measurement of hydrogen peroxide inside and outside of cells. *Mol Cells*. 2010; 29(6): 539-549.
 25. Basir HRG, Karbasi A, Ravan AP, Abbasalipourkabir R, Bahmani M. Is human umbilical cord mesenchymal stem cell-derived conditioned medium effective against oxidative and inflammatory status in CCl4-induced acute liver injury? *Life Sci*. 2022; 305: 120730.
 26. Florido J, Martinez-Ruiz L, Rodríguez-Santana C, López-Rodríguez A, Hidalgo-Gutiérrez A, Cottet-Rousselle C, et al. Melatonin drives apoptosis in head and neck cancer by increasing mitochondrial ROS generated via reverse electron transport. *J Pineal Res*. 2022; 73(3): e12824.
 27. Lorestani S, Hashemy SI, Mojarad M, Keyvanloo Shahrestanaki M, Bahari A, Asadi M, et al. Increased glutathione reductase expression and activity in colorectal cancer tissue samples: an investigational study in Mashhad, Iran. *Middle East J Cancer*. 2018; 9(2): 99-104.
 28. Rashidi Z, Aleyasin A, Eslami M, Nekoonam S, Zendedel A, Bahramrezaie M, et al. Quercetin protects human granulosa cells against oxidative stress via thioredoxin system. *Reprod Biol*. 2019; 19(3): 245-254.
 29. Li B, He X, Zhuang M, Niu B, Wu C, Mu H, et al. Melatonin ameliorates busulfan-induced spermatogonial stem cell oxidative apoptosis in mouse testes. *Antioxid Redox Signal*. 2018; 28(5): 385-400.
 30. Anjum S, Rahman S, Kaur M, Ahmad F, Rashid H, Ansari RA, et al. Melatonin ameliorates bisphenol A-induced biochemical toxicity in testicular mitochondria of mouse. *Food Chem Toxicol*. 2011; 49(11): 2849-2854.
 31. Jou MJ, Peng TI, Yu PZ, Jou SB, Reiter RJ, Chen JY, et al. Melatonin protects against common deletion of mitochondrial DNA-augmented mitochondrial oxidative stress and apoptosis. *J Pineal Res*. 2007; 43(4): 389-403.
 32. Xu D, Liu L, Zhao Y, Yang L, Cheng J, Hua R, et al. Melatonin protects mouse testes from palmitic acid-induced lipotoxicity by attenuating oxidative stress and DNA damage in a SIRT1-dependent manner. *J Pineal Res*. 2020; 69(4): e12690.
 33. He X, Ma Q. Redox regulation by nuclear factor erythroid 2-related factor 2: gatekeeping for the basal and diabetes-induced expression of thioredoxin-interacting protein. *Mol Pharmacol*. 2012; 82(5): 887-897.
 34. Zhou J, Zhang S, Zhao X, Wei T. Melatonin impairs NADPH oxidase assembly and decreases superoxide anion production in microglia exposed to amyloid-beta1-42. *J Pineal Res*. 2008; 45(2): 157-165.
 35. Yu L, Fan C, Li Z, Zhang J, Xue X, Xu Y, et al. Melatonin rescues cardiac thioredoxin system during ischemia-reperfusion injury in acute hyperglycemic state by restoring Notch1/Hes1/Akt signaling in a membrane receptor-dependent manner. *J Pineal Res*. 2017; 62(1).
 36. Gameiro PA, Laviolette LA, Kelleher JK, Iliopoulos O, Stephanopoulos G. Cofactor balance by nicotinamide nucleotide transhydrogenase (NNT) coordinates reductive carboxylation and glucose catabolism in the tricarboxylic acid (TCA) cycle. *J Biol Chem*. 2013; 288(18): 12967-12977.
 37. Yin F, Sancheti H, Cadenas E. Silencing of nicotinamide nucleotide transhydrogenase impairs cellular redox homeostasis and energy metabolism in PC12 cells. *Biochim Biophys Acta*. 2012; 1817(3): 401-409.
 38. Zhai M, Li B, Duan W, Jing L, Zhang B, Zhang M, et al. Melatonin ameliorates myocardial ischemia reperfusion injury through SIRT3-dependent regulation of oxidative stress and apoptosis. *J Pineal Res*. 2017; 63(2).
 39. Jiang L, Shestov AA, Swain P, Yang C, Parker SJ, Wang QA, et al. Reductive carboxylation supports redox homeostasis during anchorage-independent growth. *Nature*. 2016; 532(7598): 255-258.
 40. Rao KNS, Shen X, Pardue S, Krzywanski DM. Nicotinamide nucleotide transhydrogenase (NNT) regulates mitochondrial ROS and endothelial dysfunction in response to angiotensin II. *Redox Biol*. 2020; 36: 101650.

Osteoblastic Differentiation of Stem Cells from Human Exfoliated Deciduous Teeth by Probiotic Hydroxyapatite

Sabereh Nouri, Ph.D.¹, Rasoul Roghanian, Ph.D.^{1*} , Giti Emtiazi, Ph.D.¹, Oguzhan Gunduz, Ph.D.²,
Rasoul Shafiei, Ph.D.¹

1. Department of Cell, Molecular Biology and Microbiology, Faculty of Biological Science and Technology, University of Isfahan, Isfahan, Iran

2. Center for Nanotechnology and Biomaterials Application and Research at Marmara University, Goztepe Campus, Istanbul, Turkey

Abstract

Objective: Multipotent cells derived from human exfoliated deciduous teeth (SHED) possess the ability to differentiate into various cell types, including osteoblasts. This study aims to simulate the growth induction and osteogenic differentiation of SHED cells using probiotics and their resultant biomaterials.

Materials and Methods: This experimental study proceeded in two stages. Initially, we evaluated the effect of autoclaved nutrient agar (NA) grown probiotic *Bacillus coagulans* (*B. coagulans*) on the SHED and MG-63 cell lines. Subsequently, probiotics grown on the Pikovskaya plus urea (PVKU) medium and their synthesised hydroxyapatite (HA) were identified using X-ray diffraction (XRD), scanning electron microscopy (SEM), energy-dispersive X-ray (EDX), and Fourier transform infrared spectroscopy (FTIR), and then used to stimulate growth and osteogenic differentiation of the SHED cell line. Osteoblast cell differentiation was assessed by morphological changes, the alkaline phosphatase (ALP) assay, and alizarin red staining.

Results: There was a substantial increase in SHED cell growth of about 14 and 33% due to probiotics grown on NA and PVKU medium, respectively. The PVKU grown probiotics enhanced growth and induced stem cell differentiation due to HA content. Evidence of this differentiation was seen in the morphological shift from spindle to osteocyte-shaped cells after five days of incubation, an increase in ALP level over 21 days, and detection of intracellular calcium deposits through alizarin red staining-all indicative of osteoblast cell development.

Conclusion: The osteogenic differentiation process in stem cells, improved by the nano-HA-containing byproducts of probiotic bacteria in the PVKU medium, represents a promising pathway for leveraging beneficial bacteria and their synthesised biomaterials in tissue engineering.

Keywords: Differentiation, Hydroxyapatite, Osteoblast, Probiotic

Citation: Nouri S, Roghanian R, Emtiazi G, Gunduz O, Shafiei R. Osteoblastic differentiation of stem cells from human exfoliated deciduous teeth by probiotic hydroxyapatite. Cell J. 2023; 25(11): 753-763. doi: 10.22074/CELLJ.2023.1999743.1276

This open-access article has been published under the terms of the Creative Commons Attribution Non-Commercial 3.0 (CC BY-NC 3.0).

Introduction

Each year, bone disorders and defects from skeletal diseases, congenital malformations, trauma, and tumour resections necessitate bone reconstruction. Conventionally, these issues are addressed using metal implants or filling with bio-active materials in medical treatments. It is crucial to have activated calcium phosphate-based materials on the metallic implant's surface or within the filler bone cement in these therapeutic techniques (1, 2). Calcium phosphate salts comprise the primary mineral component of vertebrate bone and teeth, among which hydroxyapatite (HA), the most thermodynamically stable calcium phosphate compound, most closely resembles bone mineral protein, and is composed of up to 70% hard tissue (3, 4). HA has extensive applications in medicine, orthopaedics, dentistry, bone tissue engineering, implant coating, drug delivery systems, and cosmetics, in addition

to sanitation, sewage treatment, and the food industry. It is used in dental floss, toothpaste, and food additives to prevent tooth decay and support dental repair (5, 6). Biomaterials that bond with host bone tissues are highly effective in initiating cell regeneration (7). HA can be synthesised through chemical and biological methods, with the current focus of nano-biotechnology on environmentally friendly biosynthesis methods. Among natural HA sources, bacteria can act as bio-manufacturing units for nano-synthesis. This process, known as biomineralisation, yields inorganic crystals while exerting unique control over their morphology and nano-structural texture (8). The best bacterial candidates for biomineralisation are probiotics, the beneficial bacteria that reside in the human body and contribute to its functioning. They have been utilised in sanitation, medicine, and the food industry for several years (9, 10). Because medical usage of nano-HA

is one of the most important of our requirements, it is critical to derive this nano-particle from a safe bacterial source so that purification and characterisation are not a later issue. When these nanoparticles reach the body, they are likely to cause inflammatory reactions; therefore, the use of pathogenic bacteria to generate nano-HA may enhance the immune response (9).

The gut microbiome plays a crucial role in regulating bone health by influencing both postnatal skeletal development and skeletal involution. Imbalances in microbiota composition and the body's response to these changes contribute to pathological bone loss; adjusting the microbiota composition through interventions like prebiotics and probiotics may help prevent or reverse this loss (11). Numerous studies have demonstrated that dietary changes can enhance bone health and modify the gut microbiota composition. Additionally, recent research has explored strategies that involve bacteria and their components to influence the proliferation and differentiation of mesenchymal stem cells (MSC) (11-13). On the other hand, HA can assist stem cells in differentiating into osteogenic cells, and thus play a significant role in tissue engineering. Equally important to the field of tissue engineering is the type of stem cells employed. Among the most advantageous are stem cells from human exfoliated deciduous teeth (SHED) (14). Deciduous teeth are a set of 20 teeth that emerge after six months of age and are typically replaced between the ages of 6 to 13 years, and they contain viable pulp within their crowns (15). Dental pulp is a jelly-like tissue at the centre of each tooth that contains connective tissue, blood vessels, and odontoblasts. SHED express MSC surface markers such as STRO-1 and CD146. Cells that contain these markers are found around the blood vessels of the pulp, which suggests that SHED may originate from the microenvironment around these vessels (14, 15).

SHED possess the capability to differentiate into odontogenic, osteogenic, neurogenic, adipogenic, myogenic, and chondrogenic lines under suitable conditions. SHED coupled with HA particles and implanted into immunocompromised animals can differentiate into odontoblasts. The capacity for odontogenic differentiation and the ability to stimulate the bone *in vitro* suggest that SHED might constitute a population of multinucleated stem cells (16, 17).

Therefore, deciduous exfoliated teeth could be an excellent source of stem cells to repair damaged tooth structures, stimulate bone regeneration, and perhaps treat neurodegenerative diseases (18). Dental stem cells obtained from extracted teeth receive more attention because isolating these pluripotent cells is relatively simple and does not involve invasive action compared to the usual sources of MSC such as bone marrow or fat (15, 17, 18). One of the most promising sources of tooth stem cells is deciduous teeth, which are lost during puberty. Stem cells from the missing tooth pulp chamber could be isolated and kept as a convenient and painless source for restorative and reconstructive treatments after losing

deciduous teeth, and permanent teeth are replaced. SHED stem cells are pluripotent and have rapid proliferative capability. Hence, they are a preferred stem cell source compared to other storable dental stem cells (18).

For HA to qualify as a biomaterial, it must possess biocompatibility and bioactivities such as osteoconductivity and osteoinductivity. Biocompatibility refers to a material's systemic and cellular compatibility with the live body (19).

The separate efficacies of probiotics and HA have been shown in studies conducted on cell cultures that examined the proliferation, mineralisation, and expression of marker genes. These studies revealed that MG-63 cells, when treated with probiotics, exhibited characteristics indicative of their commitment to osteoblasts, including increased proliferation and differentiation (20).

While some studies have examined the influence of bacterial probiotic components on the proliferation and differentiation of stem cells, the primary objective of our present research is to explore the possibility of a safe probiotic [*Bacillus coagulans* (*B. coagulans*)] to produce non-toxic HA through biomineralisation. Additionally, we aim to assess the potential of probiotic debris, with its synthesised HA as a byproduct, to enhance the multiplication of MG-63 cells and promote proliferation and differentiation in SHED.

Materials and Methods

Production of bacterial synthesised hydroxyapatite

The project was found to be in accordance to the ethical principle and the national norms and standards for conducting Medical Research in Iran (IR. UI.REC.1402.017)

In this experimental study, we cultured a standard probiotic bacterial strain of *B. coagulans* (ATCC 7050) on nutrient agar (NA, Merck, Germany) and Pikovskaya plus urea (PVKU) medium that consisted of 10 g/L dextrose, 5 g/L $\text{Ca}_3(\text{PO}_4)_2$, 0.2 g/L NaCl, 0.2 g/L KCl, 0.1 g/L $\text{MgSO}_4 \cdot 7\text{H}_2\text{O}$, 0.5 g/L yeast extract, 0.002 g/L $\text{FeSO}_4 \cdot 7\text{H}_2\text{O}$, 0.002 g/L $\text{MnSO}_4 \cdot \text{H}_2\text{O}$, 15 g/L agar-agar, (pH=7.2), and 0.1% urea (Merck, Germany). After five days, the bacteria were harvested, dried at room temperature (25°C), and autoclaved for 15 minutes at 121°C. The PVKU-derived biomass was incinerated at 600°C for two hours in a furnace (Nabertherm, Germany) to eliminate any biologically active material from the HA production (21). Then, the synthesised biomaterial was characterised. The dried bacterial biomass harvested from the PVKU medium was named PVKUS and the dried bacterial biomass harvested from the NA medium was named NAS. We used 1 mg/ml of PVKUS and NAS for the cell line treatments.

Characterisation of bacterial synthesised hydroxyapatite

Synthesised HA from *B. coagulans* grown on PVKU

medium was identified by X-ray diffraction (XRD, D8 Advance, Bruker, Germany) at 35 kV and 30 mA in reflection mode with Cu K α ($\lambda=1.540598$ Å radiation) with a scanning speed of $0.04^\circ \text{ s}^{-1}$, scanning electron microscopy (SEM), energy-dispersive X-ray (EDX) analysis at 20 kV (Philips XI30, The Netherlands), and Fourier transform infrared spectroscopy (FTIR; FT/IR-6300, JASCO Corp., Japan) in the chemical bond absorption range of $350\text{-}4000 \text{ cm}^{-1}$ (21, 22).

3-(4,5-dimethylthiazol-2-yl)-2,5-diphenyltetrazolium bromide assay

SHED and the MG-63 cell line (donated by Professor Torabi Nejad Research Centre, Department of Dentistry, Isfahan University of Medical Sciences, Isfahan, Iran) were separately treated with 1 mg/ml PVKUS and 1 mg/ml NAS in Dulbecco's Modified Eagle Medium High Glucose [DMEM-H10% foetal bovine serum (FBS), 1% penicillin/streptomycin, Bio Idea] and incubated in a humidified atmosphere of 95% air and 5% CO₂ at 37°C. The growth rate and viability of the cells were assessed by the 3-(4,5-dimethylthiazol-2-yl)-2,5-diphenyltetrazolium bromide (MTT) method after three, five, and seven days. The cell lines were subjected to viability analysis and compared to an untreated control group. The experimental procedure involved removing the medium from each well, washing the wells with PBS, and subsequently adding 400 μL of medium and 40 μL of MTT solution (5 mg/mL) to each well. After four hours of incubation at 37°C, the supernatant was removed, and 400 μL of dimethyl sulphoxide (DMSO, Sigma, USA) was added to each well. Following a 20-minute incubation in a dark room, the absorbance was measured at 590 nm using a multi-mode reader (Synergy HTX, USA) (23). The cell viability assay was performed in three replications. Then, the population doubling number (PDN) was determined by utilising the following formula:

$$\text{PDN} = \log(N/N_0) \times 3.31$$

In this equation, N represents the final population cell number after three, five, and seven days, and N₀ represents the initial population number (24).

Osteoblastic differentiation of human exfoliated deciduous teeth

Characterisation of osteodifferentiation was performed by observed morphological changes, measurement of alkaline phosphatase (ALP) activity, and staining of calcium deposits with alizarin red. The osteoblastic differentiation study for SHED was conducted by treating SHED with an autoclaved sample from the PVKU medium (PVKUS). We added 2×10^4 SHED cells to each well of a six-well plate. PVKUS+DMEM-H medium were added to some of the

wells. The negative control wells had only DMEM-H, whereas the positive control wells contained osteogenic medium (STEMCELL Technologies, Canada). The plate was maintained in a humidified atmosphere of 95% air and 5% CO₂ at 37°C, and we changed the media every three days. After 7, 14, and 21 days we assessed for osteogenic differentiation by conducting the osteoblastic differentiation tests in triplicate (25, 26).

Morphological observation

The changes in SHED cell morphology were checked following osteogenic differentiation across three-time points (7, 14, and 21 days) under an inverted microscope (Motic AE31, China). Images of the cell changes were captured.

Alizarin red staining

After 21 days of osteogenesis induction, the cells were subjected to alizarin red staining to investigate the presence of calcium deposits for bone nodule formation. First, the cells were fixed in 400 μL of 10% formaldehyde for 30 minutes and then washed twice with PBS. Next, 400 μL of a 2% alizarin red stain (pH=4.2) solution was added to each well and the plate was allowed to incubate at room temperature for 15 minutes. After incubation, the solution was aspirated, and the cells were washed with distilled water. The stained cells were then observed under light microscopy, and images were captured. In order to quantitatively determine the optical density, 400 μL of 10% acetic acid was placed in each well and left to incubate for 30 minutes. Subsequently, the cell layer was gently scraped and combined with acetic acid in a microtube, and thoroughly mixed by vortexing. The sample was then heated at 85°C for 10 minutes, cooled on ice, and finally centrifuged at 20 000 g for 15 minutes. The resulting supernatant was carefully transferred to a 96-well plate, and the optical density (OD) value was measured at a single wavelength of 405 nm (27, 28).

Alkaline phosphatase activity

For osteogenic differentiation, we used the ALP assay. At 7, 14, and 21 days of culture, we removed the medium and rinsed the cells with PBS in order to eliminate any residual culture medium. The cells were trypsinised, placed in a falcon tube, and centrifuged at 300 g for 10 minutes. The supernatant was removed and cells were washed with PBS. Then, 200 μL of 0.8% (v/v) Triton x100 was added to a falcon tube for cell lysis to rupture the cell membranes and release the ALP molecules. The tubes were subjected to two rounds of centrifugation at 1600 g and 4°C for 10 minutes each in order to evaluate ALP activity. Approximately 10 μL of cell extract was added to each well of the 96-

well plates. Subsequently, each 96-well plate received the following additions: 40 μl of magnesium sulphate (w/v), 10 μl of p-nitrophenyl phosphate (w/v), and 40 μl of bicarbonate-carbonate buffer ($\text{NaNO}_3\text{-Na}_2\text{CO}_3$) (w/v) with a pH of 10.0 (PARSAZMOON, Iran). Next, the cells were placed in a controlled environment at a temperature of 37°C and allowed to incubate for 30 minutes. Following the incubation period, 100 μl of NaOH was mixed with each sample to halt the enzymatic process. A spectrophotometer was employed to measure the OD at a wavelength of 405 nm. The ALP enzyme activity was quantified using a unit (U), where one unit represents the release of 1 μmol p-nitrophenol per minute at a temperature of 37°C (29).

Statistical analysis

In this study, we used descriptive statistics and presented the results in graph form. Statistical analysis was performed using a Prism statistical software package (GraphPad Software, Inc., La Jolla, CA, USA). Two-way ANOVA and Tukey multiple comparison tests were employed for mean comparison. A significance level of $P < 0.05$ was considered statistically significant.

Results

Synthesis and characterisation of the bacterial hydroxyapatite

B. coagulans (ATCC 7050 Iranian Biological Resource Centre) was chosen due to its beneficial properties and widespread use as a probiotic in the food and medical industries (30). After cultivation on PVKU and NA media, the bacterial mass was harvested and dried. The consumption of calcium and insoluble phosphate from PVKU medium was observed by the presence of a clear zone that formed around the cultivation line on the cultural medium, a finding consistent with previous results (21). Based on this data, bacilli can synthesise biomaterials by biomineralising calcium and insoluble phosphate internally (31), which leads to purification of the biomineralised biomaterial for further investigations.

X-ray diffraction analysis

XRD patterns indicate that the synthesised HA peaks (Fig.1A) align with the standard XRD graph reference of the International Centre for Diffraction Data (ICDD) for HA (09-0432) as depicted in Figure 1B (22). Crystallinity of the synthesised HA was confirmed by the preference for orientation along the (211) and (212) planes. The Scherer equation was used to determine crystal size from the XRD peaks (22) and indicated the HA size to be 80-100 nm. The results corroborate the ability of probiotic *B. coagulans* to produce HA in a PVKU medium, as established in our previous study (21).

Scanning electron microscopy imaging and energy-dispersive X-ray analysis

SEM images (Fig.2A) revealed the braided morphological features of bacterial HA and the crystal size of the HA (range: 80-100 nm). The elemental composition and Ca/P ratios of HA were determined by EDX. The Ca/P ratio was 1.9, which was close to the stoichiometric human bone HA ratio (Fig.2B).

Fourier transform infrared spectroscopy

The Fourier transform infrared spectroscopy (FTIR) spectrum of the synthesised HA (Fig.2C) showed the presence PO_4^{3-} , OH^- , and CO_3^{2-} chemical groups, all typical of conventional HA (32, 33). Strong IR absorption bands were exhibited by the PO_4^{3-} group at 400-700 cm^{-1} and 1000-1100 cm^{-1} . The adsorbed water band was broad, and spanned from 2000 to 3000 cm^{-1} , with a distinct peak at 3427 cm^{-1} and a weaker peak at 1800 cm^{-1} . CO_3^{2-} peaks that corresponded to the natural HA were observed between 1400 and 1500 cm^{-1} (34).

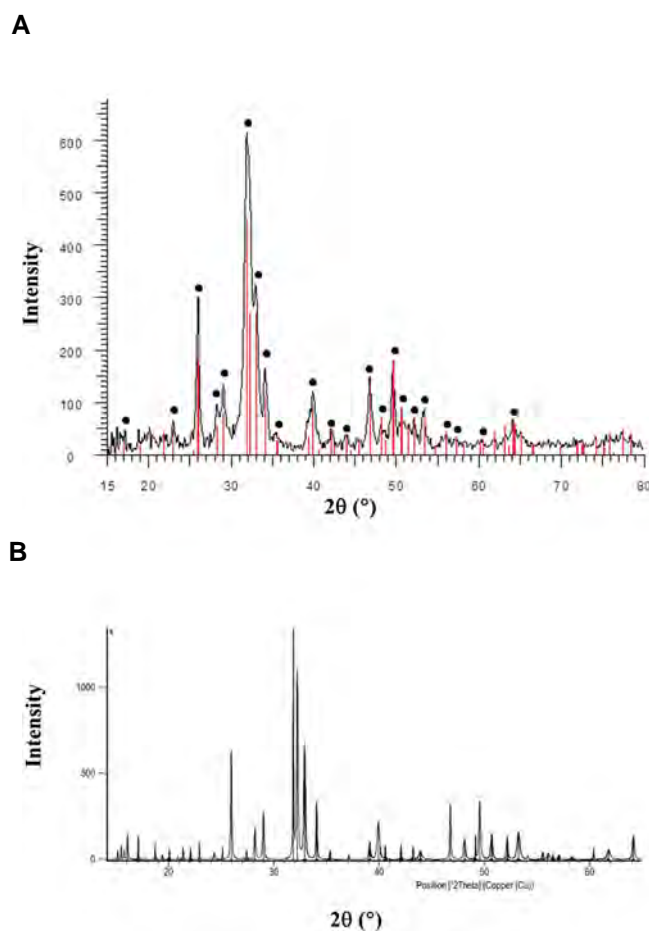


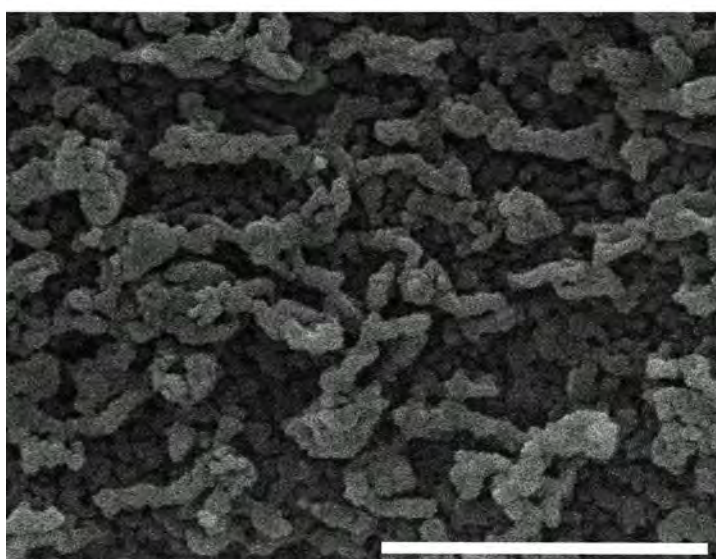
Fig.1: X-ray diffraction of synthesized HA. **A.** XRD pattern of *Bacillus coagulans* (*B. coagulans*) mediated HA. **B.** ICDD database for the standard peak of HA. XRD; X-ray diffraction, HA; hydroxyapatite, ICDD; International Centre for Diffraction Data, and \bullet ; Hydroxyapatite.

Cell viability

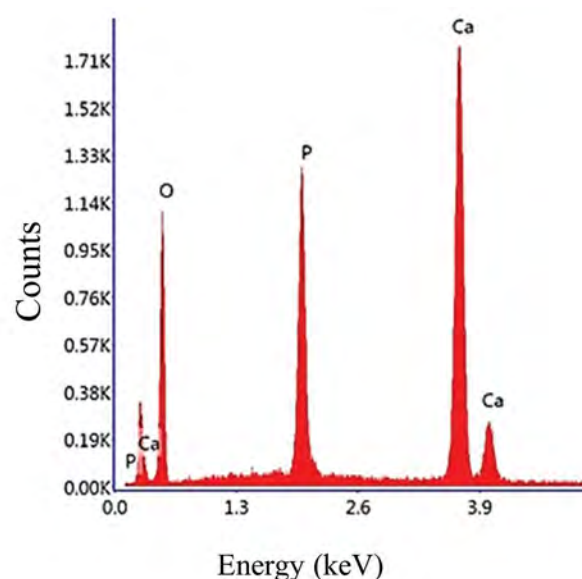
The effects of NAS and PVKUS on the viability and the proliferation rate of the SHED and MG-63 lines were examined by MTT. The results are reported as the OD of the viable cells compared to the untreated SHED control. Figure 3A and B show cellular viability and PDN for SHED. Figure 3C and D depict the graphs for cellular viability and PDN of the MG-63 cells. These graphs represent the data obtained after culturing both cell types for three, five, and seven days. ANOVA findings confirmed that NAS and PVKUS did not

show any toxicity and had highly significant ($P < 0.001$) growth induction (14 and 33%, respectively) on SHED. PVKUS was significantly more effective than NAS in increasing MG-63 cell viability. The cell PDN calculated for NAS and PVKUS showed that the PDN (Fig. 3B, D) was significantly higher for cells treated with PVKUS compared to the control and cells treated with NA ($P < 0.001$). Therefore, we chose PVKUS for osteoblastic differentiation of stem cells because of its significantly more proliferative effect on the SHED and MG-63 cell lines.

A



B



C

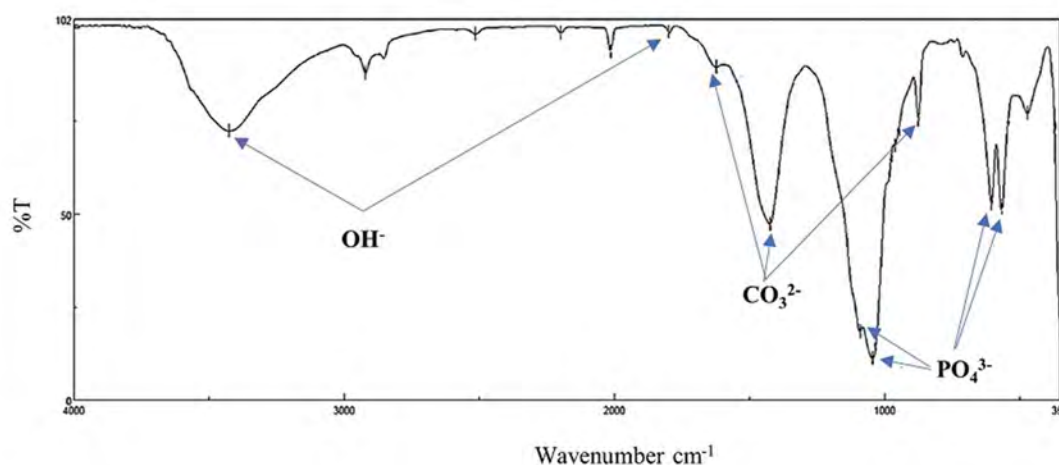


Fig.2: Characterisation of bacterial HA. **A.** SEM micrographs (scale: 300 nm). **B.** EDX graph and **C.** FTIR spectra graph of obtained probiotic bacterial nano HA from *Bacillus coagulans* (*B. coagulans*). SEM; Scanning electron microscopy, EDX; Energy-dispersive X-ray, FTIR; Fourier transform infrared spectroscopy, and HA; hydroxyapatite.

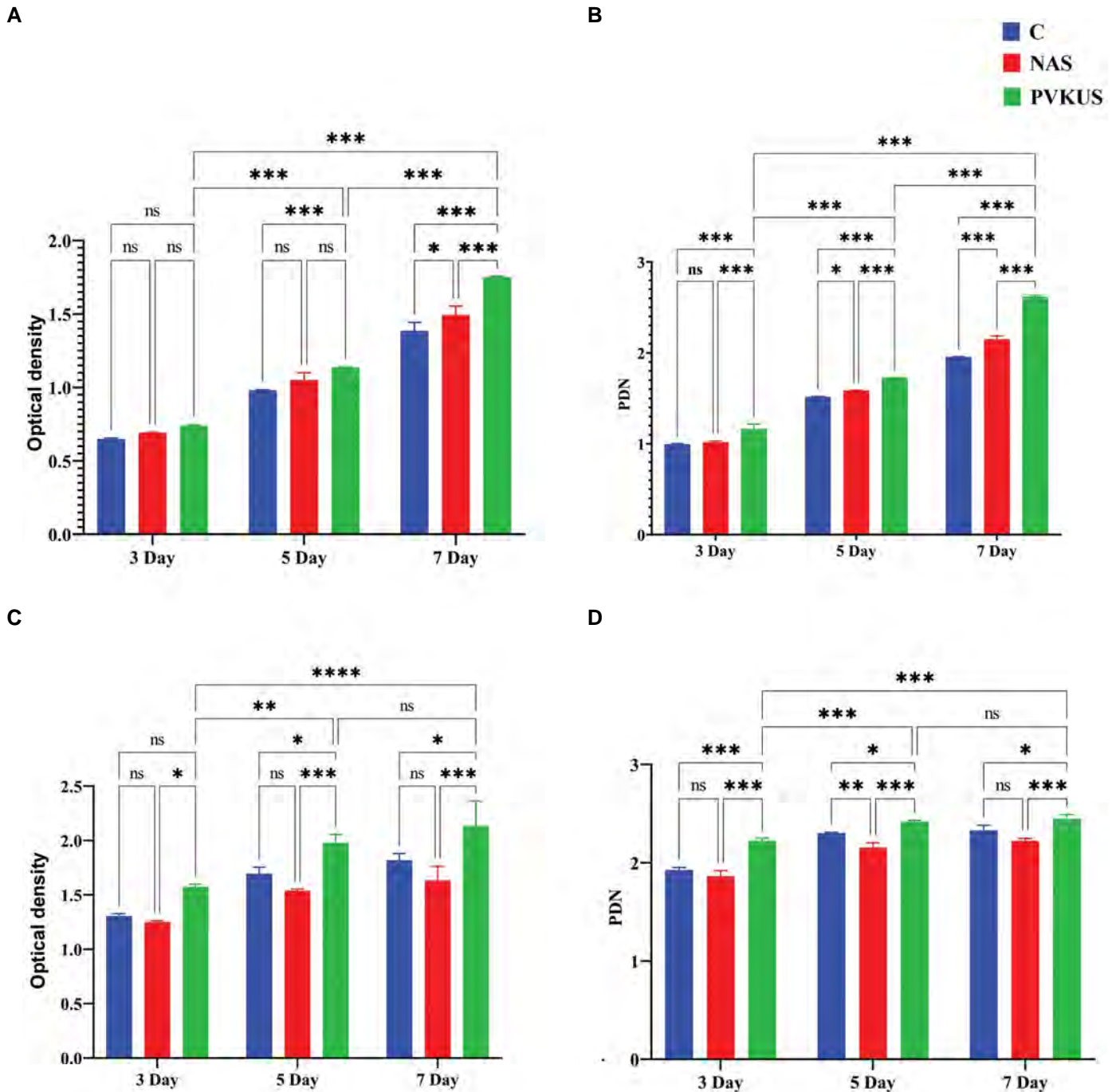


Fig.3: Cell viability. **A, B.** The effect of NAS and PVKUS [samples grown on NA and PVKU media, respectively] on SHED and **C, D.** MG-63 cell line viability. 3-(4,5-dimethylthiazol-2-yl)-2,5-diphenyltetrazolium bromide (MTT) reduction assays were used to evaluate cells treated with the same dose at different time points. The results revealed differences in OD between the treated and control cells. Untreated cells are considered as the control. Data are expressed as the mean \pm SD. Statistical analysis is obtained from the results of two-way ANOVA. *, $P < 0.1$, **, $P < 0.01$, ***, $P < 0.001$, ****, $P < 0.0001$, ns; Not significant, NA; Nutrient agar, PVKU; Pikovskaya plus urea, SHED; Human exfoliated deciduous teeth, and OD; Optical density.

Osteoblastic differentiation of human exfoliated deciduous teeth

Morphological observation

Cellular shape is a significant indicator for characterising and evaluating cell quality (35). For osteogenic differentiation, we treated the SHED cell line with PVKUS and assessed the morphological alterations. The SHED cell lines cultured in osteogenic medium and basic DMEM-H medium were considered to be the positive and

negative controls, respectively. We observed a spindle-shaped morphology and high capacity to attach to plastic surface in the DMEM-H medium. After five days, some of the cells treated with PVKUS began to change their morphology from spindle-shaped to a stellate shape and appeared more polygonal, which would be an osteocyte-associated feature (36). There was a homogeneous population of polygonal cells in the treated cells after four and 21 days of incubation

(Fig.4G-I); also, we observed a similar morphological variation in the SHED cell line in osteogenic medium (Fig.4D-F). However, there was no observed changed in morphology detected in the SHED cell line grown in DMEM-H medium (Fig.4A-C).

Alizarin red staining

Mineral nodule formation is frequently employed as a means to evaluate the osteogenic differentiation of SHED. Alizarin red staining serves as an indicator of nodules that resemble mineralised structures. In this study, we used alizarin red to stain the intracellular calcium. This staining method is widely recognized for its utility in evaluating bone differentiation and as a marker for mineralisation (27). The visualization of a coloured complex within the cells indicated successful osteoblastic differentiation of SHED and the presence of a newly formed mineralised matrix (Fig.5). Alizarin

red staining indicated that SHED grown in osteogenic medium and PVKUS significantly ($P < 0.001$) created a calcified matrix after 21 days of culture. The undifferentiated control SHED grown in DMEM-H medium showed no alizarin red staining.

Alkaline phosphatase activity

The results of two-way ANOVA show that the ALP activity of the SHED group treated with PVKUS (0.181 ± 0.002 U/mg) was significantly higher than the SHED group treated with primary DMEM medium (0.021 ± 0.006 U/mg) and was equal to the SHED group treated with osteogenic medium (0.181 ± 0.001 U/mg) after 21 days ($P < 0.001$). No significant increase in ALP levels was observed in cells treated with basic DMEM-H medium during 21 days (Fig.6). The results were similar to other researchers' findings that showed increased ALP levels during SHED differentiation (29).

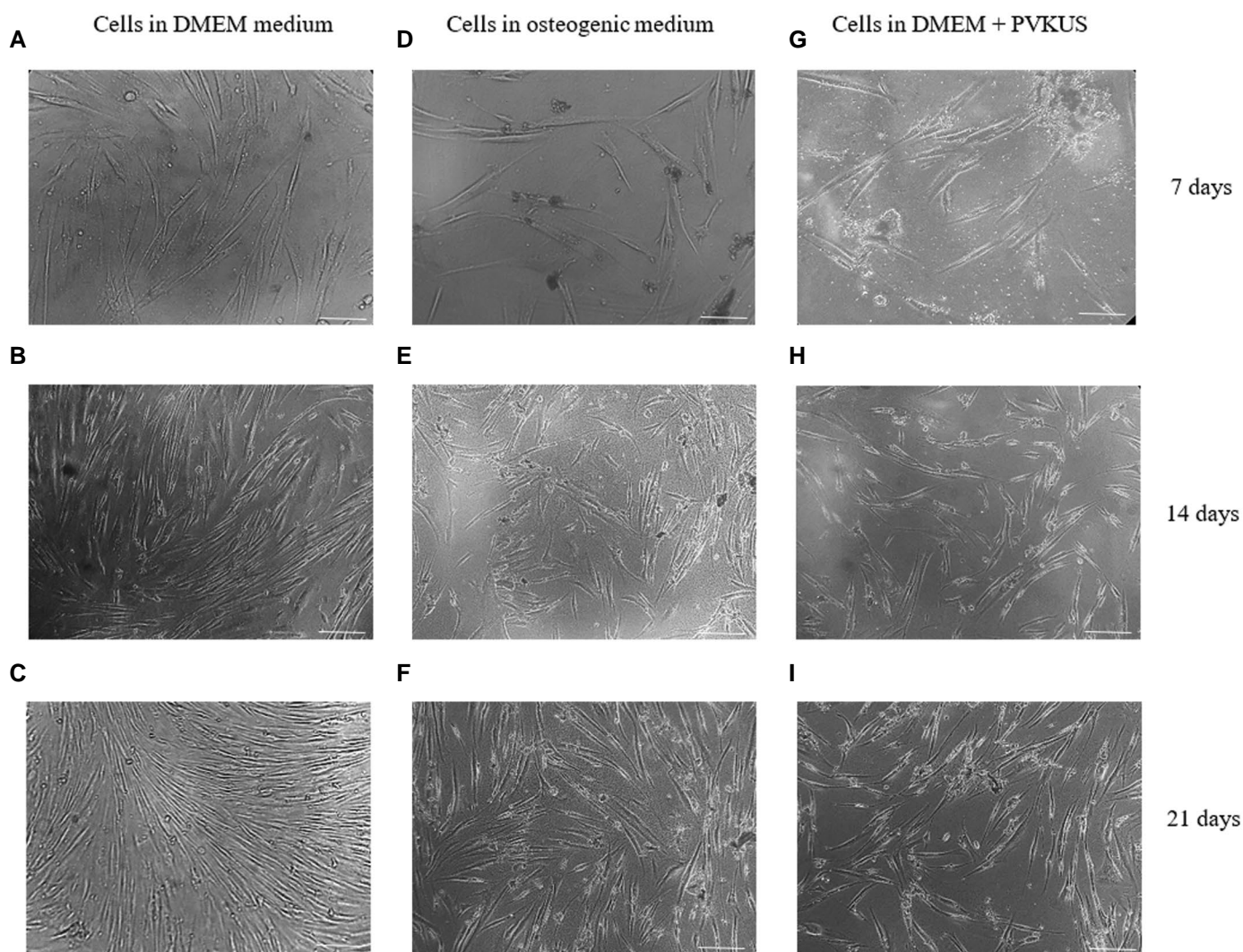


Fig.4: Cell morphological alteration during differentiation. **A-C.** SHED cultured in DMEM-H medium is the negative control (scale bar: 100 μ m), **D-F.** SHED cultured in osteogenic medium is the positive control, and **G-H.** Morphological changes of SHED during osteogenic differentiation from a spindle-shape to stellate-shaped polygon as observed by phase-contrast microscopy after 7, 14, and 21 days. SHED; Human exfoliated deciduous teeth, DMEM; Dulbecco's Modified Eagle Medium, and PVKU; Pikovskaya plus urea.

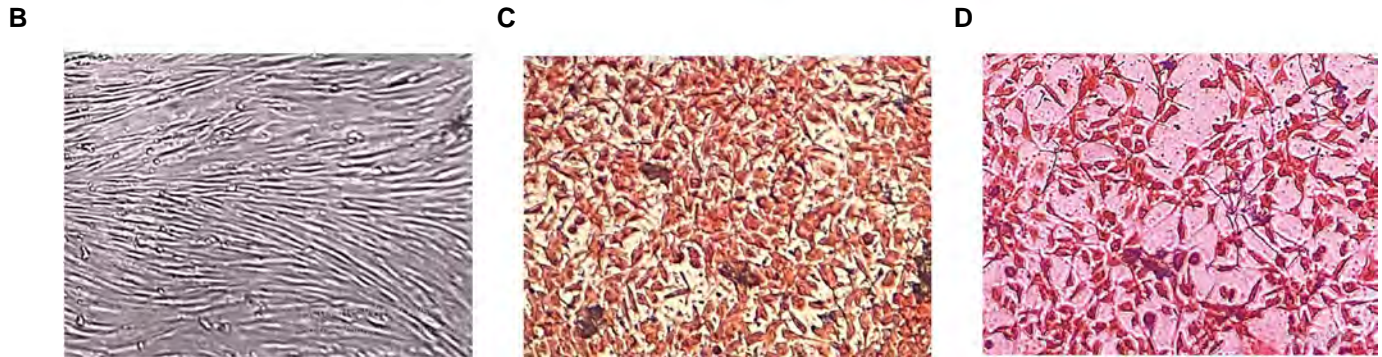
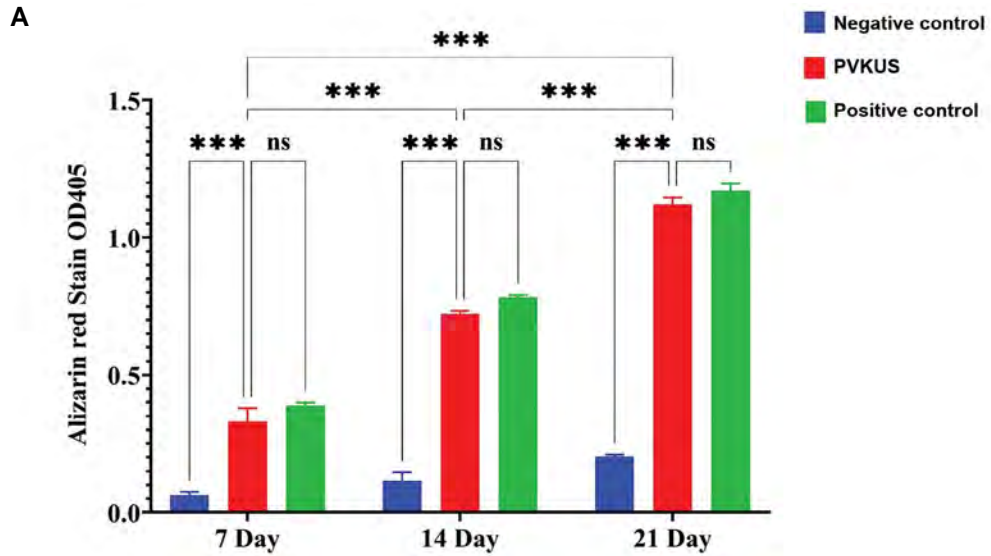


Fig.5: Alizarin red-stained mineralized nodules formed by differentiated cells. **A.** Quantitative measurement, **B.** Normal culture medium containing DMEM supplemented with 10% FBS is the negative control, **C.** The formation of a coloured complex within the cells shows osteoblastic differentiation of SHED with PVKUS [debris of the cultured *Bacillus coagulans* (*B. coagulans*) on PVKU medium], and **D.** Cells cultured with an osteogenic differentiation medium are the positive control (scale bar: 30 μ m). Statistical analysis is obtained from the results of two-way ANOVA. The results are expressed as mean \pm SD. ***, $P < 0.001$, ns; Not significant, DMEM; Dulbecco's Modified Eagle Medium, FBS; Fetal bovine serum, SHED; Human exfoliated deciduous teeth, and PVKU; Pikovskaya plus urea.

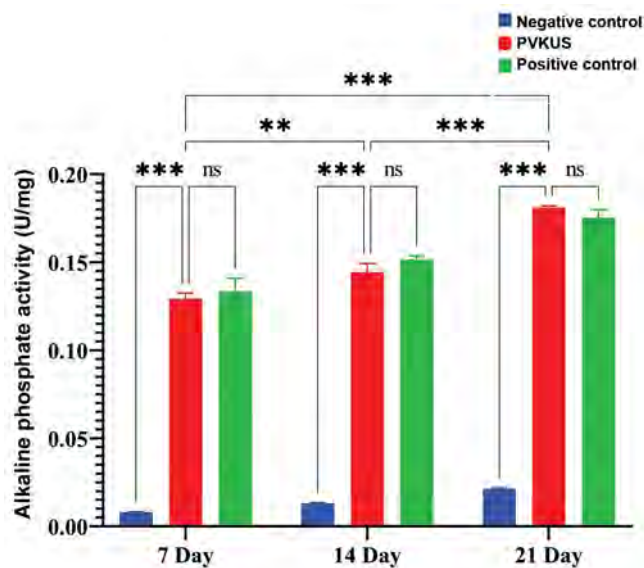


Fig.6: ALP activity of the SHED with PVKUS [debris of the cultured *Bacillus coagulans* (*B. coagulans*) on PVKU medium]. SHED cultured with DMEM-H without treatment is the negative control and SHED grown in osteogenic medium is the positive control. Data are expressed as mean \pm SD. Statistical analysis obtained from results of two-way ANOVA. **, $P < 0.01$, ***, $P < 0.001$, ns; Not significant, ALP; Alkaline phosphatase, SHED; Human exfoliated deciduous teeth, PVKU; Pikovskaya plus urea, and DMEM-H; Dulbecco's Modified Eagle Medium High Glucose.

Discussion

In this investigation, the probiotic *B. coagulans* was utilised to biosynthesize nano-HA. The XRD pattern results exhibited sharp peaks, which confirmed crystallisation of the bio-organic phase on the surface of HA that were stabilised by bacteria that acted as chelating agents (31). SEM images revealed a braided or woven particle morphology with clumped distributions in a uniform nanoscale dimension that indicated consistent crystal development within the bacteria. Woven HA is typically found in bone structure, as well as in fractures and pathological situations, and it represents the first bone type to form during initial bone formation (32). Previous research has suggested the necessity of nanoscale HA for the human bone tissue surface and textural suitability for defective bone replacement (37). The presence of typical chemical groups of standard HA in the synthesised nano-HA, as confirmed by FTIR spectra, corroborate this characterisation (32-34). *B. coagulans*, a potential probiotic, has the capability to consume insoluble phosphate and calcium from the culture medium to synthesise HA crystals. This was evidenced by the identification of the purified powder from grown bacteria on PVKU medium. The formation of calcite and HA nanocrystals were reported previously in pathogenic bacteria and a limited number of non-pathogenic bacteria (21, 31).

Studies conducted on MG-63 cell cultures provided evidence that support the effectiveness of probiotics and HA. The results of these studies have shown that when probiotics were administered to MG-63 cells, they underwent increased proliferation and differentiation, which suggested their commitment to osteoblasts. MG-63 cells are commonly used as a model to study the viability, adhesion, and proliferation of bone cells. Moreover, the literature confirms that the MG-63 cell line maintains a stable phenotype and closely resembles human MSCs (20). This resemblance has significantly contributed to the widespread use of MG-63 cells in evaluating the compatibility of biomaterials intended for orthopaedic purposes and exploring bone metabolism that concerns osteoblast-like cells.

Recent studies have shown that debris from *Bacillus* sp. is not toxic to stem cells, while exhibiting inhibitory effects on cancerous cells (38). The surfactin production of *Bacillus* species, which was reported to stimulate cell proliferation and differentiation in some studies, was also noteworthy. It enhanced the production of hypoxia-inducible factor-1 α and vascular endothelial growth factor, increased the movement of keratinocytes through the mitogen-activated protein kinase, Wnt/ β -catenin pathway and nuclear factor- κ B signalling pathways, and controlled the release of inflammatory cytokines and the change in macrophage phenotype (23). Given that the PVKUS and MG-63 stimulated greater proliferation in SHED in this investigation, it became clear that the HA synthesised from bacteria impacted cell multiplication in a way not reported in previous studies. Nano-HA

acts as a catalyst for bone formation by promoting the differentiation and activity of osteoblasts through the provision of sufficient calcium and phosphate in the vicinity of SHED, thereby facilitating bone regeneration. Nano-HA, characterised by its small crystal size, creates higher levels of stress at the interface between cells and crystals compared to conventional flat-surfaced HA. The increased cell extension on the surface of nano-HA facilitates the exchange of calcium ions, which promotes the differentiation of MSC into osteoblasts. Furthermore, nano-HA can facilitate the attachment of specific cells that rely on surface adhesion by adsorbing extracellular matrix proteins such as fibronectin and growth factors like osteonectin (14, 39).

Morphological change serves as a marker of cell differentiation, as the cellular shape is a key factor in characterising and assessing cell quality (35). These morphological changes were consistent with previous research (40). While other studies investigating the osteogenic differentiation potential of stem cells have primarily employed cell-damaging techniques (such as staining, gene expression), assessing osteogenic potentiality using cellular morphology is a simple, direct, and non-invasive procedure. Several studies have revealed a relationship between osteogenic differentiation potentiality and cellular shape. Previous research has indicated that the stellate shape of stem cells is positively associated with the expression of osteogenic differentiation marker genes and the shape of osteocytes. It has been observed that cell geometry shows a significant correlation with the differentiation into osteogenic lineages (26, 35). Intracellular calcium deposits stained by alizarin red and the increase in ALP levels in cells during treatment with synthesised HA confirmed cell differentiation. Calcium deposits particularly found in bone tissues and ALP activity are significant indicators of early bone cell differentiation. These findings align with previous studies that used alizarin red staining to ascertain osteoblastic maturation and mineralisation (29). In recent studies, there has been a focus on exploring strategies that involve probiotic bacteria and their components to influence the proliferation and differentiation of MSCs. Additionally, it has been reported that HA can facilitate the differentiation of stem cells into osteogenic cells, which makes it a valuable component in tissue engineering. The present study successfully generated HA from probiotics, providing dual advantages in terms of its effects on stem cells and its potential application in tissue engineering (11, 12).

We propose a differentiation mechanism by probiotic and synthesised HA. Osteogenic differentiation is induced by adding probiotic debris as specific chemical inducers or growth factors to the culture medium. The chemical inducers initiate a cascade of signalling pathways such as the Wnt/ β -catenin pathway within the dental pulp stem cells. Activation of this pathway promotes the expression of genes related to osteogenesis. The activated signalling pathways stimulate the expression of genes associated

with osteogenic differentiation. These genes include transcription factors such as RUNX2, osterix, and bone morphogenetic proteins. The differentiated dental pulp stem cells, now known as osteocytes, begin to deposit synthesised bacterial HA. As the osteocytes continue to deposit the mineralised matrix, it gradually forms a network of bone tissue. Over time, the newly formed bone tissue undergoes maturation and remodelling, which involves the activity of osteoclasts and osteoblasts to maintain bone homeostasis. Some researchers have investigated differentiation through expression (27, 29) and others through assessment of enzymatic and phenotypic properties (25, 26). We also used the latter method in this work.

Conclusion

The results of this study demonstrated that neither probiotic debris nor bacterial HA showed any toxic effect on SHED; rather, they enhanced the proliferation rate of the stem cells. PVKUS induced osteogenic differentiation of the SHED, which was confirmed by MTT, ALP assay, alizarin red staining, and morphological observation. HA production by probiotic bacteria was confirmed by sintering the bacterial mass at 600°C to remove the organic matter, followed by analysis of the obtained powder by XRD, FTIR, and SEM. Probiotics are frequently used in cosmetics, sanitation, the food industry, nutritional supplements, and medicine, with proven benefits. The current research reveals a dual advantage of probiotics that produce HA nanoparticles. It has been demonstrated that *B. coagulans* could prevent and treat peri-implant diseases and oral-dental infections. Meanwhile, HA particles in sanitation, medicine, and food industries could be applied to repair bones and teeth. Thus, the direct usage of probiotics that produce HA is recommended for achieving both goals.

Acknowledgements

The authors wish to thank the University of Isfahan for financial support of this work. The authors declare that they have no conflict of interests.

Authors' Contributions


S.N.; Conceptualization, Methodology, Validation, Formal analysis, Investigation, and Writing - original draft. R.R.; Supervision, Resources, Writing - review and editing, Project administration, and Funding acquisition. G.E.; Conceptualization, Methodology, Supervision, and Resources. O.G., R.S.; Writing - review, editing, and validation. All authors read and approved the final submitted manuscript.

References

- Zhao R, Chen S, Zhao W, Yang L, Yuan B, Ioan VS, et al. A bioceramic scaffold composed of strontium-doped three-dimensional hydroxyapatite whiskers for enhanced bone regeneration in osteoporotic defects. *Theranostics*. 2020; 10(4): 1572-1589.
- Pillai S, Upadhyay A, Khayambashi P, Farooq I, Sabri H, Tarar M, et al. Dental 3D-printing: transferring art from the laboratories to the clinics. *Polymers (Basel)*. 2021; 13(1): 157-182.
- Fang J, Li P, Lu X, Fang L, Lü X, Ren F. A strong, tough, and osteoconductive hydroxyapatite mineralized polyacrylamide/dextran hydrogel for bone tissue regeneration. *Acta Biomater*. 2019; 88: 503-513.
- Shi H, Zhou Z, Li W, Fan Y, Li Z, Wei J. Hydroxyapatite based materials for bone tissue engineering: a brief and comprehensive introduction. *Crystals*. 2021; 11(2): 149-167.
- Sudradjat H, Meyer F, Loza K, Epple M, Enax J. In vivo effects of a hydroxyapatite-based oral care gel on the calcium and phosphorus levels of dental plaque. *Eur J Dent*. 2020; 14(02): 206-211.
- Babayevska N, Woźniak-Budych M, Litowczenko J, Peplińska B, Jarek M, Florczyk P, et al. Novel nanosystems to enhance biological activity of hydroxyapatite against dental caries. *Mater Sci Eng C Mater Biol Appl*. 2021; 124: 112062.
- Kantharia N, Naik S, Apte S, Kheur M, Kheur S, Kale B. Nano-hydroxyapatite and its contemporary applications. *J Dent Res Sci Dev*. 2014; 1(1): 15.
- Nouri S, Roghanian R, Emtiazi G. Review on biological synthesis of nano-hydroxyapatite and its application in nano-medicine. *Iran J Med Microbiol*. 2021; 15(4): 369-383.
- Aleixandre-Tudó JL, Castelló-Cogollos L, Aleixandre JL, Aleixandre-Benavent R. Tendencies and challenges in worldwide scientific research on probiotics. *Probiotics antimicrob proteins*. 2020; 12(3): 785-797.
- Behera J, Ison J, Voor MJ, Tyagi N. Probiotics stimulate bone formation in obese mice via histone methylations. *Theranostics*. 2021; 11(17): 8605-8623.
- Mendi A, Aktaş B, Aslım, B. Mesenchymal stem cell-probiotic communication: beneficial bacteria in preconditioning. In: Haider KH, ed. *Handbook of stem cell therapy*. Singapore: Springer Nature Singapore; 2022: 1-20.
- Yan Q, Cai L, Guo W. New advances in improving bone health based on specific gut microbiota. *Front Cell Infect Microbiol*. 2022; 12: 821429.
- Zaiss MM, Jones RM, Schett G, Pacifici R. The gut-bone axis: how bacterial metabolites bridge the distance. *J Clin Invest*. 2019; 129(8): 3018-3028.
- Karbalaie KH, Tanhaei S, Rabiee F, Kiani-Esfahani A, Masoudi NS, Nasr-Esfahani MH, et al. Stem cells from human exfoliated deciduous tooth exhibit stromal-derived inducing activity and lead to generation of neural crest cells from human embryonic stem cells. *Cell J*. 2021; 23(1): 140-142.
- Bhandi S, Alkahtani A, Mashyakh M, Abumelha AS, Albar NHM, Renugalakshmi A, et al. Effect of ascorbic acid on differentiation, secretome and stemness of stem cells from human exfoliated deciduous tooth (SHEDs). *J Pers Med*. 2021; 11(7): 589.
- Baghban EM, Bagheri F, Zandi M, Nejati E, Zomorodian E. Study of mesenchymal stem cell proliferation and bone differentiation on composite scaffolds of PLLA and nano hydroxyapatite with different morphologies. *Cell J*. 2011; 12(4): 469-476.
- Miura M, Gronthos S, Zhao M, Lu B, Fisher LW, Robey PG, et al. SHED: stem cells from human exfoliated deciduous teeth. *Proc Natl Acad Sci USA*. 2003; 100(10): 5807-5812.
- Hayashi Y, Kato H, Nonaka K, Nakanishi H. Stem cells from human exfoliated deciduous teeth attenuate mechanical allodynia in mice through distinct from the siglec-9/MCP-1-mediated tissue-repairing mechanism. *Sci rep*. 2021; 11(1): 20053.
- Blokhuis TJ, Arts JJ. Bioactive and osteoinductive bone graft substitutes: definitions, facts and myths. *Injury*. 2011; 42 Suppl 2: S26-S29.
- Mullick P, Das G, Aiyagari R. Probiotic bacteria cell surface-associated protein mineralized hydroxyapatite incorporated in porous scaffold: in vitro evaluation for bone cell growth and differentiation. *Mater Sci Eng C Mater Biol Appl*. 2021; 126: 112101.
- Nouri S, Roghanian R, Emtiazi G, Shafiei R. Biosynthesis of nanocalcite and nano-hydroxyapatite by the probiotic bacteria of bacillus subtilis and bacillus coagulans. *Appl Food Biotechnol*. 2022; 9(4): 275-286.
- Murugesan V, Vaiyapuri M, Murugesan A. Fabrication and characterization of strontium substituted chitosan modify hydroxyapatite for biomedical applications. *Inorg Chem Commun*. 2022; 142: 109653.
- Yan L, Liu G, Zhao B, Pang B, Wu W, Ai C, et al. Novel biomedical functions of surfactin A from *Bacillus subtilis* in wound healing promotion and scar inhibition. *J Agric Food Chem*. 2020; 68(26): 6987-6997.
- Cerci E, Erdost H. Phenotypic characterization and differentiation of mesenchymal stem cells originating from adipose tissue. *Turk J Vet Anim Sci*. 2019; 43(6): 834-845.

25. Tetè G, Capparè P, Gherlone E. New application of osteogenic differentiation from hiPS stem cells for evaluating the osteogenic potential of nanomaterials in dentistry. *Int J Environ Res Public Health*. 2020; 17(6): 1947.
26. KarbalaieMahdi A, Moridi K, Ghollasi M. Evaluation of osteogenic differentiation of human mesenchymal stem cells (hMSCs) on random and aligned polycaprolactone-polyaniline-gelatin scaffolds. *BiolImpacts*. 2023; 13(2): 123-132.
27. Su WT, Wu PS, Huang TY. Osteogenic differentiation of stem cells from human exfoliated deciduous teeth on poly (ϵ -caprolactone) nanofibers containing strontium phosphate. *Mater Sci Eng C Mater Biol Appl*. 2015; 46: 427-434.
28. Khorolsuren Z, Lang O, Pallinger E, Foldes A, Szabolcs GG, Varga G, et al. Functional and cell surface characteristics of periodontal ligament cells (PDLs) on RGD-synthetic polypeptide conjugate coatings. *J Periodontol Res*. 2020; 55(5): 713-723.
29. Hagar MN, Yazid F, Luchman NA, Ariffin SHZ, Wahab RMA. Comparative evaluation of osteogenic differentiation potential of stem cells derived from dental pulp and exfoliated deciduous teeth cultured over granular hydroxyapatite based scaffold. *BMC Oral Health*. 2021; 21(1): 263.
30. Adibpour N, Hosseinihezad M, Pahlevanlo A, Hussain MA. A review on *Bacillus coagulans* as a Spore-Forming Probiotic. *Appl Food Biotechnol*. 2019; 6(2): 91-100.
31. Ghashghaei S, Emtiazi G. Production of hydroxyapatite nanoparticles using tricalcium-phosphate by *alkalindiges illinoisensis*. *J Nanomater Mol Nanotechnol*. 2013; 2(5).
32. Esmailkhanian A, Sharifianjazi F, Abouchenari A, Rouhani A, Parvin N, Irani M. Synthesis and characterization of natural nano-hydroxyapatite derived from turkey femur-bone waste. *Appl Biochem Biotechnol*. 2019; 189(3): 919-932.
33. Elbasuney S. Green synthesis of hydroxyapatite nanoparticles with controlled morphologies and surface properties toward biomedical applications. *J Inorg Organomet Polym Mater*. 2020; 30(12): 899-906.
34. Núñez D, Elgueta EY, Varaprasad K, Oyarzún P. Hydroxyapatite nanocrystals synthesized from calcium rich bio-wastes. *Mater Lett*. 2018; 230: 64-68.
35. Kelly DJ, Jacobs CR. The role of mechanical signals in regulating chondrogenesis and osteogenesis of mesenchymal stem cells. *Birth Defects Res C Embryo Today*. 2010; 90(1): 75-85.
36. Escobar LM, Bendahan Z, Bayona A, Castellanos JE, González MC. Effect of vitamins D and E on the proliferation, viability, and differentiation of human dental pulp stem cells: an in vitro study. *Int J Dent*. 2020; 2020: 8860840.
37. Armiento AR, Hatt LP, Sanchez Rosenberg G, Thompson K, Stoddart MJ. Functional biomaterials for bone regeneration: a lesson in complex biology. *Adv Funct Mater*. 2020; 30(44): 1909874.
38. Asadi S, Soleimani N. Anticancer effect of fractions from *staphylococcus aureus* and *bacillus atrophaeus* on the proliferation and death of human breast cancer cell line (MCF-7). *Int J Enteric Pathog*. 2020; 8(4): 116-121.
39. Liang W, Ding P, Li G, Lu E, Zhao Z. Hydroxyapatite nanoparticles facilitate osteoblast differentiation and bone formation within sagittal suture during expansion in rats. *Drug Des Devel Ther*. 2021; 15: 905-917.
40. Wang X, Li G, Liu Y, Yu W, Sun Q. Biocompatibility of biological material polylactic acid with stem cells from human exfoliated deciduous teeth. *Biomed Rep*. 2017; 6(5): 519-524.

Adipose Tissue-Derived Mesenchymal Stem Cells Alter Metabolites of Brain Cholesterol Homeostasis in An Alzheimer's Model

Mehrnaz Karimi Darabi, Ph.D.^{1,2,3}, Zahra Nazeri, M.Sc.^{1,2,3}, Arash Rafeinia, Ph.D.⁴, Seyedeh Pardis Pezeshki, M.Sc.^{1,2,3}, Alireza Kheirollah, Ph.D.^{1,2,5}, Yaghoob Farbood, Ph.D.^{6,7}, Maryam Adelipour, Ph.D.¹, Shirin Azizidoost, Ph.D.⁸, Maryam Cheraghzadeh, Ph.D.^{1,2*} 

1. Department of Clinical Biochemistry, Faculty of Medicine, Ahvaz Jundishapur University of Medical Sciences, Ahvaz, Iran
2. Cellular and Molecular Research Center, Medical Basic Science Research Institute, Ahvaz Jundishapur University of Medical Sciences, Ahvaz, Iran
3. Student Research Committee, Ahvaz Jundishapur University of Medical Sciences, Ahvaz, Iran
4. Sirjan School of Medical Sciences, Sirjan, Iran
5. Surgery Department, Geisel School of Medicine at Dartmouth, Hanover, NH, United States
6. Department of Physiology, Faculty of Medicine, Ahvaz Jundishapur University of Medical Sciences, Ahvaz, Iran
7. Persian Gulf Physiology Research Centre, Basic Medical Sciences Research Institute, Ahvaz Jundishapur University of Medical Sciences, Ahvaz, Iran
8. Atherosclerosis Research Centre, Ahvaz Jundishapur University of Medical Sciences, Ahvaz, Iran

Abstract

Objective: Disruption of cholesterol homeostasis in Alzheimer's disease (AD) plays a crucial role in disease pathogenesis, making it a potential therapeutic target. Mesenchymal stem cells (MSCs) show promise in treating cognitive impairment and provide a novel therapeutic approach. This study aims to investigate the effects of MSCs on specific metabolites associated with brain cholesterol homeostasis in an AD rat model.

Materials and Methods: In this experimental study, animals were divided into three groups: control, AD, and AD+MSCs. AD was induced using amyloid beta (A β) and confirmed through the Morris water maze (MWM) behavioural test and Congo red staining. MSCs were extracted, characterised via flow cytometry, subjected to osteoblast and adipose differentiation, and injected intraventricularly. The cholesterol metabolite levels were measured using gas chromatography-mass spectrometry (GC)-MS and compared among the groups.

Results: Treatment with MSCs significantly improved memory function in the AD+MSCs group compared to the AD group and the number of beta-amyloid plaques decreased according to histological assessment. Disturbances in the brain cholesterol metabolites that included desmosterol, 7-dehydrocholesterol, 24S-hydroxycholesterol, 27-hydroxycholesterol and cholesterol were observed in the AD group compared to the control group. Treatment with MSCs resulted in significant alterations in the levels of these metabolites.

Conclusion: The findings indicate that MSC therapy has the potential to improve AD by modulating brain cholesterol homeostasis and promoting the differentiation of stem cells into nerve cells. The results emphasize the importance of investigating the role of cholesterol metabolites in the context of MSC therapy to gain deeper insights into underlying mechanisms of the therapeutic efficacy of MSCs in AD.

Keywords: Alzheimer's Disease, Desmosterol, 7-Dehydrocholesterol, 24-Hydroxycholesterol, 27-Hydroxycholesterol

Citation: Karimi Darabi M, Nazeri Z, Rafeinia A, Pezeshki SP, Kheirollah A, Farbood Y, Adelipour M, Azizidoost Sh, Cheraghzadeh M. Adipose tissue-derived mesenchymal stem cells alter metabolites of brain cholesterol homeostasis in an alzheimer's model. Cell J. 2023; 25(11): 764-771. doi: 10.22074/CELLJ.2023.1999622.1272

This open-access article has been published under the terms of the Creative Commons Attribution Non-Commercial 3.0 (CC BY-NC 3.0).

Introduction

Alzheimer's disease (AD) is a devastating disease of the nervous system (1), and a disruption in cholesterol homeostasis plays a role in its development. Although the brain comprises approximately 2% of the body's total weight, it contains approximately 25% of the body's cholesterol. This fact highlights the crucial role of cholesterol in the brain. Brain cholesterol is essential for numerous functions, including synapse formation and nerve signal transmission (2). Cholesterol homeostasis

is critical for the normal functioning of nerve cells (3), and its disturbance is considered a risk factor for the development of AD. Therefore, brain cholesterol homeostasis is preserved via a precise regulatory process that involves cholesterol biosynthesis and the elimination of its metabolites (4).

Brain tissue cholesterol is produced in neurons and astrocytes by two separate pathways, namely Kandutsch-Russell and Bloch (Fig.1). Defects in either of these

Received: 06/April/2023, Revised: 05/August/2023, Accepted: 13/August/2023

*Corresponding Address: P.O.Box: 6135715794, Department of Clinical Biochemistry, Faculty of Medicine, Ahvaz Jundishapur University of Medical Sciences, Ahvaz, Iran

Email: cheraghzade_m@ajums.ac.ir



Royan Institute
Cell Journal (Yakhteh)

pathways cause serious damage to the nervous system (3). The precursors of cholesterol in the Kandutsch-Russell and Bloch pathways are 7-dehydrocholesterol and desmosterol, respectively, which are synthesized by the enzymes 7-dehydrocholesterol reductase (DHCR7) and 24-dehydrocholesterol reductase (DHCR24) (5). Excess cholesterol in neurons and astrocytes is converted into more polar metabolites known as oxysterols, which are excreted into the circulation through the blood-brain barrier (BBB). Oxysterols are key signalling compounds for brain function, and it is believed that cholesterol may perform part of its function in the brain through these metabolites (6). One of these compounds is 24-hydroxycholesterol, which is generated in neurons from excess cholesterol by the enzyme 24-hydroxylase (CYP46A1) (7). By binding to liver X (LX) receptors, 24-hydroxycholesterol induces the expressions of *APOE* and *ABCA1* genes, thereby regulating the influx of cholesterol from astrocytes to neurons. Another important oxysterol is 27-hydroxycholesterol, which is produced by the enzyme 27-hydroxylase (*CYP27A1*), and can activate LX receptors (2). It seems that the pathway of cholesterol homeostasis changes during the formation of amyloid beta ($A\beta$) plaques and

other mechanisms of AD, and it is significant in the development of this disease. This pathway might also play a role in AD pathogenesis and can be a consequence of neurodegeneration (8). Thus, considering the importance of maintaining cholesterol homeostasis, this pathway can be considered a therapeutic target for AD treatment.

To date, a definitive treatment for AD remains elusive, and available medications only serve to slow disease progression and alleviate symptoms (9). In recent years, stem cell therapy has emerged as a promising research methodology. Stem cells are believed to exert their therapeutic effects by migrating to the site of injury where they differentiate into specific cell types and establish vital connections and synapses (10). There is a growing interest in utilising stem cells to treat central nervous system disorders. The significance of cholesterol homeostasis, particularly specific cholesterol metabolites like 24-hydroxycholesterol, plays a crucial role in memory and learning. Therefore, the objective of this study is to investigate the impact of adipose tissue-derived mesenchymal stem cells (MSCs) on the levels of various metabolites involved in the cholesterol homeostasis pathway in the brain tissue of an animal model of AD.

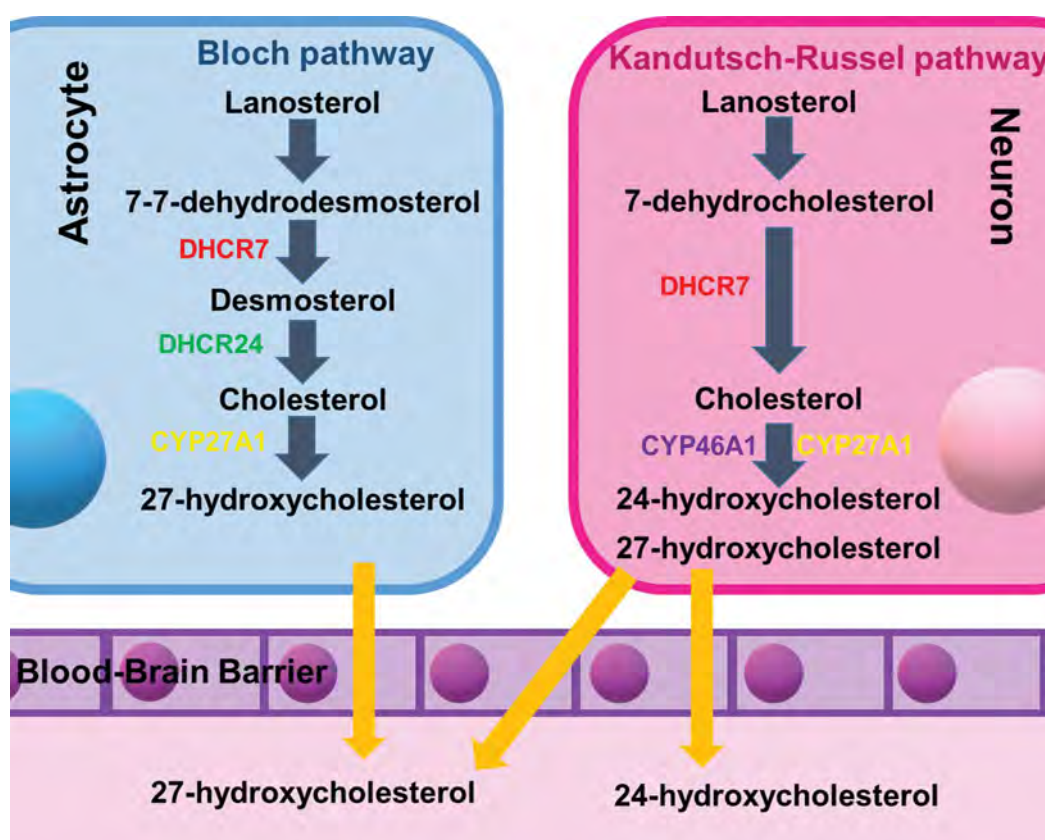


Fig.1: Pathway of cholesterol synthesis and oxysterol formation in neurons and astrocytes. DHCR7; 7-dehydrocholesterol reductase and DHCR24: 24-dehydrocholesterol reductase.

Materials and Methods

Animals

In this experimental study, 24 male Wistar rats that weighed 250-300 g were acquired from the Animal Centre of Ahvaz Jundishapur University of Medical Sciences (Ahvaz, Iran). The animals were kept at 21-25°C with controlled humidity and a 12/12 hour light/dark cycle with lights on at 7:00 AM as well as unlimited access to food and water. All animal procedures were carried out according to the guidelines of the Ethics Committee and the Centre of Research on Laboratory Animals at Ahvaz University of Medical Sciences, Ahvaz, Iran (IR.AJUMS.ABHC.REC.1400.106). The animals were divided into three groups: i. The control group (n=8) received a single bilateral intrahippocampal (I.H.P.) injection of 5 µl sterile phosphate-buffered saline (PBS), ii. The AD group (n=8) received 5 µM/µL/rat Aβ bilateral I.H.P., and iii. The AD+MSCs group (n=8) received a single bilateral intraventricular injection of 1×10⁶ MSCs, 30 days after the stereotaxic injection of Aβ.

Preparation of synthetic amyloid beta oligomers

The Aβ 1-42 peptide was activated with PBS. Briefly, Aβ1-42 was dissolved in PBS and stored at -70°C. For the aggregation protocol, sterile PBS was added to bring the peptide to a final concentration of 1 µg/µL, and then incubated for five days at 37°C.

Stereotaxic surgery

The animals were first anaesthetised by an intraperitoneal injection of ketamine/xylazine (90:10 mg/kg), and their heads were shaved and fixed in a stereotaxic apparatus. For the control group, we used a 10-µL Hamilton syringe to inject 5 µl PBS and bilateral injections of 5 µl Aβ (2.5 µL per side at a rate of about 1 µL/minutes) into the hippocampus of the CA1 region at the coordinates of AP=-4.3, ML= ± 2.4, and DV=-2.6 mm (Paxinos and Watson stereotaxic rat brain atlas) (11). For the AD+MSCs group, the animals were first treated with Aβ to induce Alzheimer's, and then 1×10⁶ MSCs (12) dissolved in PBS was injected intraventricularly at the coordinates of AP=-1.2, ML= ± 2, and DV=-3.8 (11).

Isolation of adipose tissue-derived mesenchymal stem cells

The animals were first anaesthetised with ketamine/xylazine, and the epididymal fat tissues of the animals were isolated. All of the isolation stages were performed under sterile conditions. The minced tissues were transferred to sterile falcon tubes that contained 1% penicillin/streptomycin (pen/strep) dissolved in PBS and subsequently washed to eliminate red blood cells and connective tissue. Next, 1 mg/mL of collagenase - was added, and the samples were placed in a shaking incubator at 37°C for 40 minutes. Afterwards, they were centrifuged for 15 minutes at 1500 rpm and the final sediment was incubated with Dulbecco's modified eagle medium, 10%

FBS, 1% pen/strep, and 1% amphotericin in a culture flask at 37°C, 5% CO₂, and 95% humidity. The medium was changed every three days (13).

Cell characterisation

Flow cytometry

Passage-3 cells were assessed by flow cytometry. For this purpose, we used conjugated antibodies anti-mouse-CD44-FITC and anti-mouse-CD90-FITC (stem cell markers), and anti-mouse-CD34-RPE and anti-mouse-CD45-RPE (hematopoietic markers) with a negative control (Denmark, Glostrup, Corporation Dako). The data were analysed by FlowJo software (version 7.6.1, FlowJo, LLC, Ashland, Oregon, United States).

Osteoblast and adipose differentiation

Passage-3 mesenchymal cells were grown in osteogenic differentiation medium (10 mM Beta glycerol phosphate, 7-10 mM dexamethasone, 10% FBS, 50 µg/mL ascorbic acid bi-phosphate, 1% pen/strep-amphotericin B) and adipogenic differentiation medium [66 nM insulin, 0.5 mM 3-isobutyl-1-methylxanthine (IBMX), 0.2 mM indomethacin, 7-10 mM dexamethasone, 10% FBS, and 1% pen/strep-amphotericin B]. The cells were incubated at 37°C and 5% CO₂ for 21 days and the medium was replaced every two days. Alizarin red and oil red O staining were conducted to confirm differentiation into osteoblasts and adipocytes, respectively (13).

Morris water maze behavioural assessment

This test is used to assess memory and spatial learning in rats. In the morris water maze (MWM) test, a round metal tank with a black wall that is 120-200 cm in diameter and 70 cm in height is filled with water to a depth of 60 cm with an optimal water temperature of 25 ± 2°C. An invisible platform with a diameter of 12 cm is positioned at a distance of 1 to 5 cm below the water surface in the centre of one of the four quadrants (northeast, southeast, northwest, or southwest). The movement and behaviour of the animals is tracked and controlled by an infrared camera placed at a height of 2 m above the central area of the tank. The animals were examined for five consecutive days. This experiment was conducted 30 days after the Aβ injection for the AD group and at 30, 60, and 90 days after the MSC injection for the AD+MSC group. During the first four days, the animal's learning process was measured based on the time spent and the distance travelled to find the hidden platform. Accordingly, each animal was randomly placed in a quadrant for 60 seconds to find the hidden escape platform and then given a 30 second rest until the next trial. On the fifth day, a probe phase was performed in order to assess the animal's memory performance. The hidden platform was removed and the percentage of time spent in the goal quadrant during a single trial, the location of the platform, and the distance moved in this quadrant were determined as the standard measure of memory (14).

Extraction of brain tissue

Each animal was anaesthetised using a combination of ketamine/xylazine, and then pinched to assess the level of anaesthesia. Next, the rat was perfused with PBS, decapitated by a specialized guillotine, and then the brain was extracted. Part of the tissue was fixed with 10% formaldehyde to prepare a slide and stained with Congo red dye to confirm formation of the A β plaques. The remainder of the tissue was collected in cryotubes and stored at -70°C.

Congo red staining

In order to detect the amyloid deposits, the prepared brain sections were subjected to Congo red staining according to the manufacturer's protocol (Commercial kit, Fartest). A light transmitter was used to detect the presence of amyloid plaques, which were observed as a pink to red colour.

Measurement of cholesterol metabolites

First, the lipid content of the brain tissue was extracted. Then, the cholesterol metabolites desmosterol, 7-dehydrocholesterol, 24-hydroxycholesterol, and 27-hydroxycholesterol were measured using a chromatograph (model 6890) coupled with a mass spectrometer (model 5973N, Agilent, America) and an HP-5MS capillary column with a stationary phase of 5% methylphenylsiloxane (length: 30 m, inner diameter: 0.25 mm, thickness of the stationary layer: 0.25 μ m) and ionisation energy of 70 eV. Briefly, 25 mg of brain tissue was homogenized with 88% methanol that contained 0.01% butylated hydroxytoluene at a temperature of 4°C using a homogenizer (Heidolph, Germany), then 100 μ L of methanol and 250 μ L of 1 M NaOH were added and the mixture was incubated for 16 hours at room temperature in the absence of light for hydrolysis. The samples were acidified with 1 M formic acid, followed by the addition of distilled water. In order to extract the solid phase, solid phase extraction columns (GL Sciences, USA) were prepared with methanol and 40 mM formic acid. The sample that contained sterol and oxysterol was removed from the column by hexane and hexane/methyl tert-butyl ether and dried at 37°C under N₂ gas flow, and then prepared in toluene for mass spectrometry (MS) analysis.

Statistical analysis

The results of all the analyses are expressed as mean \pm standard error of the mean (SEM) for continuous variables. Differences between the three groups were determined using a one-way ANOVA test in GraphPad Prism software, version 6 (Dotmatics, California). The level of significance was considered to be $P < 0.05$.

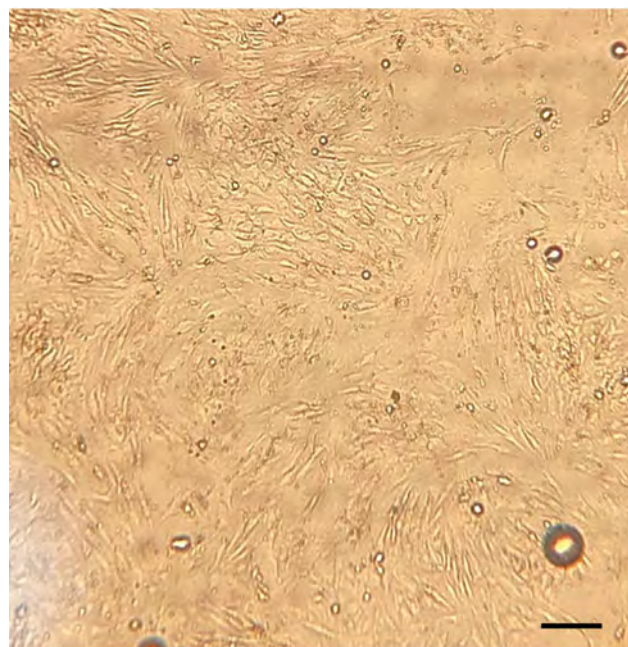
Results

Characteristics of mesenchymal stem cells

In the initial culture, adipose-derived MSCs with

a fibroblast-like or spindle-shaped appearance with distinct nuclei were grown, which were observed by light microscopy (Fig.2).

A



B

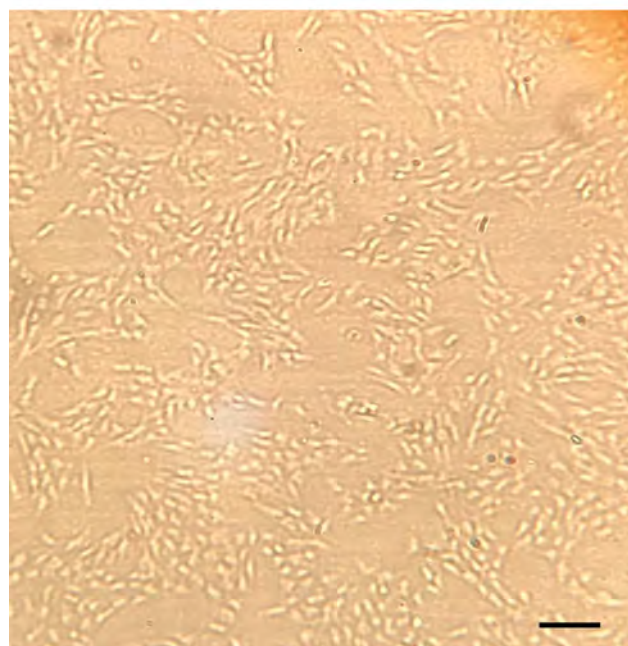


Fig.2: Isolation of MSCs from adipose tissue. MSCs culture. **A.** Primary stage. **B.** First passage (scale bar: 100 μ m). MSC; Mesenchymal stem cells.

Flow cytometry

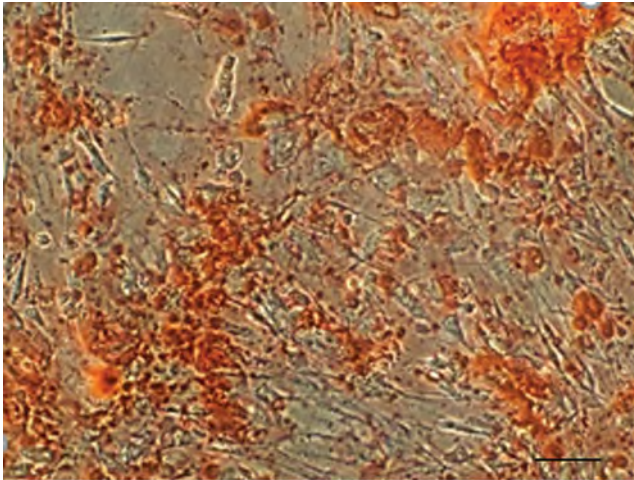
MSCs extracted from adipose tissue expressed CD44 (98.98%) and CD90 (94.34%), which are stem markers for these cells. The hematopoietic markers, CD34 (0.13%) and CD45 (0.43%), had very low expression (Fig.S1, See

Supplementary Online Information at www.celljournal.org.

Differentiation of mesenchymal stem cells into osteocytes and adipocytes

Figure 3 shows that the multipotent adipose MSCs differentiated into osteocytes and adipocytes.

A



B

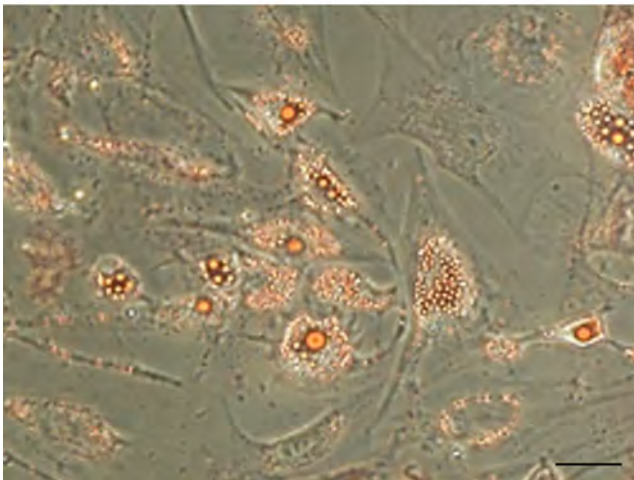


Fig.3: Differentiation of adipose mesenchymal stem cells (MSCs) into adipocytes and osteoblasts. **A.** Osteoblasts stained with alizarin red (scale bar: 100 μ m). **B.** Adipocytes stained with oil red O (scale bar: 50 μ m).

Spatial learning and memory in the Morris water maze test

Spatial memory of animals from all three groups was examined four weeks after the A β injection. In the probe trial, the AD group had a significantly less percentage of time spent in the target quadrant than the control and AD+MSC groups ($P=0.0001$), which indicated impaired spatial learning and memory. This scale showed a significant increase in the AD+MSC group compared to the AD group ($P=0.0001$, Fig.4). There was no difference in swimming speed between all of the studied groups.

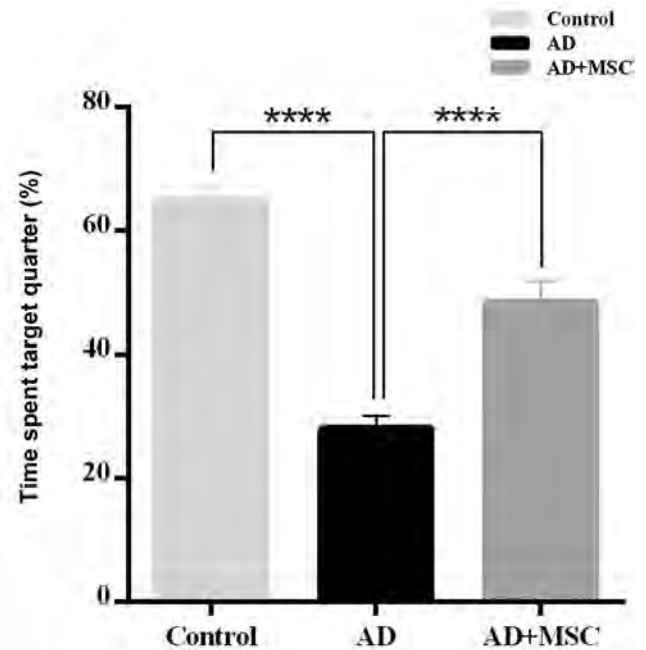


Fig.4: MWM behavioural test diagram shows the effect of A β and MSCs on spatial memory of animals from all three groups. The AD group shows a significant reduction in the percentage time spent in the target quadrant in the probe trial ($P=0.0001$). There is a significant increase in the AD+MSC group compared to the AD group ($P=0.0001$). MWM; Morris water maze, A β ; Amyloid beta, MSC; Mesenchymal stem cell, AD; Alzheimer's disease, and ****; $P<0.0001$.

Histology

Sections from the animals' brains were stained with Congo red to detect the A β plaques. This dye has a high affinity for binding to insoluble A β plaques. In the control group (Fig.5A), no amyloid plaque was observed, while, Figure 5B shows the presence of these plaques in the brain slices of the animals 30 days after the A β injection. The number of these plaques in the AD+MSC group was significantly reduced 90 days after administration of the MSCs (Fig.5C).

Gas chromatography-mass spectrometry

Desmosterol, which is the precursor of cholesterol synthesis in astrocytes, was significantly increased in the AD group compared to the control group ($P=0.0001$), while the level of this metabolite in the AD+MSC group showed a significant reduction compared to the AD group ($P=0.0001$, Fig.6A). In this regard, the measurement of 7-dehydrocholesterol, which is the precursor of cholesterol in the Kandutsch-Russell pathway in neurons, was similar to the results observed with desmosterol (Fig.6B). A significant increase in cholesterol was observed in the AD group compared to both the control and AD+MSC groups ($P=0.0001$, Fig.6C). Metabolite 24-hydroxycholesterol, a by-product of the Bloch pathway in astrocytes, was significantly decreased in the AD group compared

to the control group ($P=0.0001$), but significantly increased in the AD+MSC group compared to the AD group ($P=0.0001$, Fig.6D). The observed results

with 27-hydroxycholesterol, a by-product of the Kandutsch-Russell pathway, were similar to those of 24-hydroxycholesterol (Fig.6E).

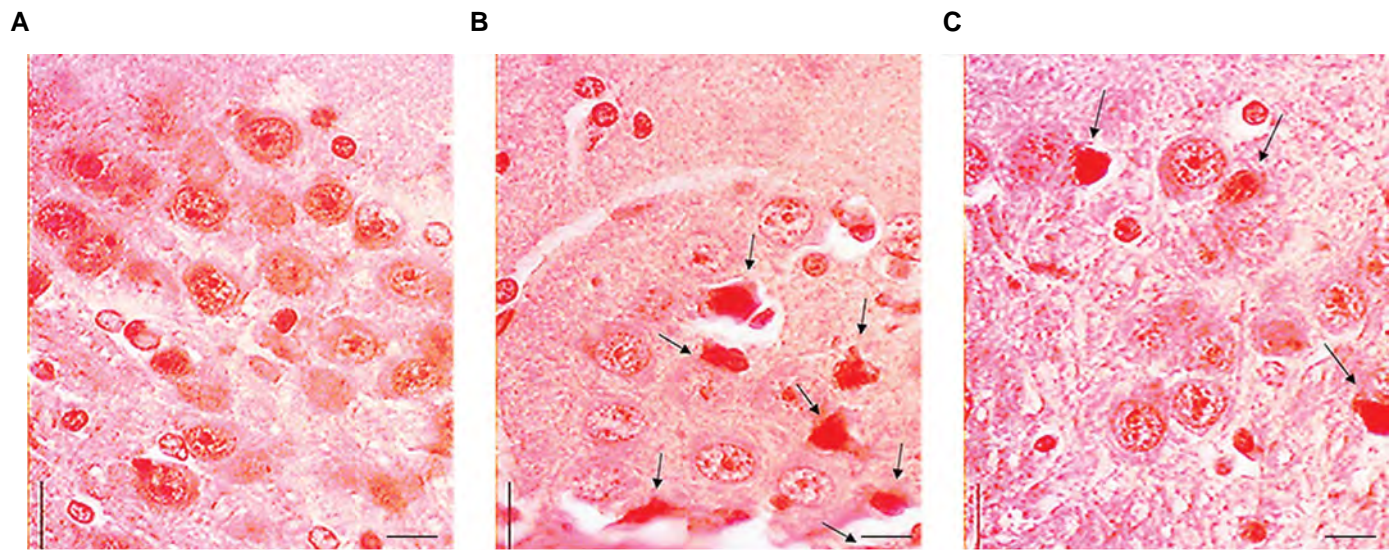


Fig.5: Congo red staining of the brain tissues. **A.** Control group, **B.** AD group, and **C.** AD+MSC group (scale bar: 20.0 μm). Black arrow shows $\text{A}\beta$. AD; Alzheimer's disease, MSCs; Mesenchymal stem cells, and $\text{A}\beta$; Amyloid beta.

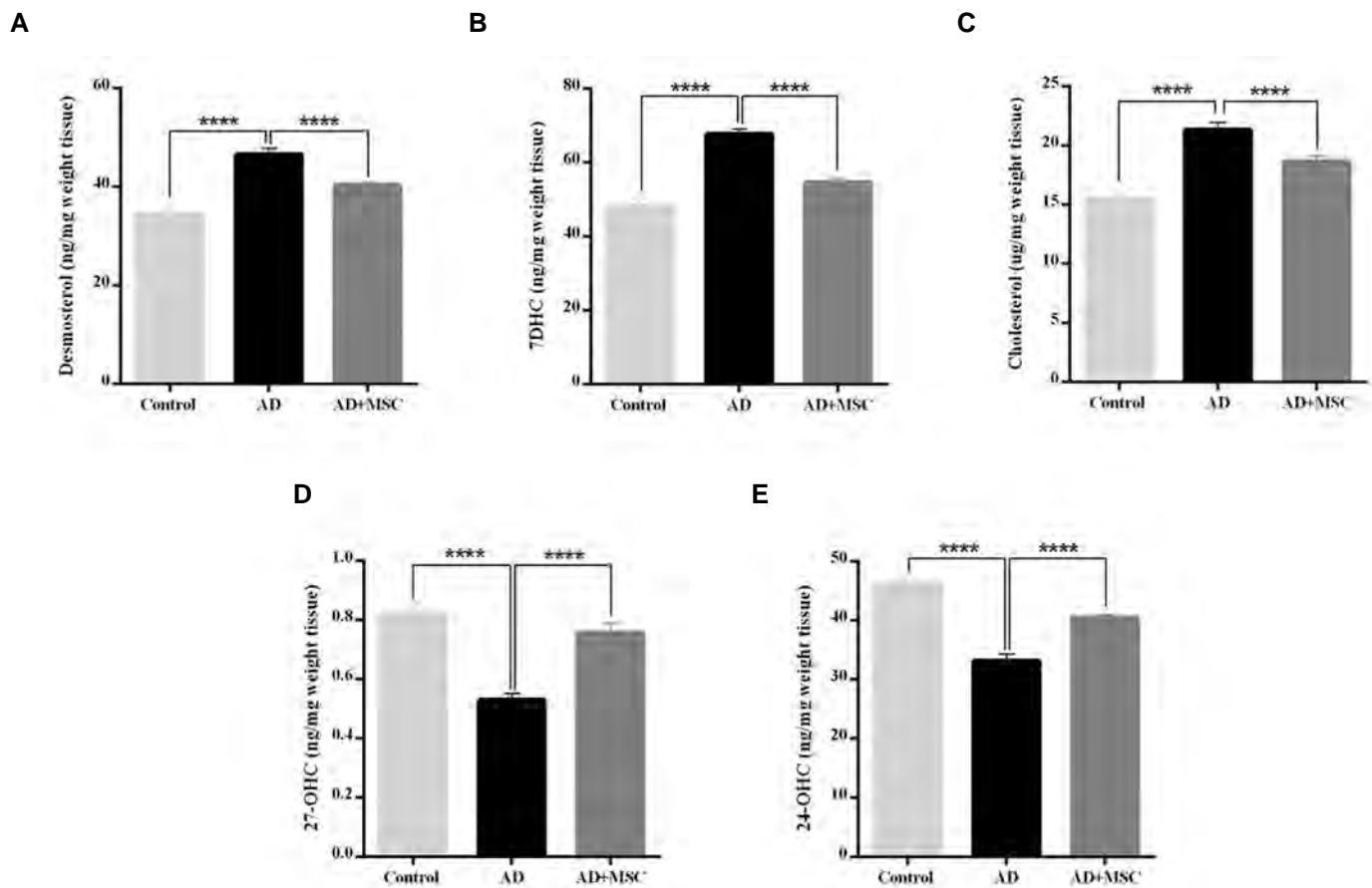


Fig.6: Measurement of cholesterol homeostasis pathway metabolites by GC-MS in the control, AD, and AD+MSC groups. **A.** Desmosterol, **B.** 7-dehydrocholesterol, **C.** Cholesterol, **D.** 24-hydroxycholesterol, and **E.** 27-hydroxycholesterol. AD; Alzheimer's disease, MSCs; Mesenchymal stem cells, GC-MS; Gas chromatography-mass spectrometry, and ****; $P \leq 0.0001$.

Discussion

AD is the most prevalent dementia in the elderly (15), and its main features are formation of amyloid plaques outside the cell and phosphorylated tau proteins inside the cell (1). The results of the current study indicate that an injection of MSCs into the Alzheimer's animal model leads to the improvement in memory, a change in the amount of A β plaques in the brains of the group that received the MSCs compared to the AD group, and significant modification in cholesterol homeostasis in the AD+MSC group compared to the AD group.

According to numerous studies on the relationship between cholesterol homeostasis and AD, disruption in the regulation of cholesterol homeostasis might reflect the basic features of AD pathogenesis, and therefore the cholesterol content of brain tissue in the AD group differs from the control group (8). In this regard, the results of our study also revealed a 38% rise in the cholesterol content in the tissue from the AD group. Potential reasons for the cholesterol increase in Alzheimer's brain tissue include the destruction of neurons, the breakdown of the plasma membrane, and the deterioration of myelin (16). Evidence has shown that the destruction of myelin leads to the release of cholesterol into the cerebrospinal fluid and extracellular space, which ultimately results in the death of nerve cells (17). On the other hand, *in vitro* studies have demonstrated that this excess cholesterol also leads to an increase in the production of A β in the brain tissue, and subsequently, these A β plaques cause extensive neuronal loss, the breakdown of myelin, and the release of excess cholesterol in the extracellular space (18). Following the injection of MSCs, the level of cholesterol in the AD+MSC group significantly decreased by 12.6% compared to the AD group. The possible mechanism is the differentiation of multipotent MSCs into various types of nerve cells, including glial cells and neurons, which can help regulate cholesterol levels by secreting a variety of beneficial cytokines and neurotrophic factors (19).

Cholesterol is synthesised *de novo* in astrocytes and neurons from a series of precursors and converted into a series of more polar metabolites to exit the brain through the BBB (20). Cholesterol is produced in astrocytes through the Bloch pathway from the 27-carbon precursor desmosterol by the enzyme DHCR24. In the current study, the level of desmosterol precursor in the AD group significantly increased by 35% compared to the control group, which is likely due to the disruption or decrease in the expression of the DHCR24 enzyme caused by the pathogenesis of AD (21).

Contrary to our results, Mohhammad et al. (4) showed a reduction in the level of desmosterol in patients compared to a control group, which prompted the speculation that other factors might also play a role in regulating desmosterol levels. One of these factors is the hormone progesterone, which inhibits cholesterol synthesis in the stage between lanosterol and cholesterol (22). However, it is hypothesised that the decrease in the level of this metabolite correlates

with AD progression, which is marked by the loss of more neurons (23). Similarly, 7-dehydrocholesterol is a precursor of cholesterol synthesis in the Kandutsch-Russell pathway, and according to the results, this metabolite showed a significant increase of 41% in the AD group compared to the control group. This increase is probably due to the decrease in the gene expression of the 7-dehydrocholesterol reductase enzyme, which converts 7-dehydrocholesterol to cholesterol (24). Disturbances in these two pathways may lead to the replacement of cholesterol by its precursors in the brain, which causes serious disorders in the nervous system (25). Similar to cholesterol, these precursors can bind to the SREBP cleavage-activating protein (SCAP) and alter its conformation, which in turn changes the level of cholesterol synthesis (2). This finding might justify the increase in cholesterol levels in the AD group compared to the control group. In this study, the injection of stem cells in the AD+MSC group significantly decreased the level of desmosterol and 7-dehydrocholesterol compared to the AD group, which supported the other findings of this study and indicated the positive effect of these cells on various aspects of this disease.

No pathway exists to destroy cholesterol in the brain; therefore, excess cholesterol is converted into 24-hydroxycholesterol and 27-hydroxycholesterol by the enzymes CYP46A1 and CYP27A1, respectively, and enters the bloodstream through the BBB (26). CYP46A1 activity and 24-hydroxycholesterol are not only necessary for memory processing but can also reduce A β levels (27). Research has shown that the presence of amyloid plaques and nerve cell destruction appeared to impair the activity of cholesterol-hydroxylating enzymes, and resulted in a 30% reduction in the level of metabolites in the brain tissue of Alzheimer's patients compared to a control group (28). In the AD+MSC group, the level of these byproducts significantly increased by 25% compared to the AD group after the injection of the MSCs. This finding is in line with the role of these metabolites and the enzymes that produce them in improving memory and reducing the level of A β . The results of the present study showed that not only the number of plaques in this group reduced, but memory and learning also improved significantly.

Numerous studies have shown that MSCs can differentiate into various types of nerve cells and can be a suitable option for cell therapy purposes in neurodegenerative diseases (29). The paracrine effects of MSCs, including the production of growth factors and anti-inflammatory cytokines, lead to nerve regeneration and myelination. MSCs likely exert phagocytic effects on abnormal A β plaques as well as anti-inflammatory effects in the AD brain via microglia, prevention of neuronal death, and enhancement of neuronal differentiation (12). Since the disorders of the cholesterol homeostasis pathway and the reduction or lack of activity of the enzymes in this pathway are more related to the loss of nerve cells, it is possible that replacing nerve cells with differentiated MSCs will cause a slight improvement in these defects,

and result in enhanced memory and a reduction in the amount of A β plaques in the animal's brain tissues.

Conclusion

Our research findings provide compelling evidence that MSC therapy has the potential benefit for improving various aspects of AD neuropathogenesis. We observed positive outcomes, including the recovery of memory function, reduced numbers of A β plaques, and modulation of cholesterol homeostasis in an animal model of AD. These results highlight the promising prospects of MSC therapy as a viable therapeutic approach for AD. Furthermore, targeting cholesterol homeostasis through MSC-based interventions may open a novel way for AD treatment. Further investigations are necessary to comprehensively understand the underlying mechanisms and optimise the therapeutic potential of MSCs in the context of AD.

Acknowledgements

We are grateful to all of our colleagues in the Cellular and Molecular Research Centre of Ahvaz Jundishapur University of Medical Sciences. This work was financially supported by the Vice Chancellor for Research Affairs, Cellular and Molecular Research Centre, Medical Basic Sciences Research Institute, Ahvaz Jundishapur University of Medical Sciences, Ahvaz, Iran [grant numbers: CMRC-0059] and is a part of a PhD thesis. All authors declare that there is no conflict of interest.



Authors' Contributions

M.Ch., A.Kh., Z.N., Y.F.; Conceptualisation, Methodology, and Software. M.K.D., S.P.P.; Data curation, Conducting experiments, Writing - Original draft preparation, and Supervision. Sh.A., M.A.; Visualisation and Investigation. A.R.; Software and Validation. M.Ch., M.K.D.: Writing- Reviewing and Editing. All authors read and approved the final manuscript.

References

- Borràs C, Mercer A, Sirisi S, Alcolea D, Escolà-Gil JC, Blanco-Vaca F, et al. HDL-like-mediated cell cholesterol trafficking in the central nervous system and Alzheimer's disease pathogenesis. *Int J Mol Sci.* 2022; 23(16): 9356.
- Petrov AM, Kasimov MR, Zefirov AL. Brain cholesterol metabolism and its defects: linkage to neurodegenerative diseases and synaptic dysfunction. *Acta Naturae.* 2016; 8(1): 58-73.
- Zhang J, Liu Q. Cholesterol metabolism and homeostasis in the brain. *Protein Cell.* 2015; 6(4): 254-264.
- Mohamed A, Smith K, de Chaves E. The mevalonate pathway in Alzheimer's disease—cholesterol and non-sterol isoprenoids. In: Zerr I, ed. *Alzheimer's disease-challenges for the future.* Canada: IntechOpen; 2015; 167-222.
- Luu W, Hart-Smith G, Sharpe LJ, Brown AJ. The terminal enzymes of cholesterol synthesis, DHCR24 and DHCR7, interact physically and functionally. *J Lipid Res.* 2015; 56(4): 888-897.
- Weigel TK, Kulas JA, Ferris HA. Oxidized cholesterol species as signaling molecules in the brain: diabetes and Alzheimer's disease. *Neuronal Signal.* 2019; 3(4): NS20190068.
- Petrov AM, Pikuleva IA. Cholesterol 24-Hydroxylation by CYP46A1: benefits of modulation for brain diseases. *Neurotherapeutics.* 2019; 16(3): 635-648.
- Varma VR, Büşra Lülecı H, Oommen AM, Varma S, Blackshear CT, Griswold ME, et al. Abnormal brain cholesterol homeostasis in Alzheimer's disease—a targeted metabolomic and transcriptomic study. *NPJ Aging Mech Dis.* 2021; 7(1): 11.
- Shen Z, Li X, Bao X, Wang R. Microglia-targeted stem cell therapies for Alzheimer disease: a preclinical data review. *J Neurosci Res.* 2017; 95(12): 2420-2429.
- Marsh SE, Blurton-Jones M. Neural stem cell therapy for neurodegenerative disorders: the role of neurotrophic support. *Neurochem Int.* 2017; 106: 94-100.
- Paxinos G, Watson C. *The rat brain in stereotaxic coordinates: hard cover edition.* 6th ed. Academic press: Elsevier; 2006.
- Naaldijk Y, Jäger C, Fabian C, Leovsky C, Blüher A, Rudolph L, et al. Effect of systemic transplantation of bone marrow-derived mesenchymal stem cells on neuropathology markers in APP/PS1 Alzheimer mice. *Neuropathol Appl Neurobiol.* 2017; 43(4): 299-314.
- Cheraghzadeh M, Hanaee-Ahvaz H, Khirolah A, Galehdari H. Platelet-rich plasma accelerates bone differentiation in human adipose-derived mesenchymal stromal cells: an experimental study. *Iran Red Crescent Med J.* 2018; 20(12): e81828.
- Chiroma SM, Mohd Moklas MA, Mat Taib CN, Baharuldin MTH, Amon Z. D-galactose and aluminium chloride induced rat model with cognitive impairments. *Biomed Pharmacother.* 2018; 103: 1602-1608.
- Sepiani A, Cheraghzadeh M, Nazeri Z, Azizidoost S, Shalbafan B, Kheirollah A. Correlation of R219K polymorphism of ABCA1 gene and the risk of Alzheimer's disease in the southwest of Iran. *Meta Gene.* 2021; 30(100961).
- Feringa FM, van der Kant R. Cholesterol and Alzheimer's disease; from risk genes to pathological effects. *Front Aging Neurosci.* 2021; 13: 690372.
- Raskin J, Cummings J, Hardy J, Schuh K, Dean RA. Neurobiology of Alzheimer's disease: integrated molecular, physiological, anatomical, biomarker, and cognitive dimensions. *Curr Alzheimer Res.* 2015; 12(8): 712-722.
- Rudajev V, Novotny J. Cholesterol as a key player in amyloid β -mediated toxicity in Alzheimer's disease. *Front Mol Neurosci.* 2022; 15: 937056.
- Hosseini SA, Mohammadi R, Noruzi S, Mohamadi Y, Azizian M, Mousavy SM, et al. Stem cell- and gene-based therapies as potential candidates in Alzheimer's therapy. *J Cell Biochem.* 2018; 119(11): 8723-8736.
- Nazeri Z, Azizidoost S, Cheraghzadeh M, Mohammadi A, Kheirollah A. Increased protein expression of ABCA1, HMG-CoA reductase, and CYP46A1 induced by garlic and allicin in the brain mouse and astrocytes-isolated from C57BL/6J. *Avicenna J Phytomed.* 2021; 11(5): 473-483.
- Martin L. Characterization of the roles of neuronal cholesterol biosynthesis and ORP4 in hippocampal neurons and glia. Presented for the M.Sc., Canada. Dalhousie University. 2018.
- Bhattarai A, Likos EM, Weyman CM, Shukla GC. Regulation of cholesterol biosynthesis and lipid metabolism: A microRNA management perspective. *Steroids.* 2021; 173: 108878.
- Jahn T, Clark C, Kerksiek A, Lewczuk P, Lütjohann D, Popp J. Cholesterol metabolites and plant sterols in cerebrospinal fluid are associated with Alzheimer's cerebral pathology and clinical disease progression. *J Steroid Biochem Mol Biol.* 2021; 205: 105785.
- Varma VR, Büşra Lülecı H, Oommen AM, Varma S, Blackshear CT, Griswold ME, et al. Abnormal brain cholesterol homeostasis in Alzheimer's disease—a targeted metabolomic and transcriptomic study. *NPJ Aging Mech Dis.* 2021; 7(1): 11.
- Gliozzi M, Musolino V, Bosco F, Scicchitano M, Scarano F, Nucera S, et al. Cholesterol homeostasis: researching a dialogue between the brain and peripheral tissues. *Pharmacol Res.* 2021; 163: 105215.
- Gamba P, Giannelli S, Staurengi E, Testa G, Sottero B, Biasi F, et al. The controversial role of 24-S-Hydroxycholesterol in Alzheimer's disease. *Antioxidants (Basel).* 2021; 10(5): 740.
- Loera-Valencia R, Goikolea J, Parrado-Fernandez C, Merino-Serrais P, Maioli S. Alterations in cholesterol metabolism as a risk factor for developing Alzheimer's disease: potential novel targets for treatment. *J Steroid Biochem Mol Biol.* 2019; 190: 104-114.
- Li D, Zhang J, Liu Q. Brain cell type-specific cholesterol metabolism and implications for learning and memory. *Trends Neurosci.* 2022; 45(5): 401-414.
- Lo Furno D, Mannino G, Giuffrida R. Functional role of mesenchymal stem cells in the treatment of chronic neurodegenerative diseases. *J Cell Physiol.* 2018; 233(5): 3982-3999.

Spinal Cord Injury Affects Gene Expression of Transmembrane Proteins in Tissue and Release of Extracellular Vesicle in Blood: In Silico and *In Vivo* Analysis

Yasmin Mirzaalikhani, M.Sc.^{1,2,3}, Nasim Eslami, Ph.D.¹, Amin Izadi, M.Sc.⁴, Faezeh Shekari, Ph.D.^{5,6*} ,
Sahar Kiani, Ph.D.^{1,3*} 

1. Department of Stem Cells and Developmental Biology, Cell Science Research Center, Royan Institute for Stem Cell Biology and Technology, ACECR, Tehran, Iran

2. Department of Developmental Biology, University of Science and Culture, Tehran, Iran

3. Department of Brain and Cognitive Sciences, Cell Science Research Center, Royan Institute for Stem Cell Biology and Technology, ACECR, Tehran, Iran

4. Department of Embryology, Reproductive Biomedicine Research Center, Royan Institute for Reproductive Biomedicine, ACECR, Tehran, Iran

5. Department of Molecular Systems Biology, Cell Science Research Center, Royan Institute for Stem Cell Biology and Technology, ACECR, Tehran, Iran

6. Advanced Therapy Medicinal Product Technology Development Center (ATMP-TDC), Cell Science Research Center, Royan Institute for Stem Cell Biology and Technology, ACECR, Tehran, Iran

Abstract

Objective: Spinal cord injury (SCI) can disrupt membrane transmission by affecting transmembrane channels or neurotransmitter release. This study aimed to explore gene expression changes of transmembrane proteins underlying SCI through bioinformatics approaches and confirming in SCI model in rats.

Materials and Methods: In this experimental study, the differentially expressed genes (DEGs) in acute and subacute SCI were obtained based on microarray data downloaded from the gene expression omnibus (GEO). Transmembrane proteins of DEGs were recognized by using the UniProt annotation and transmembrane helices prediction (TMHMM) methods. The model of SCI was established through a weight-dropping procedure in rats. To confirm the SCI model, hematoxylin and eosin (H&E) staining was performed. Total mRNA was extracted from spinal cord tissues, and the RNA expression profile of some of the significantly changed genes in the previous part that has been confirmed by real-time polymerase chain reaction (PCR). Blood was collected from rats before sacrificing. Extracellular vesicles (EVs) were isolated by high-speed centrifugation from plasma. For the assessment of protein expression, western blotting was used.

Results: Based on bioinformatics analysis, we candidate a set of membrane proteins in SCI's acute and sub-acute phases, and confirmed significant upregulation in *Grm1*, *Nrg1*, *CD63*, *Enpp3*, and *Cxcr4* between the acute and control groups and downregulation in *Enpp3* between acute and subacute groups at the RNA level. Considering *CD63* as an EV marker, we examined the protein expression of *CD9* and *CD63* in the plasma-derived EVs, and *CD9* has significant expression between acute and control groups. We also demonstrate no significant *CD63* and *Cxcr4* expressions between groups.

Conclusion: Our results provide new insight into the relationship between candidate transmembrane protein expression and different stages of SCI using in-silico approaches. Also, results show the release of EVs in blood in each group after SCI helping enlarge strategies to enhance recovery following SCI.

Keywords: Differentially Expressed Genes, Extracellular Vesicles, Membrane Protein, Signaling Pathways, Spinal Cord Injury

Citation: Mirzaalikhani Y, Eslami N, Izadi A, Shekari F, Kiani S. Spinal cord injury affects gene expression of transmembrane proteins in tissue and release of extracellular vesicle in blood: in silico and in vivo analysis. Cell J. 2023; 25(11): 772-782. doi: 10.22074/CELLJ.2023.2004115.1320

This open-access article has been published under the terms of the Creative Commons Attribution Non-Commercial 3.0 (CC BY-NC 3.0).

Received: 06/June/2023, Revised: 27/August/2023, Accepted: 30/October/2023

*Corresponding Addresses: P.O.Box: 16635-148, Department of Molecular Systems Biology, Cell Science Research Center, Royan Institute for Stem Cell Biology and Technology, ACECR, Tehran, Iran

P.O.Box: 16635-148, Department of Stem Cells and Developmental Biology, Cell Science Research Center, Royan Institute for Stem Cell Biology and Technology, ACECR, Tehran, Iran

Emails: faezehshekari@royaninstitute.org, sahar_kiani@royaninstitute.org



Royan Institute
Cell Journal (Yakhteh)

Introduction

Spinal cord injury (SCI) is one of the most important causes of sensory and motor disorders (1). The side effects may vary widely, from pain to loss of movement (2). Microscopic events following tissue injury, including inflammation, apoptosis, necrosis, and glial scar formation, are more important consequences of SCI (3). The acute phase, which begins when an injury occurs, causes a rupture of capillary networks and damage to the blood-spinal barrier, causing bleeding, activation of microglia, and the influx of inflammatory agents into the lesion site (4). In the subacute phase, astrocytes, along with extracellular matrix proteins, begin to form glial scars (5). Activation of astrocytes helps to restore ion homeostasis reducing edema and inflammation (6). Based on many studies, most recovery occurs before entering the chronic stage, especially at the subacute phase that is the optimal time to perform treatments such as cell transplantation (7). Therefore, a comparison of these phases is important.

About 30% of the entire human genome encodes membrane proteins (8). Approximately two out of third of the drug targets are membrane proteins (60-70%) (9). Membrane proteins in the nervous system, specially transmembrane proteins which are integral membrane proteins, play an important role in the development (10), generation, and transmission of electrical messages (11). Damage to the cell surface proteins frequently occurs following damage to neural cells, which can cause problems with synthesis and transmission between neurons (12). They can play an important role in inflammation that are upregulated by sensing changes in the nervous system microenvironment (13). Therefore, investigation of changes in the gene expression of transmembrane proteins after SCI is important.

Extracellular vesicles (EVs) released from almost all cell types. The possibility of isolating them from different biofluids, makes EVs valuable biomarkers to be analysed for the diagnosis or prognosis of various conditions (14). Recent studies show that EVs participate in the progression of spinal cord secondary injury by transporting parent cell-specific signaling cargoes that change the function of recipient cells within the central nervous system (15). Also, EV-mediated functions are altered in association with many pathological features of neurotrauma (16). In contrast, EVs have emerged as alternatives to cell-based therapies due to their potential for improved safety and therapeutic efficacy across diverse regenerative applications (17). Additionally, due to EVs' diagnosis, therapeutic and cell-targeting potential, they have emerged as a suitable candidate for cell-free therapies in SCI (16).

Since finding key proteins in different stages is important for controlling molecular events following SCI, we hypothesized that the expression of some

genes may differ in acute and subacute phases and there will be some common genes in the two phases. Indeed, due to the importance of transmembrane proteins, we aimed to study them with a bioinformatics approach and using available datasets. In this study, we investigated changes in the expression of transmembrane protein genes before and after injury and also introduced altered signaling pathways following injury. Also, after confirming the SCI model, the selected transmembrane proteins were examined at the RNA and protein levels. Due to the results, plasma-derived EVs playing an important role in molecular events after SCI, were isolated and characterized in different groups and compared together.

Materials and Methods

Microarray data

In this experimental study, the expression profiles of GSE464 (GPL6247; Affymetrix, Inc., Santa Clara, CA, USA), GSE45006, GSE46988, and GSE2599 based on the Affymetrix Rat Gene 1.0 ST Array were obtained from the Gene Expression Omnibus (GEO) database (<http://www.ncbi.nlm.nih.gov/geo/>; accessed August 2021) (Fig.S1, See Supplementary Online Information at www.celljournal.org) (18). Data included noninjured spinal cord control samples and contusion spinal cord at 7-, 14-, 28-, and 35-days post-lesion.

In the acute phase, the expression profiles of GSE464, GSE45006, and GSE46988 were selected. Each dataset included a control group and a SCI group (7 days after the injury, which is in the acute phase) to compare gene expression.

To compare gene expression in the subacute phase, the expression profiles of GSE464, GSE45006, and GSE2599 were selected. Each dataset has a control group and groups of spinal cord injuries (14, 28, and 35 days after injury that are in the subacute phase interval) (Table S1, See Supplementary Online Information at www.celljournal.org).

Differentially expressed genes analysis

For genes with different expression enrichment analysis, comparisons between 7-, 14-, 28-, and 35-day post-SCI groups vs. control groups were performed using the GEO2R tool. Then, the genes with a threshold of adjusted $P \leq 0.05$ were screened out as DEGs. Furthermore, genes with \log_2FC (fold-change) ≥ 1.5 or ≤ -1.5 were categorized as up and down-regulated expressed, respectively. Venn diagrams were plotted for three datasets in each phase, and the overlaps of DEGs in at least two datasets were obtained.

Gene Ontology and signaling pathway enrichment analyses

Pathway enrichment analysis for the identified

up and down-expressed genes was performed by the Enrichr tool (19) considering KEGG (2019), Reactome (2016), Wikipathway (2019) libraries, and Biological Process for Gene Ontology analysis. All pathways in different libraries with an adjusted $P \leq 0.5$ were selected and merged. Then, to draw the interaction network of the gene ontology, we used the ShinyGO v0.75 database ($P < 0.5$) for shared expressed genes in both stages demonstrating a hierarchical clustering tree that summarizes the correlation between significant signaling pathways and network plots displays relationships between enriched pathways (20).

Membrane protein annotation

For membrane protein annotation, we utilized our previously published approach (21, 22). Firstly, we downloaded all the rat's membrane proteins from UniProt (23) (release 2021_03) and investigated the overlap of DEGs and plasma membrane annotated proteins. To determine whether these reported proteins were integral membrane containing transmembrane (TM) domains, we predicted the TM helices using TMHMM (v 2.0) (24) and also SignalP (v 5.0) (25) confirmation for proteins with a single TM. Therefore, proteins with single or fewer helices and also signal proteins are excluded for further analysis.

Experimental animals and spinal cord injury model establishment

Twenty adult male Wistar Rats (220-270 g) were used in this study. All animals were housed double per cage in a room under a controlled condition, (ad libitum food and water, $22 \pm 2^\circ\text{C}$, 12 hours dark/light cycle). All animals were randomly divided into five groups; intact groups, acute laminectomy (sham) group, acute injury group, subacute laminectomy (sham) group, and subacute injury group (Table S2, See Supplementary Online Information at www.celljournal.org). Animals were anesthetized by intraperitoneal injection of Ketamine (80 mg/kg) and Xylazine (20 mg/kg). To expose the spinal cord at the T9-T10 level, we performed a laminectomy with a dental drill. A 10 g weight dropped on the exposed spinal cord from 25 mm height via an NYU-impactor. After spinal cord compression, the muscles and skin were sutured. Animals were kept on a hot stage in 37°C for recovery. After SCI surgery, dextrose saline (10 ml) for 5 days and Enrofloxacin (5 mg/Kg) for 7 days was injected into each animal. Manual bladder discharge was performed twice daily until every animal regained full bladder control (Fig.S2, See Supplementary Online Information at www.celljournal.org).

To confirm the contusion SCI model, hematoxylin and eosin (H&E) staining was performed on sagittal and transverse sections of the spinal cord 7 days after the surgery.

Ethics statement

All of the procedures conducted on animals were approved by The Institutional Animal Care Using Committee (IACUC) at The Royan Institute, Iran. All animal experiments were performed by international guidelines that approved by the Royan Ethics Committee (IR.ACECR.ROYAN.REC.1400.122). All efforts were made to decrease the suffering of the animals used and reduce the number of animals used in this research.

Behavioral assessment

The Basso, Beattie, and Bresnahan (BBB) (26) score is a scale of 0 (complete hind limb paralysis) to 21 (normal motor activity) that rat models in injury groups were placed in a surrounded field and observed for 3 minutes which can confirm spinal cord injury. First, each rat's bladder was emptied to avoid affecting its behavior. Then BBB Scale locomotor tests of all rats were blindly performed after SCI in 3-, 7-, and 14-days post-injury. Finally, the average integer value of each rat was recorded.

Histological analysis

Animals were sacrificed and perfused transcardially with 4% paraformaldehyde ($\text{pH}=7.4$). The spinal cords of the upper and lower 10 mm entered on the injured site with bone that were collected and kept in 4% paraformaldehyde for 10 days and fixed in formalin for 24 hours with bone. The tissue was dehydrated in gradient alcohol, then cleared in xylene, and embedded in paraffin. Subsequently, the embedded tissues were cut into 5- μm thick slices. The sagittal section contained the full length of the longitudinal axis of the tissues, passing through the center of the spinal cord, and the transverse section was located at the site of the injury. Next, these sections were stained with H&E.

Real-time polymerase chain reaction

To isolate RNA from each injured spinal cord which was kept in RNA later at -80°C after sacrificing the animal, Trizol (Kiagene/Kiazist) was used. cDNA was synthesized via Royan Biotech kit, according to the company's guidelines. It was used as a template in real-time polymerase chain reaction (RT-PCR) analyses and quantifying the RNA levels of *Grm1*, *Nrg1*, *Scn1*, *Kcna1*, *Cxcr4*, *CD63*, and *Enpp3* genes. mRNA expression levels were normalized against the reference gene *GAPDH* and measured using the $45-\Delta\text{CT}$ method, which is the result of subtracting ΔCT from the total number of cycles (which is 45 in this study). The final volume was 10 μl which included cDNA (2 μl , 12.5 ng/ μl), forward and reverse primers (5 pmol/ μl), SYBER Green (2.5 μl), and DEPC treated

water up to the final volume. The concentration of RNA for each cDNA reaction is 2000 ng. Three biological replicates and two independent technical replicates were used in all experiments.

Extracellular vesicles isolation and characterization

EVs were isolated from plasma using differential centrifugation. Since we are going to focus on the membrane proteins, we isolated EVs by high-speed centrifugation at 20,000 g for 60 minutes. Isolated EVs were stored at -80°C .

Western blotting

Protein expression of EVs was measured using western blot for CD9, CD63 (EVs markers), and Cxcr4 proteins. The protein concentration of each group was determined by BCA assay kits. Samples (10 μg) were separated by 10% SDS-PAGE electrophoresis (Fig. S3, See Supplementary Online Information at www.celljournal.org). The probed proteins were transferred to Bio-RAD polyvinylidene fluoride membranes using an electroblotting transfer system (Bio-Rad) 25V for 150 minutes at room temperature (RT). Then polyvinylidene difluoride membranes (PVDF) membranes were blocked overnight at 4°C buffered with 2% bovine serum albumin (BSA) in Tris-saline plus 0.1% Tween for 1 hour and incubated with primary antibodies [anti-CD9 (Sc13118, Santacruz; 1:1000), and anti-CD63 (Sc-5275, Santacruz; 1:200) and anti-Cxcr4 (sc-6190, Santacruz; 1:200)]. The membranes were washed three times with Tris buffered saline with tween 20 (TBST) and then incubated with anti-goat secondary antibodies (diluted at 1:2000) at room temperature for 1 hour. At the end, the membranes were rinsed three TBST, and incubated with Super Signal West Femto Substrate (ThermoFisher Scientific) and bands visualized by using the Alliance Q9 Advanced Chemiluminescence Imager gel documentation system. According to the SDS-PAGE gel (Fig.S3, See Supplementary Online Information at www.celljournal.org) image, the band intensities were normalized to the loading control and quantified using ImageJ software version 1.46 (National Institute of Health, USA).

Statistical analysis

All results were analysed using GraphPad Prism v.9 software (GraphPad, USA). The qRT-PCR and western blot data analysed through one-way ANOVA and Tukey post-test and the data was presented by means \pm SD. $P < 0.05$ were considered significant.

Results

Data pre-processing and differentially expressed genes screening in spinal cord injury

DEGs between the SCI and control samples at both

stages were screened. In both phases, genes that were common to at least two datasets are presented in Figure S4 (See Supplementary Online Information at www.celljournal.org). After removing duplicate genes, in total, 3382 and 745 genes with a threshold of adjusted $P \leq 0.05$ as DEGs have been reproducibly reported in acute and subacute datasets respectively.

After choosing genes with $\log_2\text{FC}$ (fold-change) ≥ 1.5 or ≤ -1.5 , 389 upregulated and 141 downregulated DEGs in the acute phase, and 143 upregulated and 62 downregulated DEGs in the subacute phase were identified. At both stages, there was a greater number of upregulated DEGs than those downregulated DEGs.

Pathway enrichment analysis

The biological process and hierarchical clusters between the shared expressed genes in both phases were detected. In hierarchical clustering trees, bigger dots indicate more significant P values. Analysis of genes commonly upregulated between acute and subacute phases by ShinyGO identified biological processes with the most significant p-value, including the immune and defense responses, and biological processes involved in interspecies interaction between organisms. Since darker nodes in ShinyGO network plots are shown as more significantly enriched gene sets, these processes are related together, and other pathways such as regulation of immune system process, inflammatory response, response to external biotic stimulus, cell activation, cytokine production, and leukocyte activation. Also, a similar analysis revealed that the commonly downregulated genes in both phases were enriched in biological processes associated with anterograde trans-synaptic signaling, chemical synaptic transmission, synaptic signaling, and cell-cell signaling (Fig.1). The hierarchical clustering tree represents related gene ontology (GO) terms grouped together based on the number of shared genes. They are related together and some pathways, including ion transport, behavior, modulation of chemical synaptic transmission, and regulation of trans-synaptic signaling. The relationship between enriched pathways is shown and two nodes with 20% or more shared genes are connected.

Moreover, we have checked our DEGs in signaling pathways with enrichment-adjusted $P \leq 0.05$ via Wikipathway, KEGG, Biological process, and Reactome databases. Some of the enriched signaling pathways that were found by at least two databases with greater input sizes that were immune response and apoptosis pathways in upregulated pathways, and also membrane transmission in downregulated pathways (Table 1).

Table 1: Enriched signaling pathways

Phase		Pathway	Term	Input/references size	Adjusted P value	Database
Acute	UP	Immune response	Regulation of immune response	14/179	1.15E-05	Biological process
			Macrophage activation involved in the immune response	5/13	3.03E-05	Biological process
			Cytokine Signaling in Immune System Homo Sapiens R-HSA-1280215	28/620	8.57E-07	Reactome
			Inflammatory response pathway WP458	4/30	0.00353	WikiPathway
		Apoptosis	Regulation of glial cell apoptotic process	2/7	0.026198	Biological process
			Apoptosis WP1254	6/81	0.003715	WikiPathway
			Apoptosis	9/141	8.45E-04	KEGG
Sub-acute	UP	Immune response	Cytokine-mediated signaling pathway	38/621	5.83E-19	Biological process
			Positive regulation of the production of molecular mediator of immune response	3/38	0.021754	Biological process
			Neutrophil activation involved in immune response	28/485	5.02E-13	Biological process
			Inflammatory response pathway WP458	3/30	3/30	WikiPathway
Acute	DOWN	Membrane transmission	Ion channel transport Homo sapiens R-HSA-983712	10/203	1.86E-05	Reactome
			GABA receptor activation Homo sapiens R-HSA-977443	6/55	2.73E-05	Reactome
			GABAergic synapse	10/90	3.54E-08	KEGG
			Calcium signaling pathway	10/189	7.70E-06	KEGG
			Neurotransmitter secretion (GO:0007269)	7/44	2.45E-06	Biological process
			Sodium ion transport (GO:0006814)	5/90	0.011817	Biological process
			Potassium ion transmembrane transport (GO:0071805)	11/139	5.95E-07	Biological process
Sub-acute		Membrane transmission	Glutamate receptor signaling pathway	5/37	8.03E-06	Biological process
			Sodium ion transmembrane transport	3/87	0.026798	Biological process
			GABAergic synapse	7/90	4.53E-07	KEGG
			Potassium ion transmembrane transport	5/139	0.002162	Biological process
			Calcium signaling pathway	8/189	0.04148	

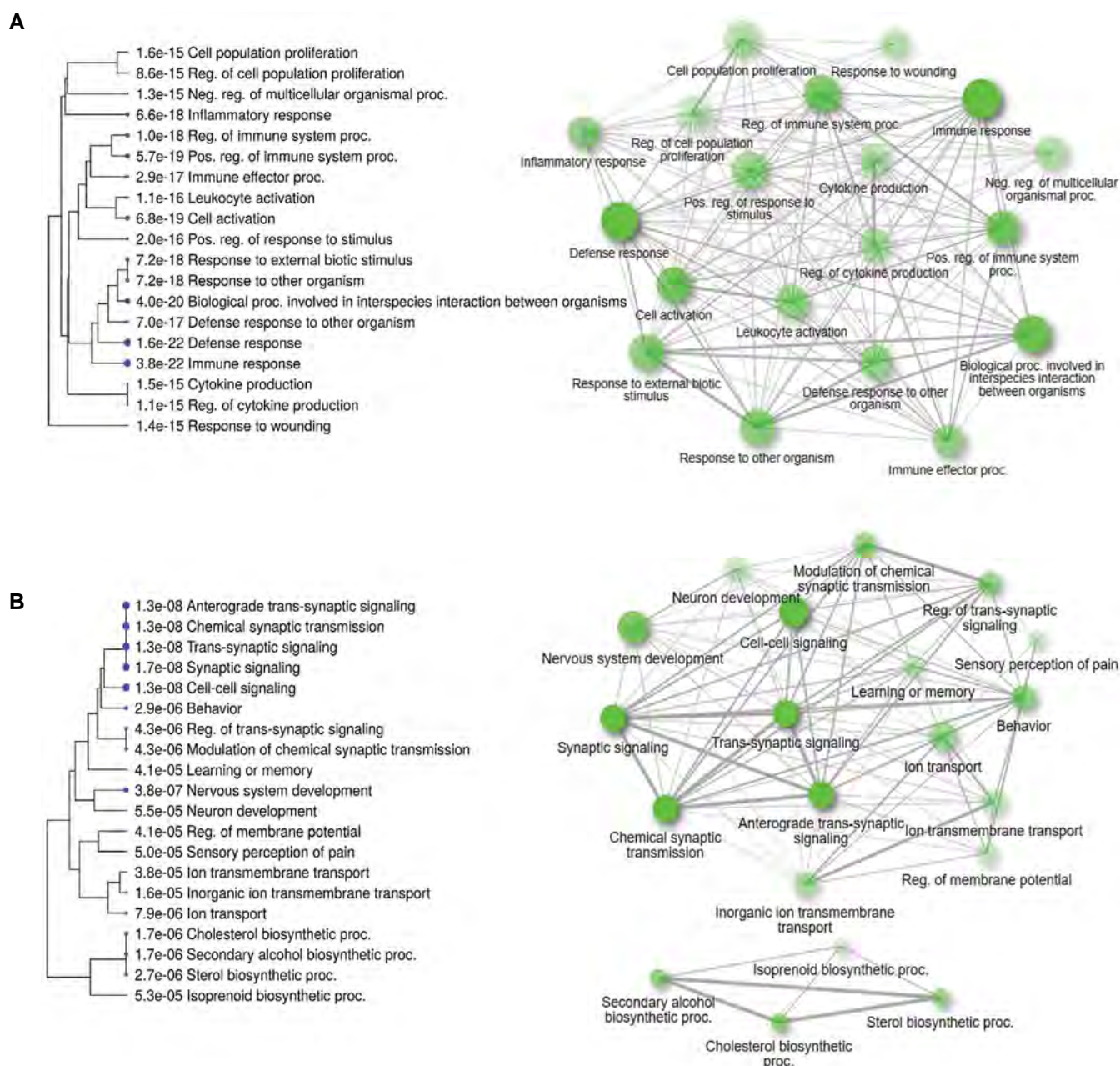


Fig.1: The biological process and hierarchical clusters between the shared expressed genes in acute and subacute phases. **A.** Upregulated and **B.** Downregulated genes in both acute and subacute phases. The intensity of color and the circles' size in networks indicate the significance of the biological process. The hierarchical clustering tree shows related GO terms grouped based on the number of shared genes (FDR $P \leq 0.05$). Bigger dots indicate more significant P values. To draw the interaction network of the gene ontology we used the ShinyGO v0.75 database. FDR; False discovery rate and GO; Gene ontology.

Analysis of differentially expressed membrane and transmembrane proteins

DEGs encoding membrane proteins in rats that were up- or down-regulated at each stage of injury were detected. In this study, proteins with more than one helix are considered transmembrane proteins. Transmembrane proteins which are upregulated or downregulated in both stages of SCI are separated. *Tlr4*, *Cd36*, *Olr1*, *Enpp3*, *Cd63*, *Ptpnc*, *Cd53*, *Adcy4*, and *Cxcr4* are upregulated, and *Kcna1*, *Scn1a*, *Gm1*, *Cnr1*, and *Nrg1* are downregulated in both phases. The rest of them are specific to one of the two phases of SCI (Fig.2).

Spinal cord injury model establishment and behavioral test

To confirm contusion SCI model H&E staining was performed in sagittal and transverse sections of the spinal cord sections 7 days after the surgery, H&E demonstrated tissue damage as well as neuronal degeneration and cell elimination around the lesion site (Fig.3).

To confirm the SCI model and to show the rate of recovery after injury, the BBB test was performed on 1, 7, and 14 days after injury, showing the motor score immediately after surgery, and at each phase, respectively

(Table S3, See Supplementary Online Information at www.celljournal.org). Up to one week after the injury, the animal had scores below five, which confirms the SCI

model. The BBB score of all animals was determined to be 21 before the SCI surgery. This score shifted to zero after surgery and remained the same for at least 3 days.

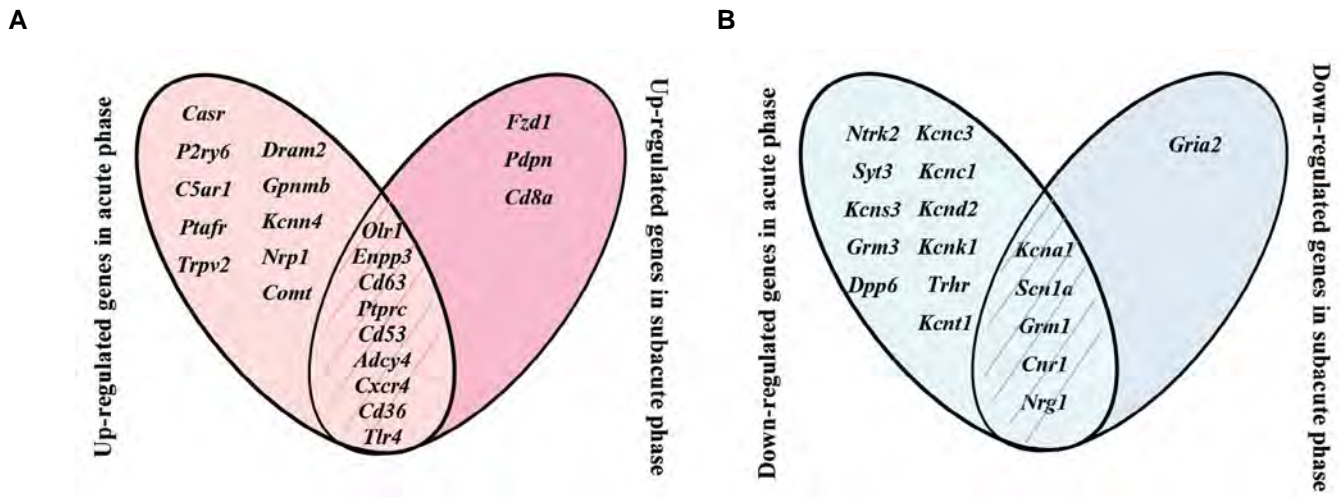


Fig.2: Upregulated and downregulated transmembrane proteins in both phases. **A.** Upregulated and **B.** Downregulated transmembrane proteins in the acute and subacute phases of injury. They also show common and specific proteins in two phases of SCI. SCI; Spinal cord injury.

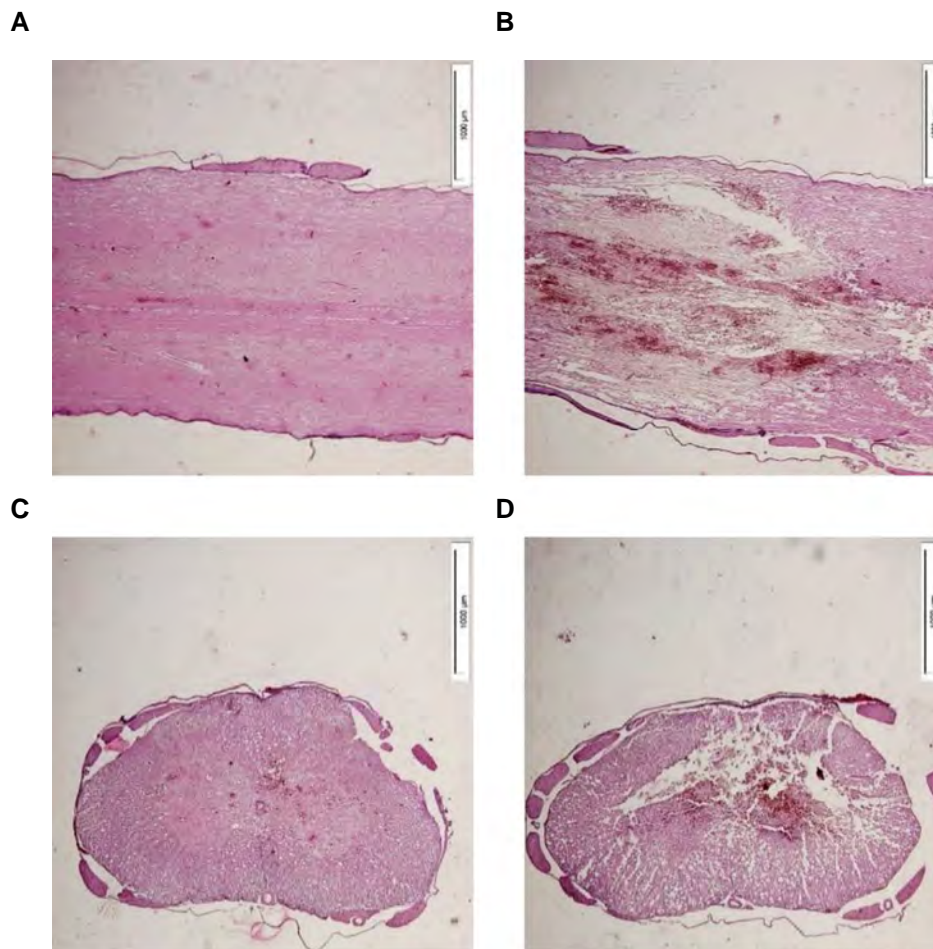


Fig.3: Spinal cord injury (SCI) model confirmation. H&E staining 1 week after SCI. **A.** H&E staining of a sagittal section of intact and **B.** injured spinal cord. The lesion site is clearly demonstrating a severe injury. **C.** Shows a transverse section of approximately the 9th thoracic level of the vertebrae which is intact. **D.** A transverse section of about the 10th thoracic vertebrae which is in the lesion site.

Gene expression at the RNA level

We examined some genes among common ones in both phases to confirm them at the RNA level. The selected genes are *Enpp3*, *Cd63*, and *Cxcr4* as upregulated genes and *Kcna1*, *Scn1a*, *Grm1*, and *Nrg1* as downregulated. In this section, the primers designed in Table S4 (See Supplementary Online Information at www.celljournal.org) are used. The melting curve of the two strands of cDNA is also shown in Figure S5 (See Supplementary Online Information at www.celljournal.org).

The genes which were upregulated in the bioinformatics part of the study were compared in the intact, sham acute, sham subacute, acute, and subacute groups. In the comparison of the sham acute groups with the acute groups, there was a considerable expression of *Cd63*. Additionally, there was a significant difference in *Cxcr4* expression between acute and intact groups as well as acute and sham groups. There was a noticeable difference in the expression of the *Enpp3* gene between the acute and subacute groups as well as between the acute and sham groups.

Also, the genes that were downregulated in the bioinformatics section of the study were compared in the intact, sham acute, sham subacute, acute, and subacute groups. There was a significant expression in this comparison between the acute group and the sham group in *Grm1*. In the acute and subacute groups, *Kcna1* and *Scn1a* genes did not have any notable expression. Additionally, there was a significant expression difference between the acute and sham groups in *Nrg1*. To compare groups, a One-way ANOVA and a Tukey post-test were applied (Fig.4).

Western blot analysis

Among all the identified genes, CD63 (EV's marker) and *Cxcr4* were selected to test their protein expression in plasma-derived EV. Western blots of plasma-derived EV have shown the expression of CD63, CD9, and *Cxcr4* in intact, sham acute, sham subacute, acute, and subacute groups. CD63 has not shown any significant expressions between groups. While there was a significant difference in CD9 expression between sham acute and intact groups as well as acute and sham acute. Also, there was no significant difference in *Cxcr4* expression between groups (Fig.5).

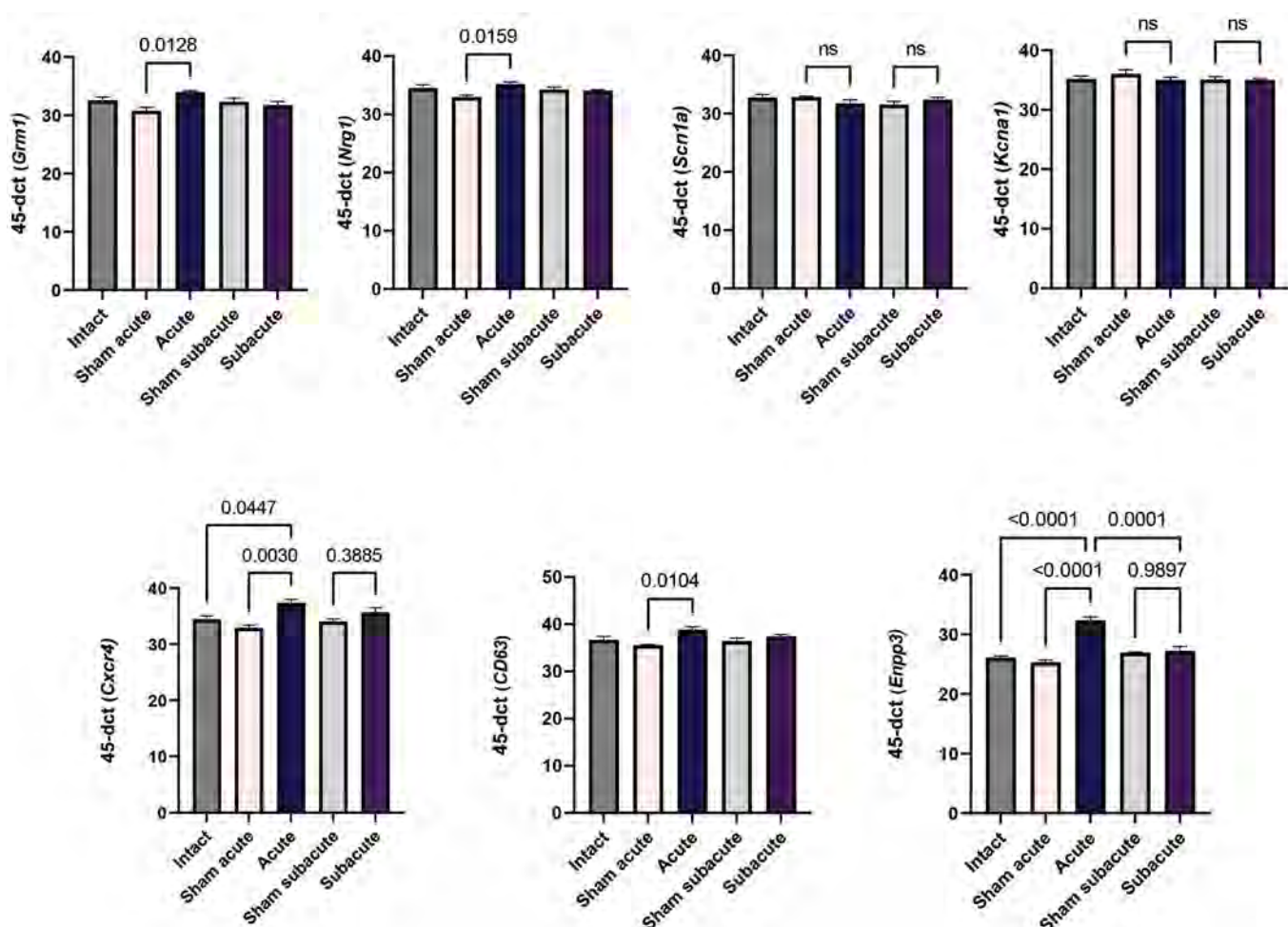


Fig.4: Quantitative RT-PCR analysis of selected genes in the spinal cord of intact, laminectomy, and injury groups in acute and subacute phases. One-way ANOVA with Tukey posttest was performed and data has been presented by means \pm SD. ns; Non-significant and RT-PCR; Real time polymerase chain reaction.

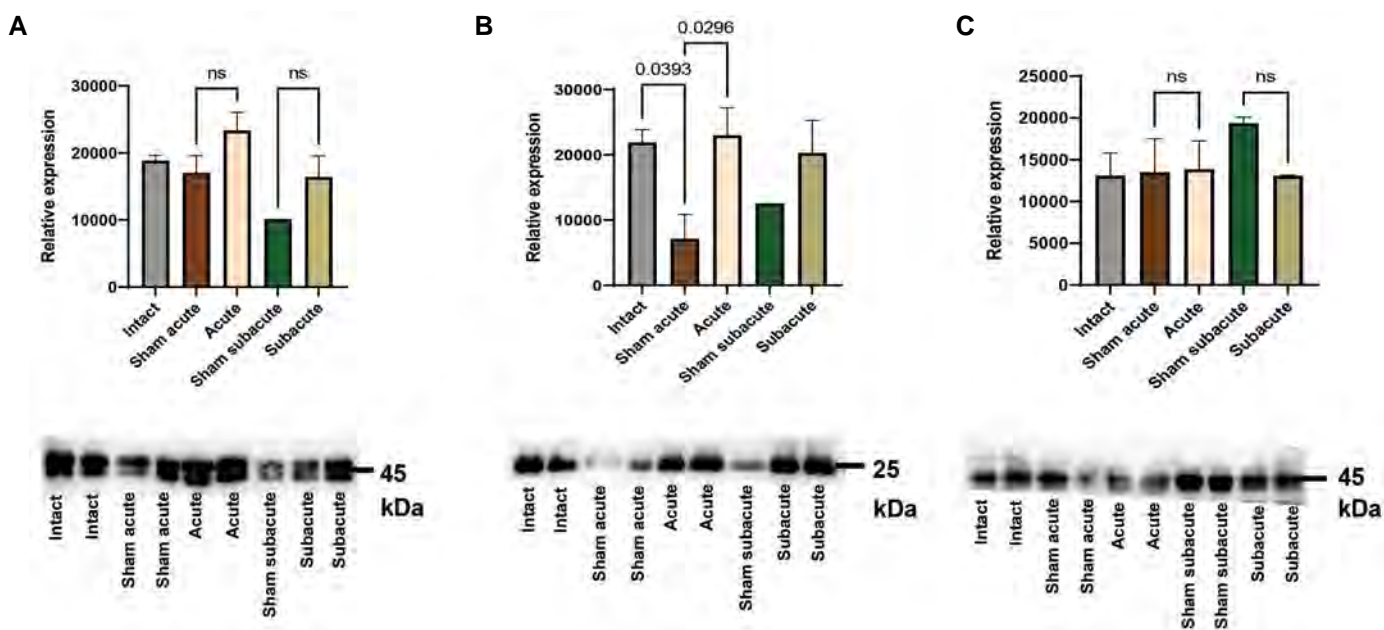


Fig. 5: Western blots of plasma derived-EV show the expression of CD63, CD9, and Cxcr4 in intact, laminectomy and injury groups. EVs were characterized by expressions of **A.** CD63 and **B.** CD9. **C.** Also, Cxcr4 protein levels were measured in all groups. 10 μ g of protein was loaded per lane. One-way ANOVA with Tukey posttest was performed and data has been presented by means \pm SD. ns; Non-significant.

Discussion

SCI is a fatal nerve injury that has irreversible effects on the sensory, motor, and nervous systems that is no complete treatment for it (27). It is important to have a comprehensive understanding of the conditions of injuries and to provide treatment strategies.

In this study, a total of 3382 DEG in the acute phase and 745 DEG in the subacute phase were found. Based on biological process enrichment, the up-regulated genes in both phases were related to the immune, defense, and inflammatory response and also cell activation and cytokine production. Also, the down-regulated genes were related to synaptic transmission, cell-cell signaling, and nervous system development. Similar results were obtained from Enrichr analysis of pathways, the most up-regulated pathways were related to the immune response such as inflammation and cytokine signaling, and apoptosis. Also, the down-regulated pathways were related to membrane transmission such as ion channel transport and neurotransmitter receptors. In 2015, research on a different dataset demonstrated that the enriched KEGG pathways of the down-regulated genes were predominantly associated with pathways of neurological diseases. While the up-regulated genes were enriched in immune response-associated pathways (28).

Due to the important role of transmembrane receptors in neurons, in the next step we defined analyses to find transmembrane proteins and obtained a short list of them that finally confirmed some of the genes among the selected genes at the RNA level. These genes included a subunit of the sodium and potassium channels and the glutamate receptor, as well as the growth factor Neuregulin genes

that were downregulated in the bioinformatics section. Additionally, the immunogenic genes *Enpp3*, *Cxcr4*, and *Cd63* were selected from the genes that were up-regulated in the previous section. Following RT-PCR for tissues, we showed significant upregulation in *Grm1*, *Nrg1*, *CD63*, *Enpp3*, and *Cxcr4* between the acute and control groups and downregulation in *Enpp3* between acute and subacute groups.

Due to the important role of EVs in cell communication, stimulation or suppression of the immune system and tissue injury, it has recently been considered as a therapeutic method. Also, considering the ability of EVs to activate or suppress many signaling pathways, in this study, we investigated the expression changes of EVs markers (29, 30). Considering *CD63* as an EV marker, to characterize EVs we examined the protein expression of *CD9* and *CD63* plasma derived-EV (31). *CD9* has significant expression between acute and control groups. We also demonstrate no significant *CD63* and *Cxcr4* expressions between groups.

According to studies on chronic pain after spinal cord injury, it has been proposed that a significant increase in *CXCL12* expression occurs in activated astrocytes. Also, the expression of the *Cxcr4* receptor increases on the surface of macroglia cells, and the connection between this ligand and the receptor causes an increase in pro-inflammatory cytokines, which will eventually lead to chronic pain (32). Moreover, studies have shown that *Enpp3* has a decreasing effect on ATP concentration in most tissues and leads to the suppression of basophil cells and mast cells. And these changes will eventually lead to the control of severe inflammation (33).

According to the bioinformatic studies in this project, we expected that the factors related to immune response and inflammation would increase in expression, and we observed this increase in both *Enpp3* and *Cxcr4* genes in the acute phase of injury.

As we mentioned, to prevent the infection and death of the animal, we used the antibiotic enrofloxacin, which in some studies has shown the mechanism of action of this drug orally leading to anti-inflammatory effects in some tissues (34). It seems that the daily use of antibiotics and serum, as well as the daily emptying of the animal's bladder, has led to the prevention of extensive inflammation and infection in the subacute phase, and it may also affect the expression of *Cd63*, which is one of the important proteins on the surface of EVs and involved in immunity and causes the adhesion of leukocytes to endothelial cells and has a role in signaling angiogenesis (35).

As we have shown, no significant difference was observed in sodium (*Scn1a*) and potassium (*Kcna1*) genes selected in the injury phases compared to the control group. Due to the important role of potassium channels and also the difference in their different isoforms, the study on the expression of these channels in neuronal damage has also been done on human data sets. Some articles reported significant changes in the *Kcna1* gene after injury. In a study, these changes were seen in the chronic phase in the mouse model. Also, they have shown the expression of another subunit of the sodium channel (*Scn8a*) was changed (36).

In our study, the *Grm1* did not significantly change between the injury groups and the control groups, but this expression was significant between the acute and subacute phases. We suppose that using ketamine to anesthetize the animal is the reason for this result, because this drug directly affects glutamate receptors and inhibits them (37).

The *Nrg1* gene, which encodes Neuregulin-1, leads to myelination of some neurons and spontaneous healing of the injury after SCI (38). It has been shown in studies that the expression of this gene decreases after injury, and severe secondary injury is formed after it (39). We guess that in our study, this change was not seen in the acute phase due to the absence of severe secondary damage in a short time after the injury occurred, and in the sub-acute phase, this lack of significance is due to the use of drugs that controlled the severity of the damage.

Generally, the possible reasons for the lack of significance in some of our genes in this study can depend on various factors. For example, the type of damage selected in bioinformatic studies was medium damage, which in this type of damage is considered to be 12-25 mm weight distance in the articles. In this research, we chose the maximum distance, 25 mm, and as seen in the histological examination, the intensity of the damage was high and scattered. Therefore, the type of injury may

have influenced the study. Moreover, there are various types of subunits and isoforms in ion channels and neurotransmitter receptors. The subunits of ion channels have different roles, including regulatory, or functional, and some of them may be active in different conditions. Also, some of these isoforms do not change when cell conditions change.

According to the mentioned cases, it can be suggested that the anesthetic drug and antibiotic used should undergo a more detailed study or be changed. Secondly, for the bioinformatics part of the work, it is possible to create more filters by changing analyses such as the amount of logFC and reaching a shorter gene list. Thirdly, in this study, we used real-time PCR for spinal cord tissue samples and the Western blotting technique for blood samples. This can be one of the explanations for the difference in expression in genes such as *Cd63*. It is suggested to investigate protein level expression in the candidate genes in tissue samples.

In the subacute phase, due to the activity of the immune system after injury, the spinal cord can undergo a slight spontaneous recovery. For example, the inflammation in the spinal cord decreases in this phase (40). Therefore, we expect that the expression of genes has undergone more changes in the acute phase, and the bioinformatics results regarding the number of genes in these two phases can support this theory.

Conclusion

Our results provide novel insight into the relationship between transmembrane protein expression and SCI by bioinformatics approaches followed up at RNA level in animal models. Also, results indicate that SCI affects EV release in the blood at different times, which can help enlarge strategies to enhance recovery following SCI.

Acknowledgments

This work was financially supported by a grant from Royan Institute to F.S. and S.K. The authors have no relevant financial or non-financial interests to disclose.

Authors' Contributions

Y.M.; Conceptualization, Methodology, Software, Formal Analysis, Writing- Original Draft, and Visualization. N.E., Y.M., A.I.; Investigation. N.E., Y.M., F.Sh.; Writing- Review and Editing. F.Sh., S.K.; Supervision, Project administration, and Funding acquisition. All authors read and approved the final manuscript.

References

1. Carpentier S, Deng W, Bottale S, Hendrickson T, Zhang L, Wudlick R, et al. Cognitive multisensory rehabilitation for sensory and motor function in adults with spinal cord injury: proof of concept. *Archives of Physical Medicine and Rehabilitation*. 2022; 103(3): e21-e22.
2. Forte G, Giuffrida V, Scuderi A, Pazzaglia M. Future treatment of neuropathic pain in spinal cord injury: the challenges of nanomedicine, supplements or opportunities? *Biomedicines*. 2022; 10(6): 1373.

3. Zhang C, Kang J, Zhang X, Zhang Y, Huang N, Ning B. Spatiotemporal dynamics of the cellular components involved in glial scar formation following spinal cord injury. *Biomed Pharmacother.* 2022; 153: 113500.
4. Zhang Y, Al Mamun A, Yuan Y, Lu Q, Xiong J, Yang S, et al. Acute spinal cord injury: Pathophysiology and pharmacological intervention (Review). *Mol Med Rep.* 2021; 23(6): 417.
5. He X, Li Y, Deng B, Lin A, Zhang G, Ma M, et al. The PI3K/AKT signalling pathway in inflammation, cell death and glial scar formation after traumatic spinal cord injury: mechanisms and therapeutic opportunities. *Cell Prolif.* 2022; 55(9): e13275.
6. Munteanu C, Rotariu M, Turnea M, Ionescu AM, Popescu C, Spinu A, et al. Main cations and cellular biology of traumatic spinal cord injury. *Cells.* 2022; 11(16): 2503.
7. Shang Z, Li D, Chen J, Wang R, Wang M, Zhang B, et al. What is the optimal timing of transplantation of neural stem cells in spinal cord injury? A systematic review and network meta-analysis based on animal studies. *Front Immunol.* 2022; 13: 855309.
8. Dobson L, Reményi I, Tusnády GE. The human transmembrane proteome. *Biol Direct.* 2015; 10: 31.
9. Chen W, Chen L, Dai Q. iMPT-FDNPL: identification of membrane protein types with functional domains and a natural language processing approach. *Comput Math Methods Med.* 2021; 2021: 7681497.
10. Jin EJ, Kiral FR, Hiesinger PR. The where, what, and when of membrane protein degradation in neurons. *Dev Neurobiol.* 2018; 78(3): 283-297.
11. Roy A. Membrane preparation and solubilization. *Methods Enzymol.* 2015; 557: 45-56.
12. Ciechanover A, Kwon YT. Degradation of misfolded proteins in neurodegenerative diseases: therapeutic targets and strategies. *Exp Mol Med.* 2015; 47(3): e147.
13. Zhao JF, Ren T, Li XY, Guo TL, Liu CH, Wang X. Research progress on the role of microglia membrane proteins or receptors in neuroinflammation and degeneration. *Front Cell Neurosci.* 2022; 16: 831977.
14. Liang Y, Lehrich BM, Zheng S, Lu M. Emerging methods in biomarker identification for extracellular vesicle-based liquid biopsy. *J Extracell Vesicles.* 2021; 10(7): e12090.
15. Rufino-Ramos D, Albuquerque PR, Carmona V, Perfeito R, Nobre RJ, Pereira de Almeida L. Extracellular vesicles: novel promising delivery systems for therapy of brain diseases. *J Control Release.* 2017; 262: 247-258.
16. Dutta D, Khan N, Wu J, Jay SM. Extracellular vesicles as an emerging frontier in spinal cord injury pathobiology and therapy. *Trends Neurosci.* 2021; 44(6): 492-506.
17. Branscome H, Paul S, Yin D, El-Hage N, Agbottah ET, Zadeh MA, et al. Use of stem cell extracellular vesicles as a "Holistic" approach to CNS repair. *Front Cell Dev Biol.* 2020; 8: 455.
18. Clough E, Barrett T. The gene expression omnibus database. *Methods Mol Biol.* 2016; 1418: 93-110.
19. Xie Z, Bailey A, Kuleshov MV, Clarke DJB, Evangelista JE, Jenkins SL, et al. Gene set knowledge discovery with enrichr. *Curr Protoc.* 2021; 1(3): e90.
20. Ge SX, Jung D, Yao R. ShinyGO: a graphical gene-set enrichment tool for animals and plants. *Bioinformatics.* 2020; 36(8): 2628-2629.
21. Shekari F, Han CL, Lee J, Mirzaei M, Gupta V, Haynes PA, et al. Surface markers of human embryonic stem cells: a meta analysis of membrane proteomics reports. *Expert Rev Proteomics.* 2018; 15(11): 911-922.
22. Shekari F, Nezari H, Larijani MR, Han CL, Baharvand H, Chen YJ, et al. Proteome analysis of human embryonic stem cells organelles. *J Proteomics.* 2017; 162: 108-118.
23. Coudert E, Gehant S, de Castro E, Pozzato M, Baratin D, Neto T, et al. Annotation of biologically relevant ligands in UniProtKB using ChEBI. *Bioinformatics.* 2023; 39(1): btac793.
24. Krogh A, Larsson B, von Heijne G, Sonnhammer EL. Predicting transmembrane protein topology with a hidden Markov model: application to complete genomes. *J Mol Biol.* 2001; 305(3): 567-580.
25. Almagro Armenteros JJ, Tsirigos KD, Sønderby CK, Petersen TN, Winther O, Brunak S, et al. SignalP 5.0 improves signal peptide predictions using deep neural networks. *Nat Biotechnol.* 2019; 37(4): 420-423.
26. Basso DM, Beattie MS, Bresnahan JC. A sensitive and reliable locomotor rating scale for open field testing in rats. *J Neurotrauma.* 1995; 12(1): 1-21.
27. Mu J, Wu J, Cao J, Ma T, Li L, Feng S, et al. Rapid and effective treatment of traumatic spinal cord injury using stem cell derived exosomes. *Asian J Pharm Sci.* 2021; 16(6): 806-815.
28. Wang W, Liu R, Xu Z, Niu X, Mao Z, Meng Q, et al. Further insight into molecular mechanism underlying thoracic spinal cord injury using bioinformatics methods. *Mol Med Rep.* 2015; 12(6): 7851-788.
29. Wang X, Botchway BOA, Zhang Y, Yuan J, Liu X. Combinational treatment of bioscaffolds and extracellular vesicles in spinal cord injury. *Front Mol Neurosci.* 2019; 12: 81.
30. Zhang J, Shi W, Qu D, Yu T, Qi C, Fu H. Extracellular vesicle therapy for traumatic central nervous system disorders. *Stem Cell Res Ther.* 2022; 13(1): 442.
31. Mathieu M, Névo N, Jouve M, Valenzuela JI, Maurin M, Verweij FJ, et al. Specificities of exosome versus small ectosome secretion revealed by live intracellular tracking of CD63 and CD9. *Nat Commun.* 2021; 12(1): 4389.
32. Luo X, Tai WL, Sun L, Pan Z, Xia Z, Chung SK, et al. Crosstalk between astrocytic CXCL12 and microglial CXCR4 contributes to the development of neuropathic pain. *Mol Pain.* 2016; 12: 1744806916636385.
33. Li FX, Yu JJ, Liu Y, Miao XP, Curry TE Jr. Induction of ectonucleotide pyrophosphatase/phosphodiesterase 3 during the periovulatory period in the rat ovary. *Reprod Sci.* 2017; 24(7): 1033-1040.
34. Strzępa A, Marcińska K, Majewska-Szczepanik M, Szczepanik M. Oral treatment with enrofloxacin creates anti-inflammatory environment that supports induction of tolerogenic dendritic cells. *Int Immunopharmacol.* 2019; 77: 105966.
35. Yeung L, Hickey MJ, Wright MD. The many and varied roles of tetraspanins in immune cell recruitment and migration. *Front Immunol.* 2018; 9: 1644.
36. Garcia VB, Abbinanti MD, Harris-Warrick RM, Schulz DJ. Effects of chronic spinal cord injury on relationships among ion channel and receptor mRNAs in mouse lumbar spinal cord. *Neuroscience.* 2018; 393: 42-60.
37. Lazarevic V, Yang Y, Flais I, Svenningsson P. Ketamine decreases neuronally released glutamate via retrograde stimulation of presynaptic adenosine A1 receptors. *Mol Psychiatry.* 2021; 26(12): 7425-7435.
38. Bartus K, Galino J, James ND, Hernandez-Miranda LR, Dawes JM, Fricker FR, et al. Neuregulin-1 controls an endogenous repair mechanism after spinal cord injury. *Brain.* 2016; 139(Pt 5): 1394-1416.
39. Kataria H, Karimi-Abdolrezaee S. Neuregulin-1: a novel regulator of glial response in spinal cord injury. *Neural Regen Res.* 2017; 12(10): 1616-1617.
40. Onifer SM, Smith GM, Fouad K. Plasticity after spinal cord injury: relevance to recovery and approaches to facilitate it. *Neurotherapeutics.* 2011; 8(2): 283-293.

Association of *MGLL* Intronic C>T Single Nucleotide Polymorphism (rs782440) with Borderline Personality Disorder: A Case-Control Study

Nazanin Hatami Bavarsad, Ph.D.¹, Leila Jahangard, M.D.², Masood Saidijam, Ph.D.³, Seyed Asaad Karimi, Ph.D.¹, Ali Reza Soltanian, Ph.D.⁴, Elahe Shahriari, M.Sc.¹, Saeid Afshar, Ph.D.^{3, 5*} ,
Abdolrahman Sarihi, Ph.D.^{1, 6*} 

1. Department of Neuroscience, School of Advanced Medical Sciences and Technologies, Hamadan University of Medical Sciences, Hamadan, Iran

2. Department of Psychiatry, School of Medicine, Hamadan University of Medical Sciences, Hamadan, Iran

3. Research Center for Molecular Medicine, Hamadan University of Medical Sciences, Hamadan, Iran

4. Noncommunicable Diseases Research Center, Hamadan University of Medical Sciences, Hamadan, Iran

5. Department of Medical Biotechnology, School of Advanced Medical Sciences and Technologies, Hamadan University of Medical Sciences, Hamadan, Iran

6. Neurophysiology Research Center, Hamadan University of Medical Sciences, Hamadan, Iran

Abstract

Objective: From the perspective of etiology, borderline personality disorder (BPD) is a multifactorial and complex disorder, hence our understanding about the molecular basis and signaling of this disorder is extremely limited. The purpose of this study was evaluating the relationship between BPD and the Monoacylglycerol lipase (*MGLL*) polymorphism rs782440 in the population of Hamadan, Iran.

Materials and Methods: In this case-control study, 106 participants including 53 patients with BPD and 53 healthy control subjects were selected by psychiatrists in the Department of Psychiatry at Farschian Sina Hospital in Hamadan. The BPD patients were selected based on the Diagnostic and Statistical Manual of Mental Disorders (*DSM-5*) form for diagnosing BPD patients. For genotyping, polymerase chain reaction (PCR) was used to amplify the desired region including the *MGLL* intronic C>T single nucleotide polymorphism (SNP) (rs782440) and afterward the amplicon was sequenced using the Sanger sequencing method. To determine the genotype of these patients, their sequences were aligned with the reference sequence of *MGLL* through the CLC genomic workbench software.

Results: The results indicated that the frequency of TT in comparison to the CC genotype was significantly different ($P=0.003$) and the risk of BPD in change from the TT genotype to CC genotype was increased by 6.679%. Regarding the frequency of allele in this group, no significant difference was observed.

Conclusion: This paper, has studied and reports for the first time, the association between *MGLL* SNP (rs782440) with BPD. The findings of the current research revealed that the TT genotype increases the risk of BPD compared to the CC genotype. Considering the lack of a suitable diagnostic biomarker for BPD, using this potential biomarker in the near future can be promising.

Keywords: Borderline Personality Disorder, Monoacylglycerol Lipase, Polymorphism

Citation: Hatami Bavarsad N, Jahangard L, Saidijam M, Karimi SA, Soltanian AR, Shahriari E, Afshar S, Sarihi A. Association of *MGLL* intronic C>T single nucleotide polymorphism (rs782440) with borderline personality disorder: a case-control study. *Cell J.* 2023; 25(11): 783-789. doi: 10.22074/CELLJ.2023.2004323.1321
This open-access article has been published under the terms of the Creative Commons Attribution Non-Commercial 3.0 (CC BY-NC 3.0).

Introduction

Borderline personality disorder (BPD) is considered as a multidimensional disorder accompanied with main symptoms including impulsivity, repetitive suicidality and dissociative symptoms like instability in impulse

control, and interpersonal relationships which appears in adolescence (between 10-18 years) or adulthood (19-25 years) (1, 2). BPD diagnosis is impeded by other overlapping disorders and lack of a biological profile or specific family history (2, 3).

Received: 08/June/2023, Revised: 04/September/2023, Accepted: 02/October/2023

*Corresponding Addresses: P.O.Box: 6517838736, Research Center for Molecular Medicine, Hamadan University of Medical Sciences, Hamadan, Iran
P.O.Box: 6517838736, Department of Neuroscience, School of Sciences and Advanced Technology in Medicine, Hamadan University of Medical Sciences, Hamadan, Iran

Emails: s.afshar@umsha.ac.ir, sarihi@umsha.ac.ir



Royan Institute
Cell Journal (Yakhteh)

From an etiological point of view, it has been confirmed that BPD is a multifactorial disorder and results from the reaction between environmental and genetic agents. Moreover, according to some familial and twin studies, heredity of BPD which has comorbidity with personality disorders like drug abuse and mood disorder varies between 30 to 70% (4, 5).

The monoacylglycerol lipase (MAGL) enzyme which is encoded by the *MGLL* gene is located on chromosome 3q21.3, and has been shown to be related to BPD (6, 7). *MGLL* is one of the enzymes of the endocannabinoid system (ECS) and belongs to the group serine hydrolase enzymes. The ESC consists of two main endogenous ligands: 2-arachidonoylglycerol (2-AG) which is degraded into arachidonic acid (AA) by MAGL, and anandamide (AEA) (8). In this regard, this enzyme has an important role in determining the amount of 2-AG and AA in the brain. These compounds are related to inflammatory pathways, hence various compound of the ECS such as MAGL could be used as a therapeutic targets (9). It is worth mentioning that the use of ECS agents, especially the anandamide-degrading enzyme fatty acid amide hydrolase (FAAH), and MAGL inhibitors in disorders like neuropsychiatric diseases, is very promising. In this regard, MAGL inhibitors for example, have exhibited anxiolytic and antidepressant effects (10-12).

Due to the high level of AEA in the serum of BPD patients and also the comorbidity of BPD with other neuropsychiatric disorders [like post-traumatic stress disorder (PTSD)] (13), the need for more investigation on the correlation between brain functions and the diseases with plasma level of ECS is extremely felt.

Single nucleotide polymorphisms (SNPs) as the most common genetic differences, have an important role in the study of human health. SNPs could be used to anticipate the risk of developing diseases, response to treatment and so on. Currently, many studies are continuing to identify associated SNPs with several disease such as cancer, diabetes, heart disease, and neurological disorder. Several studies have focused on finding diagnostic biomarkers for various neurological diseases (13-16). Hence, some interesting studies have been conducted on the relationship of ECS related gene polymorphisms with some physiological functions such as psychophysiological modes (such as depression and anxiety), eating disorders, regulation of energy balance, appetite, and also drug (marijuana and alcohol) abuse (10, 17-19). Considering the important role of this gene in the ECS and BPD, the rs782440 SNP, the effects of which was only evaluated on plasma low-density lipoprotein cholesterol, and lack of any in-depth study on the role of *MGLL* in the pathogenesis of BPD, the aim of this study was evaluating the association between BPD and *MGLL* intronic C>T SNP (rs782440).

Materials and Methods

Participants

In this case-control study, all the participants were from a local community in Hamadan, Iran. Diagnosis of BPD was done on the basis of criteria of the Diagnostic and Statistical Manual of Mental Disorders (DSM-5) by psychiatrists (Clinical psychiatric interview) in the psychology department of Farshchian Sina Hospital in Hamadan, Iran. The most important diagnostic criteria for BPD are: impulsivity, repetitive suicidality and dissociative symptoms like instability impulse control, interpersonal relationships and the use of immature defense mechanisms in relationships such as projection, projective identification and splitting. First, a written informed consent was taken from all participants. Next, each subject was given a health and illness assessment form to fill out. The screening population consisted of 110 Iranian subjects consisting 55 patients with BPD and 55 healthy control subjects (20). All of the case participants in this study were collected from patients admitted to the psychiatry department of Farshchian Sina Hospital in years from 2021 to 2022. The inclusion criteria in the study were the clinical diagnosis of BPD based on DSM-5 and informed consent to participate in the study. Exclusion criteria included lack of informed consent and clinical diagnosis of concurrent psychotic disorders and major depressive disorder. All procedures and study protocols applied in the present study were approved by the Mental Health Research Committee at Medical School of Hamadan University of Medical Sciences (IR.UMSHA.REC.1399.942).

DNA extraction and genotyping

Five ml of the Subjects' blood was drained into a vacuum tube with EDTA. The DNA was extracted from the blood samples via the genome DNA extraction kit DNG (Sinaclon, Iran) and was stored in -20°C. The sanger sequencing method was used for the genotyping of *MGLL* intronic C>T SNP (rs782440). The primer pair for sanger sequencing was designed through the Allele ID 6 software and the specificity of the designed primer pair was evaluated with NCBI Primer BLAST. The designed primers (F: AACTAACAGCAGGCAGGTTGACA and R: AACTAACAGCAGGCAGGTTGACA) with amplicon size 459 bp were synthesized by TAG Copenhagen (Denmark). Moreover, the temperature program in the thermal cycler was as follows: Initial denaturation was done for 5 minutes at 95°C and continued to the next steps by 35 cycles of 95°C for 30 seconds, 62°C for 30 seconds, and 72°C for 45 seconds and final extension for 5 minutes at 72°C.

Finally, PCR amplicons were sequenced with Sanger sequencing (ABI 3500). The genotype for each sample

was evaluated through aligning the sequenced amplicon and reference genome sequence using the CLC Genomic Workbench software version 11.0.1 (Fig.1) (16).

Statistical analysis

In the study, qualitative values such as sex and education were described by frequency and percentage. Also, to describe quantitative variables (e.g., age), mean ± SD was used. The Chi-Square test was used to verify the establishment of the Hardy-Weinberg equilibrium. However, due to lack of this equilibrium, the expectation-maximization (EM) algorithm method was used to estimate allelic frequencies by the R software (version 3.2.2). The Chi-square test was used to compare the demographic variables in case and control groups. In addition, Logistic regression was used to compare the phenotypes and alleles frequencies in the case and control groups. Univariate and Multiple logistic regression models were used to obtain crude and adjusted odds-ratios, respectively.

Dominant and recessive genetic models were used to further compare the association between the variants in the case and control groups. The significance level in this research was considered less than 0.05. The proportion of T allele of the rs782440 codon is equal to 49.5% in controls (20), and we assumed that its frequency between the cases is about 50%. Considering that the maximum significant difference was $d=0.2$, a type I error level of 5% and test power of 90%, the sample size in each group was estimated to be 48 samples, while in this study 53 samples were used in each group.

Results

The present study was conducted on a sample of 106

patients, including 53 cases and 53 controls, who were selected in regards to age and gender. In the control group, 38.2% of the subjects belonged to the age group between 15-24 years, 56.4% were 25-34 years old, and 5.5% of them were in the 35 to 45 range of age. Moreover, 27.3% were female and 72.2% were male. On the other hand, in the case group, 41.8% of the patients were 15-24 years old, 41.8% were 25-34 and 16.4% were 35-45. Moreover, regarding gender, in the BPD group 25.5% were female and 74.5% were male.

Since the Hardy-Weinberg equilibrium was not established, allele frequencies (C and T) were estimated via the EM algorithm, (Table 1). According to the obtained results, 37 subjects (42.5%) in the control group and 28 patients (37.8%) in the case group possessed the T allele.

Moreover, by using the logistic regression model, it was observed that the case and control groups showed no significant differences in terms of the frequency of C and T alleles (OR=1.26, CI=0.645-2.91, P=0.55). The TT genotype compared to the CC genotype had a significant difference in both case and control groups and the TT genotype increased the risk of BPD by 6.679% compared to the CC genotype (OR=6.679, CI=1.974-22.596, P=0.002).

On the other hand, the results of the current study revealed a significant difference between the TC and CC genotypes in both groups and the TC genotype increased the risk for BPD by 4/817% compared to the CC genotype (OR=4.817, CI=1.324-17.527, P=0.02) (Table 2).

In fact, one reason why we did not find the allele significant in this study but found the genotypes significant, could be that the frequency of TT is much higher than CC genotypes.

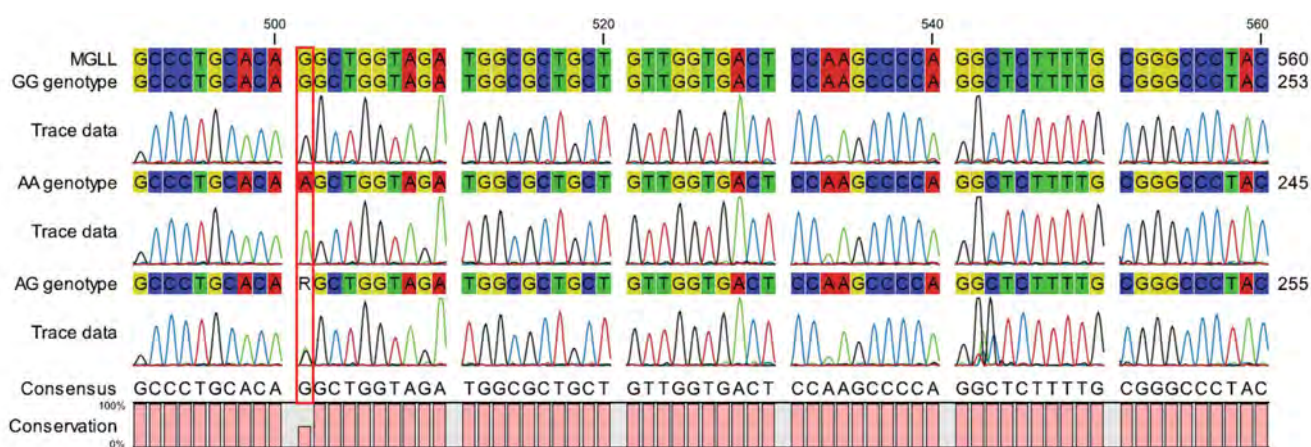


Fig.1: Sanger sequencing analysis for three samples. Sequence analysis for three samples including GG, AA, and AG genotypes are shown.

Table 1: Demographic information of participants

Variables	Control n (%)	Case n (%)	Chi-square (df)	P value
Age (Y)				
15-24=1	21 (38.2)	23 (41.8)	4.276 (2)	0.12
25- 34=2	31 (56.4)	23 (41.8)		
35-45=3	3 (5.5)	9 (16.4)		
Sex				
Female	15 (27.3)	14 (25.5)	0.047 (1)	0.83
Male	40 (72.7)	41 (74.5)		
Education				
Under-educated=0	3 (5.5)	29 (52.7)	29.792 (1)	0.001
Diploma and above=1	52 (94.5)	26 (47.3)		

Table 2: Genotype and allele frequencies distribution in BPD patients and healthy control subjects

Allele/Genotype/Model	Control	Case	OR-CI (95%)	P value	Adjusted OR-CI (95%)	P value
Allele, n (%) [*]						
T	37 (42.5)	28 (37.8)	1.216 (0.645-2.91)	0.55 ^{**}	–	–
C (ref)	50 (57.5)	46 (62.2)	–	–	–	–
Genotype, n (%)						
TT	33 (61.1)	21 (39.6)	6.629 (1.974-22.596)	0.002 ^{**}	7.08 (1.977-25.374)	0.003 ^{***}
TC	17 (31.5)	15 (28.3)	4.817 (1.324-17.527)	0.02 ^{**}	3.483 (0.892-13.601)	0.07
CC (ref.)	4 (7.4)	17 (32.1)	-	–	–	–
Recessive model						
TT	33 (61.1)	21 (39.6)	2.395 (1.102-5.203)	0.03 ^{**}	2.364 (1.057- 5.286)	0.04 ^{***}
TC+CC	21 (38.9)	32 (60.4)	–	–	–	–
Dominant model						
TT+TC	50 (92.6)	36 (67.9)	5.903 (1.831-19.027)	0.003 ^{**}	5.847 (1.762-19.395)	0.004 ^{***}
CC	4 (7.4)	17 (32.1)	–	–	–	–

*; Allele frequencies T and C were estimated by the expectation-maximization (EM) algorithm, because the Hardy-Weinberg equilibrium was not observed, **; The P values were determined using univariate logistic regression model, ***; The P values were determined using multiple-logistic regression model. In this model, the results were adjusted by sex and age, OR; Odds ratio, and CI; Confidence interval.

Discussion

For gaining deeper understanding regarding the pathology of BPD, clarification for ambiguities of the neurotransmitter systems and genetic factors related to BPD is necessary (21). The *MGLL* gene has been studied polymorphically in diseases with similar signaling pathways (20, 22, 23) but it has not yet been investigated in BPD.

The aim of this study was investigating the effect of *MGLL* intronic C>T SNP (rs782440) on BPD. Therefore, the fundamental role of the genetic basis of BPD and the relationship between the desired polymorphism and etiology of BPD was clarified and strengthened. This SNP is located in the intronic region of long arm of chromosome 3. The bioinformatics prediction analysis indicated that this intronic region contains a distal enhancer-like signature (EH38E2235794). This SNP which affects the CTCF-bound sequence may have a role in regulation of *MGLL* expression (<http://genome.ucsc.edu>).

In the current study it was hypothesized and the results confirmed that the risk of BPD increased with some genotypes such as the TT and AT genotypes, compared to the CC genotype but no significant difference in the frequency of alleles C and T was found, from which it could be inferred that the frequency of the TT genotypes is much higher than the CC genotypes. Moreover, despite the significant correlation between BPD and the ECS, according to our knowledge, this report is the first study to examine the link between one of the genetic polymorphisms of ECS and BPD.

The lifelong perspective of BPD from adolescence to adulthood is characterized by a change in symptoms of BPD such as affective dysregulation, suicidality and impulsivity at the age of 10-18 years toward abnormal interpersonal relationships, functional abnormality, as well as subsequent recurrence and collapse period as the main symptoms in adulthood (24, 25). In this study overlaps of other neuropsychiatric disorder symptoms with BPD were considered, so in this respect patients were selected by psychiatrists based on the Diagnostic and Statistical Manual of Mental Disorders (DSM-5) scale.

Previous studies have revealed a connection between various aspects and characteristics of BPD with some genes or their variants (FKBP5a co-chaperone of the glucocorticoid receptor) (26), the oxytocin receptor (OXTR) (27), and monoamine oxidase-A (MAOA-L) (28). Moreover, recent studies have indicated that both *SERT* and *BDNF* genes are associated with BPD symptoms (29). In the current report, the association between the *MGLL* gene and BPD has been studied for the first time.

The ECS related genes polymorphisms can affect some psychophysiological modes such as depression, anxiety, eating disorders, regulation of energy balance, appetite, and also drug abuse (10, 17-19). Furthermore, the relation between the *MGLL* gene and various disorders like brain tumors, nicotine dependency, inflammatory pain and

metabolic diseases has been revealed (20, 30-32). For example, the rs3773159 variant of *MGLL* was associated with type 2 diabetes, while the rs684358 variant of *MGLL* was associated with high body mass index (BMI) (33, 34).

Similarly, Ouellette et al. (20) have conducted a related study on gene variants of *MGLL* and low density lipoprotein which are involved in the same signaling pathway, as *MGLL* is involved in the metabolic pathways related to lipoprotein TG. The result of their research which is consistent with the results of the current study, revealed that in *MGLL* intronic C>T SNP (rs782440), the TT genotype shows a higher risk for particle size of LDL.

In one study regarding the effect of dronabinol (Cannabinoid Agonist) on the colonic motility of Patients with Irritable Bowel Syndrome, showed a modest relation between *MGLL* variant and colonic motility and tone (35). Such studies are in line with the current paper about the *MGLL* gene, but similar to BPD it requires more studies.

However, in contrast to the results of the current study and previously mentioned studies regarding the involvement of ECS variant genes, in a study of association of 15 genetic variants genes of ECS such as *FAAH* and *MGLL*, using 91 German subjects with anorexia nervosa (AN), no major association between this SNP with AN was found (36). Taking into consideration weight and diet, using ECS compound changes as a biomarker can be enlightening to some extent (37, 38).

Anandamide (AEA)-degrading enzyme (FAAH) and ECS receptors including CB1 and CB2 (18, 39) are the main members of ECS. A series of studies have also been done on ECS and drugs that may be abused. One of them, revealed that *MGLL* in connection with *FAAH* and *CBI*, is associated with mood changes caused by THC, so that inhibition of *MGLL* mimics the pseudo-antidepressant properties of THC. In accordance with this issue, childhood adversity and cannabis abuse have been associated with *MGLL* SNP (rs604300) (40).

It is worth mentioning that in contrast to the present study, a study conducted on Japanese population in the context of alcoholism with 14 variants of the *MGLL* gene, did not show any significant effects of these genotype on alcoholism (22).

In addition, the findings of this study is in line with the study of Harismendy et al. (33), showing a relationship between two locus-variants of *MGLL* with extreme obesity and also clarified the connection between *MGLL* intron 3 locus interval of rs684358 with BMI.

Conclusion

The results have revealed that *MGLL* intronic C>T SNP (rs782440) has a great effect on the psychopathology of BPD and may be helpful as a potential both in the treatment field and in new and challenging studying programs. However, it is suggested that more research should be conducted in order to provide further knowledge regarding the role of various compounds of ECS such as

MGLL, *FAAH*, *CBI*, *CB2*, etc. Furthermore, various types of polymorphisms in diseases and disorders related to the ECS system, such as BPD, addiction, eating disorders, anxiety, depression, and complex post-traumatic stress disorder have been shown.

For gaining clear knowledge regarding *MGLL*, further research at genetic, molecular, pathophysiological, and physiological levels must be conducted. Moreover, the current study faced some limitations therefore more specialized investigations in different contexts of BPD and statistical populations is required.

Acknowledgments

This research was a part of the Ph.D. thesis of Nazanin Hatami at The Department of Neurosciences, Faculty of new Sciences and Technologies in Medicine, Hamadan University of Medical Sciences and was funded by the research deputy of Hamadan University of Medical Sciences and Neurophysiology Research Center (Grant Number: 1400011045), Hamadan, Iran. There is no conflict of interest in this study.

Authors' Contributions



S.A.K., N.H.B., L.J., M.S., A.S., S.A.; Conceptualization, Methodology, and Software. N.H.B., L.J., M.S., A.S., S.A.; Writing- Reviewing and Editing. A.S., S.A., M.S.; Data curation and Supervision. N.H.B., A.S., S.A.; Writing- Original draft preparation. A.R.S.; Statistical analysis. N.H.B., E.Sh.; Visualization and Investigation. N.H.B., S.A.; Software and Validation. All authors read and approved the final manuscript.

Reference

- Chanen AM, Betts JK, Jackson H, Cotton SM, Gleeson J, Davey CG, et al. A comparison of adolescent versus young adult outpatients with first-presentation borderline personality disorder: findings from the MOBY randomized controlled trial. *Can J Psychiatry*. 2022; 67(1): 26-38.
- Kaplan B, Yazici Gulec M, Gica S, Gulec H. The association between neurocognitive functioning and clinical features of borderline personality disorder. *Braz J Psychiatry*. 2020; 42(5): 503-509.
- Mulder RT, Newton-Howes G, Crawford MJ, Tyrer PJ. The central domains of personality pathology in psychiatric patients. *J Pers Disord*. 2011; 25(3): 364-377.
- Lubke GH, Laurin C, Amin N, Hottenga JJ, Willemsen G, van Grootheest G, et al. Genome-wide analyses of borderline personality features. *Mol Psychiatry*. 2014; 19(8): 923-929.
- Siever LJ, Torgersen S, Gunderson JG, Livesley WJ, Kendler KS. The borderline diagnosis III: identifying endophenotypes for genetic studies. *Biol Psychiatry*. 2002; 51(12): 964-968.
- Aliczki M, Varga ZK, Balogh Z, Haller J. Involvement of 2-arachidonoylglycerol signaling in social challenge responding of male CD1 mice. *Psychopharmacology (Berl)*. 2015; 232(12): 2157-2167.
- Bhatia G, Bansal V, Harismendy O, Schork NJ, Topol EJ, Frazer K, et al. A covering method for detecting genetic associations between rare variants and common phenotypes. *PLoS Comput Biol*. 2010; 6(10): e1000954.
- McAllister LA, Butler CR, Mente S, O'Neil SV, Fonseca KR, Piro JR, et al. Discovery of trifluoromethyl glycol carbamates as potent and selective covalent monoacylglycerol lipase (MAGL) inhibitors for treatment of neuroinflammation. *J Med Chem*. 2018; 61(7): 3008-3026.
- Grabner GF, Eichmann TO, Wagner B, Gao Y, Farzi A, Taschler U, et al. Deletion of monoglyceride lipase in astrocytes attenuates lipopolysaccharide-induced neuroinflammation. *J Biol Chem*. 2016; 291(2): 913-923.
- Bedse G, Bluett RJ, Patrick TA, Romness NK, Gaulden AD, Kingsley PJ, et al. Therapeutic endocannabinoid augmentation for mood and anxiety disorders: comparative profiling of FAAH, MAGL and dual inhibitors. *Transl Psychiatry*. 2018; 8(1): 92.
- Ogawa S, Kunugi H. Inhibitors of fatty acid amide hydrolase and monoacylglycerol lipase: new targets for future antidepressants. *Curr Neuropharmacol*. 2015; 13(6): 760-775.
- Wang Y, Gu N, Duan T, Kesner P, Blaskovits F, Liu J, et al. Monoacylglycerol lipase inhibitors produce pro- or antidepressant responses via hippocampal CA1 GABAergic synapses. *Mol Psychiatry*. 2017; 22(2): 215-226.
- Kolla NJ, Mizrahi R, Karas K, Wang C, Bagby RM, McMain S, et al. Elevated fatty acid amide hydrolase in the prefrontal cortex of borderline personality disorder: a [¹¹C]CURB positron emission tomography study. *Neuropsychopharmacology*. 2020; 45(11): 1834-1841.
- Izzo NJ, Yuede CM, LaBarbera KM, Limegrover CS, Rehak C, Yurko R, et al. Preclinical and clinical biomarker studies of CT1812: A novel approach to Alzheimer's disease modification. *Alzheimers Dement*. 2021; 17(8): 1365-1382.
- Moradi S, Tapak L, Afshar S. Identification of novel noninvasive diagnostics biomarkers in the parkinson's diseases and improving the disease classification using support vector machine. *Biomed Res Int*. 2022; 2022: 5009892.
- Salem E, Keshvari A, Mahdavinhezad A, Soltanian AR, Saidijam M, Afshar S. Role of EFNA1 SNP (rs12904) in tumorigenesis and metastasis of colorectal cancer: a bioinformatic analysis and HRM SNP genotyping verification. *Asian Pac J Cancer Prev*. 2022; 23(10): 3523-3531.
- Ando T, Tamura N, Mera T, Morita C, Takei M, Nakamoto C, et al. Association of the c.385C>A (p.Pro129Thr) polymorphism of the fatty acid amide hydrolase gene with anorexia nervosa in the Japanese population. *Mol Genet Genomic Med*. 2014; 2(4): 313-318.
- Lazary J, Eszlari N, Juhasz G, Bagdy G. A functional variant of CB2 receptor gene interacts with childhood trauma and FAAH gene on anxious and depressive phenotypes. *J Affect Disord*. 2019; 257: 716-722.
- Palmer RHC, McGeary JE, Knopik VS, Bidwell LC, Metrik JM. CNR1 and FAAH variation and affective states induced by marijuana smoking. *Am J Drug Alcohol Abuse*. 2019; 45(5): 514-526.
- Ouellette C, Rudkowska I, Lemieux S, Lamarche B, Couture P, Vohl MC. Gene-diet interactions with polymorphisms of the *MGLL* gene on plasma low-density lipoprotein cholesterol and size following an omega-3 polyunsaturated fatty acid supplementation: a clinical trial. *Lipids Health Dis*. 2014; 13: 86.
- Joyce PR, Stephenson J, Kennedy M, Mulder RT, McHugh PC. The presence of both serotonin 1A receptor (HTR1A) and dopamine transporter (DAT1) gene variants increase the risk of borderline personality disorder. *Front Genet*. 2014; 4: 313.
- Iwasaki S, Ishiguro H, Higuchi S, Onaivi ES, Arinami T. Association study between alcoholism and endocannabinoid metabolic enzyme genes encoding fatty acid amide hydrolase and monoacylglycerol lipase in a Japanese population. *Psychiatr Genet*. 2007; 17(4): 215-220.
- Tardelli M. Monoacylglycerol lipase reprograms lipid precursors signaling in liver disease. *World J Gastroenterol*. 2020; 26(25): 3577-3585.
- Newton-Howes G, Clark LA, Chanen A. Personality disorder across the life course. *Lancet*. 2015; 385(9969): 727-734.
- Zanarini MC, Frankenburg FR, Reich DB, Conkey LC, Fitzmaurice GM. Treatment rates for patients with borderline personality disorder and other personality disorders: a 16-year study. *Psychiatr Serv*. 2015; 66(1): 15-20.
- Amad A, Ramoz N, Peyre H, Thomas P, Gorwood P. FKBP5 gene variants and borderline personality disorder. *J Affect Disord*. 2019; 248: 26-28.
- Zhang M, Liu N, Chen H, Zhang N. Oxytocin receptor gene, childhood maltreatment and borderline personality disorder features among male inmates in China. *BMC Psychiatry*. 2020; 20(1): 332.
- Kolla NJ, Meyer J, Sanches M, Charbonneau J. Monoamine oxidase-a genetic variants and childhood abuse predict impulsiveness in borderline personality disorder. *Clin Psychopharmacol Neurosci*. 2017; 15(4): 343-351.
- Salinas V, Villarreal J, Silva H, Herrera L, Jerez S, Zazueta A, et al. SERT and BDNF polymorphisms interplay on neuroticism in borderline personality disorder. *BMC Res Notes*. 2020; 13(1): 61.
- Hohmann AG. Inhibitors of monoacylglycerol lipase as novel anal-

- gesics. *Br J Pharmacol.* 2007; 150(6): 673-675.
31. Li X, Gao S, Li W, Liu Z, Shi Z, Qiu C, et al. Effect of monoacylglycerol lipase on the tumor growth in endometrial cancer. *J Obstet Gynaecol Res.* 2019; 45(10): 2043-2054.
 32. Muldoon PP, Chen J, Harenza JL, Abdullah RA, Sim-Selley LJ, Cravatt BF, et al. Inhibition of monoacylglycerol lipase reduces nicotine withdrawal. *Br J Pharmacol.* 2015; 172(3): 869-882.
 33. Harismendy O, Bansal V, Bhatia G, Nakano M, Scott M, Wang X, et al. Population sequencing of two endocannabinoid metabolic genes identifies rare and common regulatory variants associated with extreme obesity and metabolite level. *Genome Biol.* 2010; 11(11): R118.
 34. Rao P, Zhou Y, Ge SQ, Wang AX, Yu XW, Alzain MA, et al. Validation of type 2 diabetes risk variants identified by genome-wide association studies in Northern Han Chinese. *Int J Environ Res Public Health.* 2016; 13(9): 863.
 35. Wong BS, Camilleri M, Busciglio I, Carlson P, Szarka LA, Burton D, et al. Pharmacogenetic trial of a cannabinoid agonist shows reduced fasting colonic motility in patients with nonconstipated irritable bowel syndrome. *Gastroenterology.* 2011; 141(5): 1638-1647. e1-7.
 36. Müller TD, Reichwald K, Brönner G, Kirschner J, Nguyen TT, Scherag A, et al. Lack of association of genetic variants in genes of the endocannabinoid system with anorexia nervosa. *Child Adolesc Psychiatry Ment Health.* 2008; 2(1): 33.
 37. Bourdy R, Hertz A, Filliol D, Andry V, Goumon Y, Mendoza J, et al. The endocannabinoid system is modulated in reward and homeostatic brain regions following diet-induced obesity in rats: a cluster analysis approach. *Eur J Nutr.* 2021; 60(8): 4621-4633.
 38. Tagliamonte S, Laiola M, Ferracane R, Vitale M, Gallo MA, Meslier V, et al. Mediterranean diet consumption affects the endocannabinoid system in overweight and obese subjects: possible links with gut microbiome, insulin resistance and inflammation. *Eur J Nutr.* 2021; 60(7): 3703-3716.
 39. Gil-Ordóñez A, Martín-Fontecha M, Ortega-Gutiérrez S, López-Rodríguez ML. Monoacylglycerol lipase (MAGL) as a promising therapeutic target. *Biochem Pharmacol.* 2018; 157: 18-32.
 40. Carey CE, Agrawal A, Zhang B, Conley ED, Degenhardt L, Heath AC, et al. Monoacylglycerol lipase (MGLL) polymorphism rs604300 interacts with childhood adversity to predict cannabis dependence symptoms and amygdala habituation: Evidence from an endocannabinoid system-level analysis. *J Abnorm Psychol.* 2015; 124(4): 860-877.
-

The Effect of Mesenchymal Stem Cells Derived-Conditioned Media in Combination with Oral Anti-Androgenic Drugs on Male Pattern Baldness: An Animal Study

Majid Kamali-Dolat Abadi, M.Sc.¹, Gholamhossein Yousefi, Ph.D.², Farzaneh Dehghani, Ph.D.^{3,4}, Ali Akbar Alizadeh, Ph.D.¹, Abolfazl Jangholi, M.Sc.⁵, Mohammad Amin Moadab, B.Sc.⁶, Maryam Naseh, Ph.D.³, Shima Parsa, M.D.⁷, Golara Nasiri, Ph.D.⁸, Negar Azarpira, M.D., Ph.D.^{7*} , Mehdi Dianatpour, Ph.D.^{9,10*} 

1. Department of Tissue Engineering and Applied Cell Sciences, School of Advance Medical Science and Technology, Shiraz University of Medical Sciences, Shiraz, Iran

2. Department of Pharmaceutics, School of Pharmacy, Shiraz University of Medical Sciences, Shiraz, Iran

3. Histomorphometry and Stereology Research Center, Shiraz University of Medical Sciences, Shiraz, Iran

4. Department of Anatomical Sciences, School of Medicine, Shiraz University of Medical Sciences, Shiraz, Iran

5. Department of Biology, Faculty of Science, Razi University, Kermanshah, Iran

6. Department of Biology, Zand Institute of Higher Education, Shiraz, Iran

7. Transplant Research Center, Shiraz University of Medical Sciences, Shiraz, Iran

8. Department of Tissue Engineering and Cell Therapy, School of Advanced Technologies in Medicine, Shiraz University of Medical Sciences, Shiraz, Iran

9. Stem Cell Technology Research Center, Shiraz University of Medical Sciences, Shiraz, Iran

10. Department of Medical Genetics, School of Medicine, Shiraz University of Medical Sciences, Shiraz, Iran

Abstract

Objective: Androgenetic alopecia (AGA) is a prevalent form of hair loss, mainly caused by follicular sensitivity to androgens. Despite developing different anti-androgen treatment options, the success rate of these treatments has been limited. Using animal models, this study evaluated the therapeutic effects of umbilical cord (UC) stem cell conditioned media (CM) combined with oral anti-androgens for hair regeneration.

Materials and Methods: In this experimental study, Poloxamer 407 (P407) was used as a drug carrier for subcutaneous testosterone injection. AGA models were treated with oral finasteride, oral flutamide, and CM injections. Samples were thoroughly evaluated and compared using histological, stereological, and molecular analyses.

Results: Injecting CM-loaded hydrogel alone or combined with oral intake of anti-androgens improved hair regeneration. These treatments could promote hair growth by inducing hair follicles in the anagen stage and shortening the telogen and catagen phases. Furthermore, the combination treatment led to an upregulation of hair induction gene expression with a downregulation of inflammation genes.

Conclusion: Through a reduction in inflammation, injection of CM-loaded hydrogel alone or combined with oral intake of anti-androgens induces the hair cell cycle with regeneration in damaged follicles. Hence, this could be a promising therapeutic method for AGA patients.

Keywords: Androgenetic Alopecia, Conditioned Media, Finasteride, Flutamide, Mesenchymal Stem Cells

Citation: Kamali-Dolat Abadi M, Yousefi Gh, Dehghani F, Alizadeh AA, Jangholi A, Moadab MA, Naseh M, Parsa Sh, Nasiri G, Azarpira N, Dianatpour M. The effect of mesenchymal stem cells derived-conditioned media in combination with oral anti-androgenic drugs on male pattern baldness: an animal study. Cell J. 2023; 25(11): 790-800. doi: 10.22074/CELLJ.2023.2008138.1377

This open-access article has been published under the terms of the Creative Commons Attribution Non-Commercial 3.0 (CC BY-NC 3.0).

Introduction

Androgenetic alopecia (AGA) is the most prevalent form of hair loss affecting 80% of men and 50% of women over their lives. AGA is influenced by androgen and characterized by persistent, gradual and patterned hair thinning in defined areas of the scalp. Genetic inheritance and androgen levels are two major risk factors for AGA (1). Notably, the binding of dihydrotestosterone (DHT), a

metabolite of testosterone, to the androgen receptor (AR) is a crucial factor in the pathogenesis of this condition. As DHT accumulates in androgen-sensitive tissues, a progressive shrinking and thinning of the affected areas occur, eventually leading to alopecia (2). Despite AGA's prevalence and adverse effects, there is currently no universally accepted treatment for this condition. Drug therapies and follicular unit transplantation are routine treatment options for AGA. However, these treatment

Received: 30/July/2023, Revised: 16/September/2023, Accepted: 07/October/2023

*Corresponding Addresses: P.O.Box: 7193635899, Transplant Research Center, Shiraz University of Medical Sciences, Shiraz, Iran

P.O.Box: 7134845794, Department of Medical Genetics, School of Medicine, Shiraz University of Medical Sciences, Shiraz, Iran

Emails: azarpiran@sums.ac.ir, dianatpour@sums.ac.ir



Royan Institute
Cell Journal (Yakhteh)

options cannot cure AGA effectively and permanently (3). Therefore, it is essential to develop novel therapeutic strategies to discover more effective treatment options.

The use of AR antagonists presents a potential therapeutic approach for AGA. Flutamide, a nonsteroidal anti-androgen drug, was shown to block the action of both endogenous and exogenous testosterone through binding to AR (4). Finasteride is the first food and drug administration (FDA)-approved oral treatment for AGA which acts through selective inhibition of type II 5 α reductase. Finasteride reduces follicular shrinkage by irreversibly binding to the enzyme and blocking the production of DHT from testosterone (5). While flutamide, finasteride, and other chemical drugs are used as primary alopecia therapies, their potential synergistic effects and undesirable side effects have remained unclear (6).

The dermal papilla (DP) of the hair follicle (HF) is a critical signalling region responsible for sustaining hair development, regulating hair formation and cycling by paracrine secretion (7). Accordingly, a poor DP microenvironment may lead to hair loss. Additionally, androgen-induced changes in autocrine or paracrine compounds of DP cells are associated with HF stem cell dysfunction (8). In this regard, regenerative medicine using cell products and tissue engineering can be a suitable treatment for hair loss. Treatments based on cell therapy are among the suggested approaches, which play an essential role in migrating endothelial cells, fibroblasts and skin cells due to proliferation intensifiers (9). Stem cell therapy is a new technique for treating hair loss (HL) using exogenous cell sources or progenitor cells (PCs), such as follicular stem cells and the umbilical cord (UC) that are used in clinical trials (10). Another approved regenerative medicine method is thermo-sensitive gel products, a simple, low-cost method with a slow-release property (11). Poloxamer 407 (P407) system is a thermo-sensitive and high-quality carrier in drug delivery. P407 is in the form of a gel at a temperature close to the body (37°C) and remains as a stable carrier at the injection site (12). In addition, several studies have shown that conditioned media (CM) can influence hair stem cell activation and angiogenesis, accelerated hair density, and increased volume in AGA patients (13, 14). Indeed, dental pulp stem cells-derived CM (dental-MS) have the ability to activate hair follicles, neural cells, adipocytes, and dentin-producing cells (13).

In the embryonic ectoderm germ layer, these multipotent cells originate from temporary neural crest cells. The ability of these stem cells to differentiate into other cells may make them useful in the treatment of different disorders. Furthermore, CM contains multiple growth factors released by stem cells, which may be effective in repairing tissue under different conditions (15).

Mesenchymal stem cells (MSCs), immature precursors derived from the mesoderm, possess self-renewal capabilities and the capacity for multilineage differentiation. Studies have demonstrated that paracrine

factors secreted in CM are primarily responsible for the therapeutic activity observed in MSC. In CM therapy, extracellular vesicles (EVs) and soluble factors are transferred to activate signalling pathways. EVs contain various components including mRNAs, miRNA, growth factors and cytokines. Retrospective human studies have demonstrated that CM regulates the hair cycle and the regeneration of hair follicles.

Early hair regression is thought to be caused by DHT, a hormone derived from testosterone. Moreover, it was found that it reduced the volume of the cellular hair matrix and reduced the duration of the anagen growth phase in genetically susceptible hair follicles. The DHT synthesis inhibitor (DHT-inhibitor) is regarded as one of the most important metabolites in hair development, although it is not able to completely alleviate hair loss. Despite this, long-term treatment of AGA with DHT inhibitors has been documented in well-controlled clinical trials to be both effective and safe. As reported by Kamishima et al. (13), androgen inhibitors are quite beneficial, especially when started at an early stage of the disease.

In this study, CM, a mixture of growth factors and peptides derived from stem cells, was loaded in P407 thermosensitive hydrogel and injected into the alopecia-induced mice model. The effects of CM-rich P407 thermosensitive gel in combination with oral anti-androgens on hair growth and its inhibitory effect on hair loss at the molecular level were investigated. In addition, we examined two forms of AGA strategy with different natures, the first one is anti-androgens, and the second one is based on cell therapy.

Materials and Methods

Isolation and characterization of human umbilical cords mesenchymal stem cells

This experimental study was approved by the Shiraz University of Medical Sciences Ethics Committee (IR.SUMS.REC.1398.855). After obtaining written informed consent, UCs were collected from women (18 to 30 years old) who underwent cesarean section. The cords were cultured in a culture plate containing minimum essential medium eagle-alpha modification (Alpha MEM) (Shellmax, USA) supplemented with 10% fetal bovine serum (FBS, Gibco, Life, USA) and 1% penicillin-streptomycin at 37°C with 5% CO₂. The culture medium was changed every three days (16). Cell surface markers, including HLADR, CD44, CD90, and CD34, were analyzed using a FACSCalibur™ flow cytometer (Becton Dickinson, USA) to confirm the isolated cells. The certainty of the mesenchymal origin of cells was also evaluated by differentiation into osteoblasts and adipocytes using each specific differentiation medium (Gibco Life, USA) (17).

Preparation of condition media

Cells were selected, trypsinized (0.25%) and cultured in DMEM/F-12 (Shellmax, USA) supplemented with

10% FBS until 70 to 80% confluency. After 48 hours of incubation in a serum-free medium, CM was harvested. The media was collected, spun at 1000 rpm for 5 minutes to remove cell debris, and filtered through a 0.22 µm syringe filter, then freeze-dried, and stored at -20°C.

Preparation of thermo-sensitive Poloxamer 407 (P407) System

Injectable thermosensitive P407 was used as a testosterone carrier for sustained-release drug delivery. The P407 powder was dissolved at a concentration of 21% in phosphate-buffered saline (PBS) and Ethanol with a volume ratio of 80/20. Then, a testosterone injection solution (ALL-TEST-2433) was added to the P407 gel at a 5 gr/ml ratio. This solution was used in the early stages of the study to induce alopecia in animals. Furthermore, P407 maintained the slow release of umbilical cord MSC-CM (UC-MSc-CM). To achieve this, a suitable amount (200 µg) of dried CM was dissolved in P407 gel without ethanol to reach a concentration of 22% at 15°C (12, 18).

Evaluating the release rate of testosterone and conditioned media loaded in the gel

UV spectroscopy was used to analyze the *in vitro* release profiles of P407-CM and P407-testosterone. The *in vitro* release of CM and testosterone was investigated by placing two vials with known concentrations of P407-CM and P407-testosterone in a shaker incubator at 37°C for 15 minutes until a gel formed. After that, 1.5 ml of phosphate buffer (pH=7.4) was added to each container. The samples were obtained at specified time intervals (periods), replaced with the same volume of pre-warmed fresh PBS, and centrifuged for 15 minutes at 12000 rpm. The absorbance was recorded at 240 nm using a UV-visible spectrophotometer. The Bradford assay was also used to assess the concentration of CM (18, 19).

Animal groups

Six-week-old male C57BL/6 mice (35-50 g) were acquired from the Shiraz University of Medical Sciences Animal Lab. For each group, six male mice were placed into separate cages to prevent interference between them. The housing and handling of mice were conducted based on the Ethics Committee guidelines in cages at ambient temperature (25 ± 2°C), and the mice were fed standard mouse chow and water ad libitum under light/dark cycles of 12 hours and 12 hours. Dorsal skin hair was shaved in 48 mice, and they were categorized into eight groups as listed in Table 1. Then subcutaneous injection of testosterone with Poloxamer 407 (P407) carrier was used to induce alopecia in mice. For injection, 0.2 ml of gel containing 2 mg of CM was used in two stages on days 1 and 21. The mice were evaluated daily for changes in hair loss and growth, and the photographs were taken in

the first and last days of the study. Finally, the mice were sacrificed 42 days after the start of the study (14, 20).

Table 1: Classification of studied mice for different treatments

Groups	Treatment
PBS	PBS=every 4 days
P407	P407=every 4 days
P.T	P.T=every 4 days
CM	P.T=every 4 days, CM=Day 1 and 21 of the study
Fl	P.T=every 4 days, Fl=everyday
CM.Fl	P.T=every 4 days, Fl=everyday, CM=Day 1 and 21 of the study
Fin	P.T=every 4 days, Fin=everyday
CM.Fin	P.T=every 4 days, Fin=everyday, CM=Day 1 and 21 of the study

PBS; Phosphate-buffered saline, P407; Poloxamer 407, P.T; Poloxamer 407+Testosterone, CM; Poloxamer 407+umbilical cord stem cell conditioned media, Fl; Oral flutamide, and Fin; Oral finasteride.

Anti-androgenic treatment

Flutamide and finasteride, an androgen antagonist and a 5-alpha reductase inhibitor, respectively, were utilized as oral anti-androgenic drugs (Table 1). The mice were fed daily with flutamide at a dose of 1.75 g/ml in soybean oil and finasteride at a concentration of 0.007 mg/ml in water.

Excisional biopsy and sample preparation

On the final day of the experiment, animals were sacrificed for histological, stereological, and molecular analysis. Samples were collected from the area between 0.5-1 mm below the dermo-epidermal junction.

Stereological analysis

A full-thickness dorsal skin sample (2×2 cm²) was removed and subsequently fixed in buffered formaldehyde for stereological assessment. The specimen was sectioned into 0.5×0.5 cm², and nine pieces were selected according to the systematic random sampling method. Using a microtome, the sample pieces were embedded in a paraffin block and sectioned with 5 µm and 20 µm thickness. Then, Heidenhain's Azan trichrome and hematoxylin-eosin were used to stain 5 µm and 20 µm sections, respectively (Fig.1A, B).

Estimation of the volume density

Microscopic skin analyses were carried out by a video-microscopy system (Nikon E-200, Tokyo, Japan). The point-counting method was utilized to estimate the volume densities of the dermis, epidermis, hypodermis, collagen bundles, and vessels. Briefly, a point grid was superimposed on the images of the 5 µm thickness skin

on the monitor using stereology software designed by Shiraz University of Medical Sciences, Shiraz, Iran (Fig.1A). The volume density (Vv) was measured using the following formula (21):

$Vv(\text{structure, reference}) = \Sigma P(\text{structure}) / \Sigma P(\text{reference})$
Where " $\Sigma(\text{reference})$ " and " $\Sigma P(\text{structure})$ " are the whole skin sections and the total points hitting the favoured structures, respectively.

Estimation of the numerical density

To obtain the numerical density (number of the cells per unit volume of the dermis; Nv) of the fibroblasts, the 20 μm slides were analyzed using the "optical dissector" method (Fig.1B), and Nv was calculated using the following formula (15):

$$Nv = [\Sigma Q / \Sigma P \times a / f \times h] \times [t / BA]$$

where " ΣQ " represents the total number of cells counted during scanning the section thickness (on average, 700 neurons and 600 oligodendrocytes per animal), " ΣP " is the total number of counting frames in all fields (130 frames per animal, on average), "a/f" and "h" are the frame area and the height of the dissector, respectively. "BA" is the block advance of the microtome (30 μm) and "t" refers to the real post-processing section thickness calculated using the microcator (25 μm). To calculate the total number of cells, the numerical density (NV) was multiplied by the reference volume (V).

Histopathology study

The biopsy sample was fixed in a 10% formalin fixative solution, embedded in paraffin, and sectioned into 3 μm thick slices for histopathology evaluation. HFs in different stages of catagen, telogen, and anagen were counted. The count was done in 10 different fields (40x) and mean \pm SD was calculated for each parameter. Compared to normal skin, any change in the number of HFs and a difference in the inflammatory reaction was considered as an intervention effect. The stage of HF growth (Anagen, Telogen and Catagen) and hair type (vellus or terminal) were evaluated.

Quantitative gene analysis

Total RNA from the treated skin tissue was extracted using the AddPrep Total RNA Extraction Kit (Addbio, Korea) based on the manufacturer's instructions. The concentration and purity of RNA were quantified using a NanoDrop ND-1000 spectrophotometer (NanoDrop Technologies, Wilmington, DE, USA). Next, cDNA was synthesized (Addbio, Korea) and used as a template for a real-time polymerase chain reaction (PCR). After cDNA synthesis, the expression of *Il-1 β* , *Il-1 α* , *Tnf- α* , *Lef-1*, *Versican*, and *Ptc-1* genes along with Beta-actin (*β -actin*) as an internal control was measured using real-time PCR. For this purpose, specific gene primers and 2x Q-PCR Master Mix SYBER GREEN Add SYBR Master

kit were used based on the manufacturer's protocol. The relative expression of the mRNA was quantified using the comparative cycle threshold method. The following primer sequences were used:

β -Actin-

F: CAGCTGAGAGGGGAAATCGTG
R: CGTTGCCAATAGTGATGACC

Il-1 β -

F: ACAAGGAGAACCAAGCAACGAC
R: GCTGATGTACCAGTTGGGGAAC

Il-1 α -

F: CTGTGCCTGTCTTGTGCCA
R: AGAGCGGATGAAGGTAAGCG

Tnf- α -

F: TGCCCCAAGGACACCCC
R: GGGCTGGGTAGAGAATGGATGA

Lef-1-

F: ACCGATGAGATGATCCCCCT
R: CCTCTTCGGGATGACTGAT

Versican-

F: TTTTACCCGAGTTACCAGACT
R: AGTAGTTGTTACATCCGTTGC

Ptc-1-

F: ACATTCAAAGAAGAACTGCGGC
R: AAAGGGAAGGAAGACGAAGG

Statistical analysis

The data was presented as mean \pm SD. GraphPad Prism software (version 8.0, La Jolla, CA) was used to generate all the graphs. The groups were analyzed using One-way ANOVA and Tukey's tests using GraphPad (Version 8.0, La Jolla, CA). Differences were reported as statistically significant if $P < 0.05$.

Results

Characterization of human umbilical cords mesenchymal stem cells and the hydrogel

To confirm the mesenchymal origin of cells, isolated cells were evaluated by differentiation into osteoblasts and adipocytes. The presence of calcium deposits indicated the potential of cells to become osteoblasts, while the presence of intracellular lipid vacuoles was noted as a distinguishing characteristic of adipocytes (17). Cells were also characterized by flow cytometry using different surface markers. The presence of positive markers, CD90 and CD44, and the absence of negative markers, HLA-DR and CD34 were confirmed on the isolated cells (Fig.1C-F).

We also evaluated the release of CM and testosterone from the gel system. We observed that CM was released from the gel system after 20 days (Fig.1G). However, approximately 60% of the testosterone was released within the first 24 hours, with complete release occurring within 160 hours (Fig.1H).

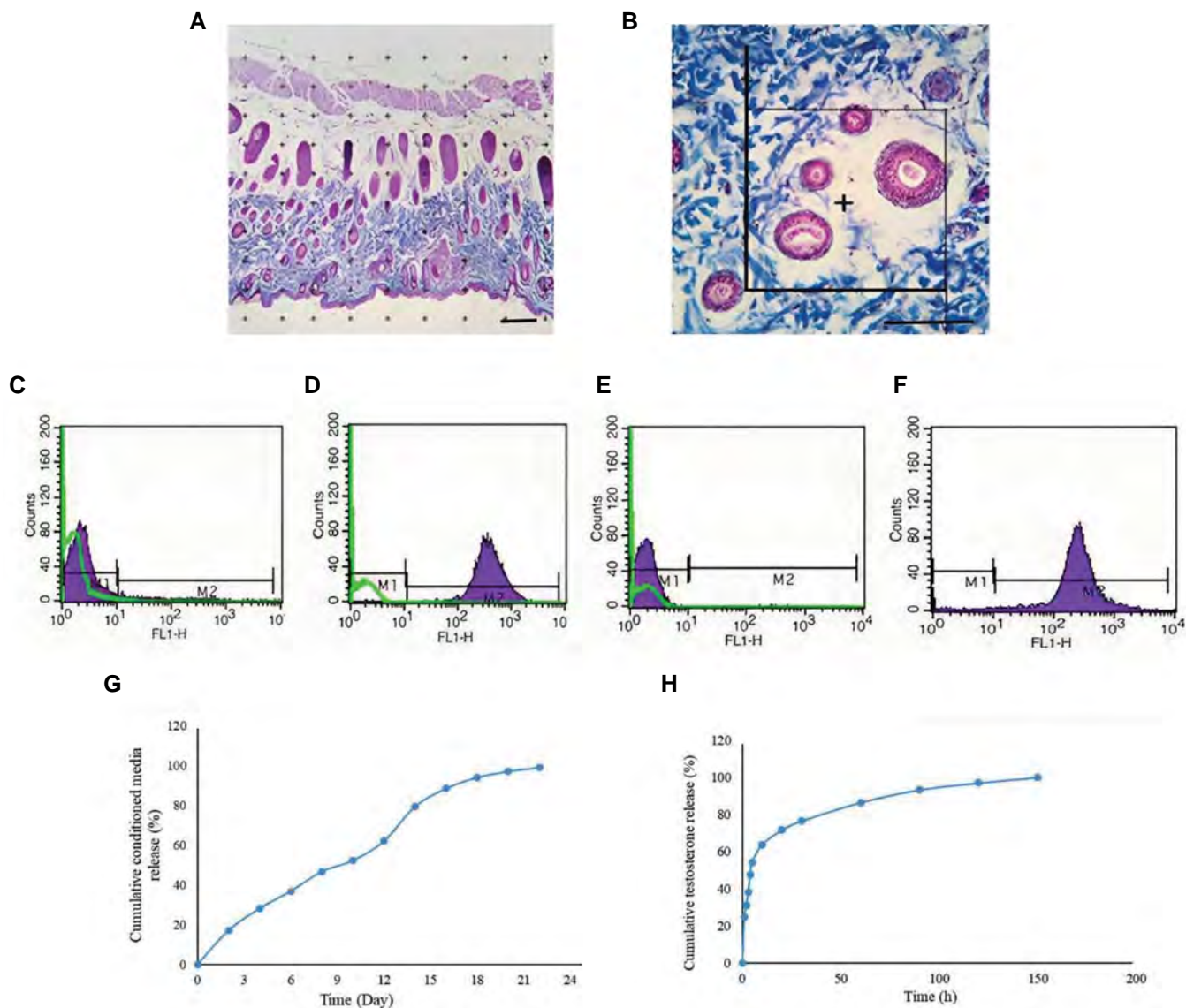


Fig.1: A schematic representation of stereological methods was used in this study. **A.** Point-counting method for calculating volume density, **B.** Optical disector method for estimating numerical density (scale bar: 50 μm). The ability of human UC-MSCs differentiation into adipocytes and osteocytes. Immunophenotyping analysis of UC-MSCs. Cells were positive for **C.** CD44, **D.** CD99 and negative for **E.** HLA-DR, **F.** CD34. The control histogram is highlighted in green. CM and testosterone release rate loaded in the hydrogel. **G.** Cumulative CM release and **H.** Cumulative testosterone release. UC-MSCs; umbilical cords mesenchymal stem cells and CM; Conditioned media.

Gross, histopathological and stereological evaluations of the treated groups

The results of gross and histopathological studies showed the increase and regeneration of HF in all treatment groups (Figs.2A-H, 3A-C). CM.FI and CM.Fin treatment resulted in the most significant effect on the anagen phase, leading to an earlier onset and a longer duration of HF growth. Regarding the HF cycle, in CM, Cm.FI and CM.Fin treated groups, the number of HF in the telogen and catagen phases were greatly reduced. The combination of CM with flutamide displayed a significant improvement in promoting HF toward the anagen phase ($P < 0.05$).

AGA is characterized by the presence of small-sized

hair follicles and a shortening anagen phase Figure 2CIII (22). Hair loss typically correlates with irregularities in HF cycling and morphology, as shown in Figure 2CIII. During the anagen state of a hair follicle, DP remains situated deep within the subcutaneous fat layer, as depicted in Figure 2CIII (23). In addition, the number of vellus and terminal hairs was evaluated between groups. Across all treated groups, vellus hairs decreased, while terminal hairs increased (Fig.3D, E). However, CM, CM.FI, and CM.Fin treated groups demonstrated a higher level of terminal hairs compared to other treated groups. Similarly, the groups treated with CM showed a significant reduction of inflammation ($P < 0.05$, Fig.3F) (24).

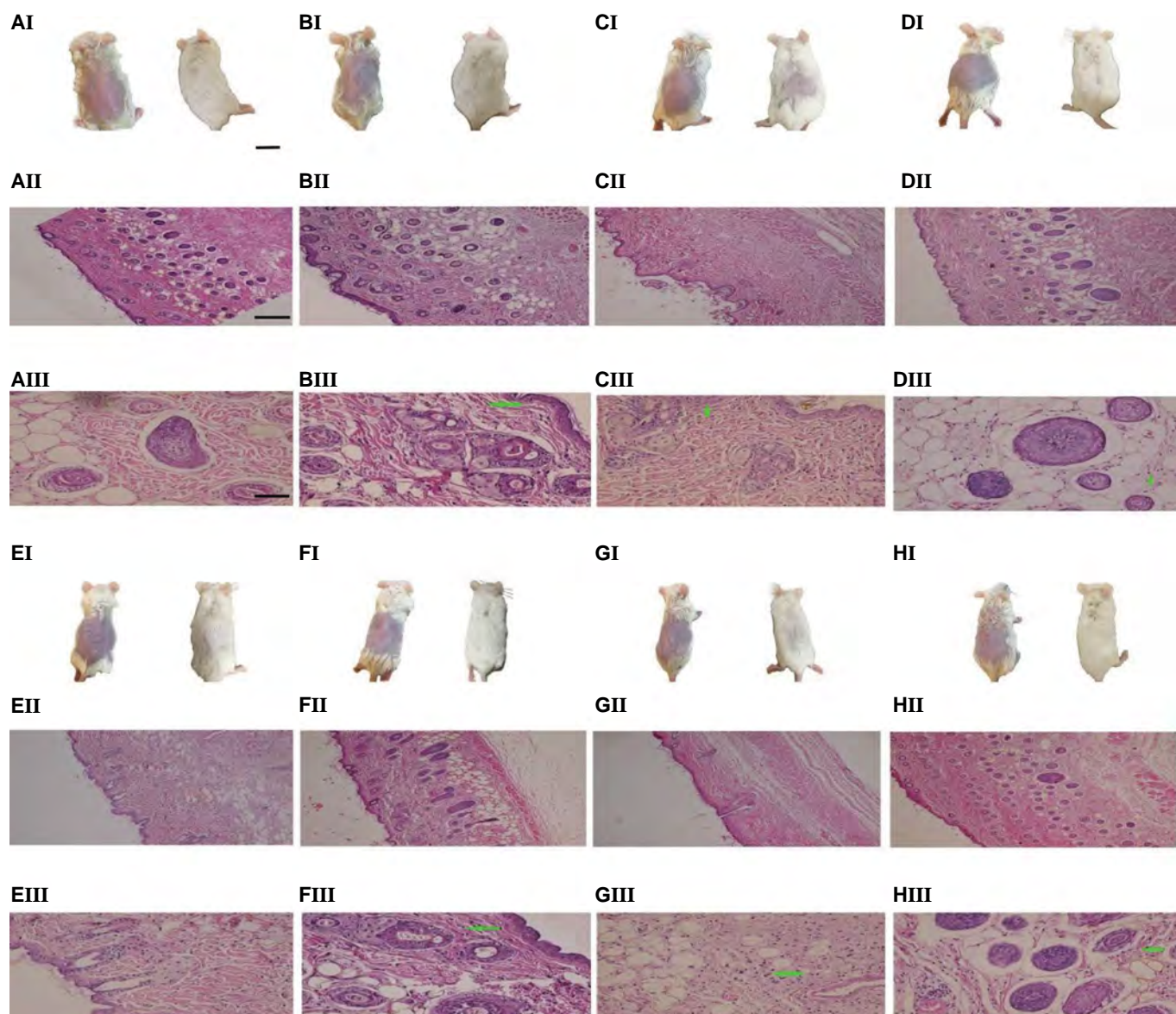


Fig.2: The gross appearance of alopecia and hematoxylin and eosin staining of HF in different treatment groups. The mice were treated using **A.** PBS, **B.** P407, **C.** P.T, **D.** C.M, **E.** F.I, **F.** C.M.F.I, **G.** F.I, and **H.** C.M.F.I. The presented photographs depict the first (left) and last (right) days of the experiment (AI-HI) (scale bar: 1 cm). AII-HII 100x (scale bar: 50 μ m). AIII-HIII 400x-Green arrow showing inflammation (scale bar: 200 μ m). HF; Hair follicle, PBS; Phosphate-buffered saline, P407; Poloxamer 407, P.T; Poloxamer 407+Testosterone, C.M; Poloxamer 407+Testosterone)+(Poloxamer 407+conditioned media), F.I; (Poloxamer 407+Testosterone)+(Oral flutamide, CM), F.I; (Poloxamer 407+Testosterone)+(Oral flutamide), Fin; (Poloxamer 407+Testosterone)+(Oral finasteride), and CM.Fin; (Poloxamer 407+Testosterone)+(Oral finasteride)+ (Poloxamer 407+conditioned media).

As shown in Figure 3, a significant difference in the volume density of the epidermis between the P.T and PBS treated groups was found ($P < 0.05$). There was also a significant difference in hypodermis between the P.T and PBS treated groups ($P < 0.05$). Although, CM, CM.FL and CM.Fin treatments could significantly prevent subcutaneous layer loss ($P < 0.05$), no significant changes in dermal volume density were observed.

As a result of treatment with P.T, FL, or Fin, collagen volume density was significantly reduced in comparison with the PBS treated group ($P < 0.05$), whereas the CM, CM.FI, and CM.Fin treated groups demonstrated significant increases in this parameter ($P < 0.05$, Fig.3J). The volume density of vessels was reduced

in the P.T, FL and Fin treated groups compared to the control group ($P < 0.001$). Moreover, it was shown that the volume densities of vessels in the CM, CM.FI, and CM.Fin groups were significantly higher than the P.T group ($P < 0.001$). Interestingly, a significant difference was seen between the FI and Fintreated animals and the CM treated group ($P < 0.01$). Combined groups with CM improved the Vessel's volume density more than either FI or Fin groups ($P < 0.001$, Fig.3K).

Conversely, the volume density of the sebaceous gland was increased in the P.T ($P < 0.001$), FL and Fin treated groups ($P < 0.01$) compared to the Control group. This parameter was reduced in the FL and Fin-treated mice ($P < 0.05$), as well as CM, CM.FI, and CM.Fin treated groups ($P < 0.001$) compared to the P.T group (Fig.3L).

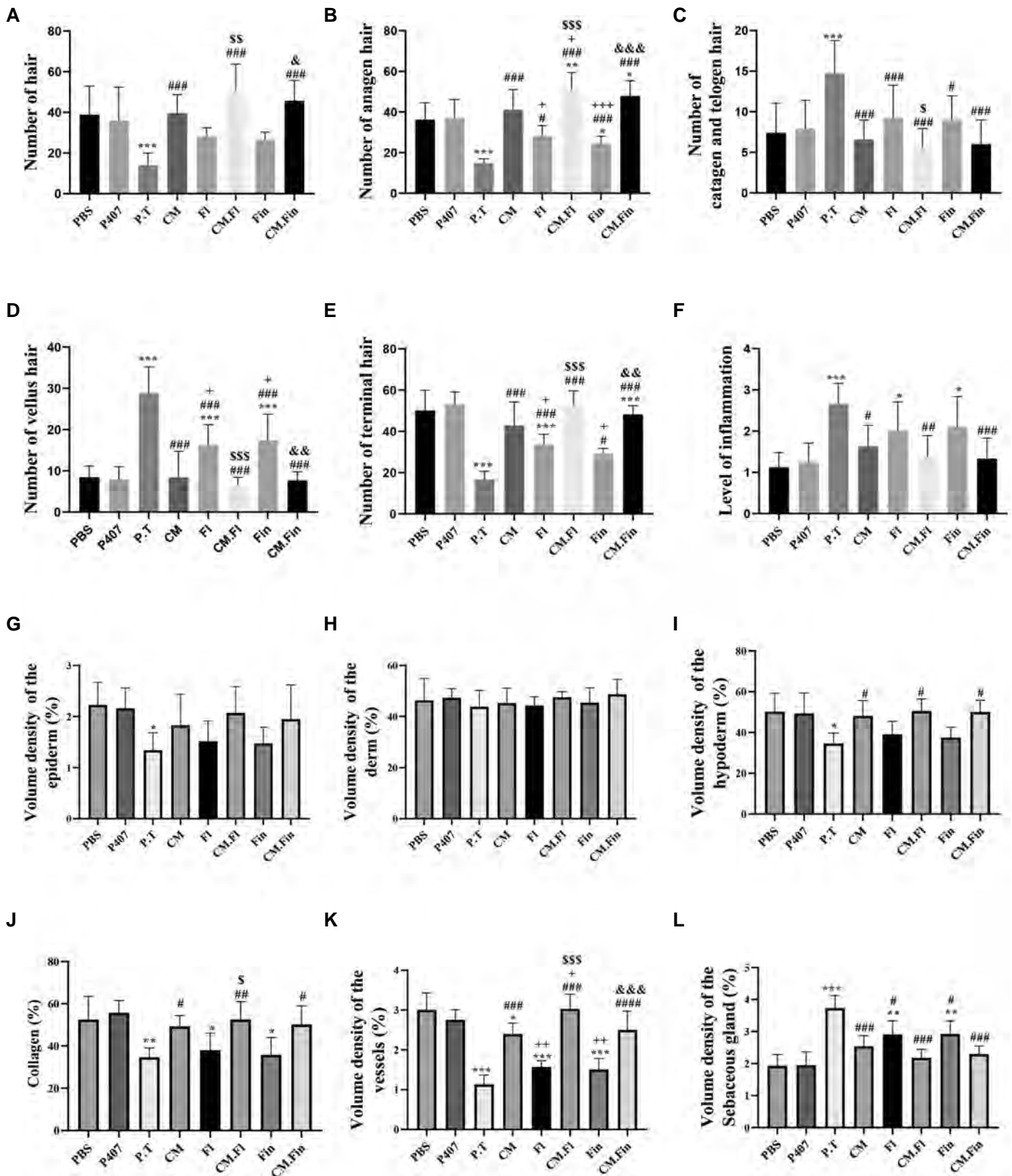


Fig.3: The effect of anti-androgen treatments and regenerative medicine on the hair follicle cycle and components of skin layers in mice. **A.** Quantitative analysis of the number of hair follicles, **B.** The number of follicles in the anagen phase, **C.** The number of follicles in the catagen or telogen phase, **D.** The number of vellus hairs, **E.** The number of terminal hairs, and **F.** The degree of inflammation. **G.** The volume density (%) of skin's layers including epidermis, **H.** Dermis, **I.** Hypodermis among the treated groups. **J.** The volume density (%) of the collagen bundle, **K.** Vessels, and **L.** Sebaceous gland in the experimental groups. Data are presented as $n=6 \pm SD$. HF; Hair follicle, PBS; Phosphate-buffered saline, P407; Poloxamer 407, P.T; (Poloxamer 407+Testosterone), C.M; (Poloxamer 407+Testosterone)+(Poloxamer 407+conditioned media), F1; (Poloxamer 407+Testosterone)+(Oral flutamide), C.M.F1; (Poloxamer 407+Testosterone)+(Oral flutamide)+(Poloxamer 407+conditioned media), Fin; (Poloxamer 407+Testosterone)+(Oral finasteride), CM.Fin; (Poloxamer 407+Testosterone)+(Oral finasteride)+(Poloxamer 407+conditioned media), *, $P<0.05$, **, $P<0.01$, ***, $P<0.001$ vs. the PBS group, #, $P<0.05$, ##, $P<0.01$, ###, $P<0.001$ vs. the P.T group, +, $P<0.05$, ++, $P<0.01$ vs. the CM group, +++, $P<0.001$ vs. the CM group, \$, $P<0.05$, \$\$, $P<0.01$, \$\$\$, $P<0.001$ vs. the FI group, &, $P<0.5$, &&, $P<0.01$, and &&&, $P<0.001$ vs. the Fin group.

The stereological data obtained for HFs and components of HFs, including medulla, cortex, inner root sheath, outer root sheath, and dermal root sheath, are listed in Table 2. The volume density of all parameters was reduced in the P.T. group in comparison to the PBS-treated animals ($P < 0.05$). These components were significantly increased in mice treated with CM, CM.FI, and CM.Fin compared to P.T group ($P < 0.05$).

As shown in Table 2, the numerical density of spinous cells in the epidermis and fibroblasts in the dermis of the P.T, FL, and Fin treated mice were lower than the PBS treated group ($P < 0.001$). These cells were significantly increased in the CM ($P < 0.01$), CM.FI, and CM.Fin treated groups ($P < 0.001$) compared to the P.T treated group. In addition, a significant difference was observed between the CM.FI and CM.Fin treated animals and CM group ($P < 0.01$). No significant

changes were found in the numerical density of basal cells between groups. Taken together, CM.FI and CM.Fin could improve the numerical density of these cells more than either FI or Fin groups ($P < 0.001$) (25).

Gene expression analysis

The expression of *Il-1 α* , *Il-1 β* , and *Tnf- α* genes were up-regulated in the alopecic models compared to the control group (Fig.4A-C). Following treatment, the expression of these genes was decreased in all groups. However, a significant reduction was found in the groups treated by CM, CM.FI, and CM.Fin compared to the other groups. A decrease in the expression of genes related to hair growth and survival, *Ptc1*, *Versican*, and *Lef* are closely associated with androgenic alopecia (Fig.4D-F). However, subsequent to treatment with CM, CM.FI, and CM.Fin, a significant upregulation of *Ptc1*, *Versican*, and *Lef* was observed within the respective groups. ($P < 0.05$).

Table 2: The mean and standard deviation of the volume density (%) of the HF and components of the HF in the experimental groups (n=6)

Group	Hair follicle (Vv)	Hair follicle component (Vv)					Fibroblast (Nv)	Epidermis cells (Nv)	
		Medulla	Cortex	Inner root sheath	Outer root sheath	Dermal root sheath		Basal	Spinousum
PBS	6.213 ± 1.205	3.750 ± 0.3852	6.120 ± 1.776	15.63 ± 3.588	31.93 ± 3.064	7.859 ± 1.789	176.7 ± 17.07	175.2 ± 28.13	533.6 ± 93.64
P407	6.400 ± 1.071	3.512 ± 0.7372	5.821 ± 1.355	15.73 ± 4.923	31.00 ± 5.161	8.079 ± 2.139	188.1 ± 33.89	176.7 ± 28.25	517.2 ± 88.09
P.T	3.372 ± 0.4764*	1.775 ± 0.4453*	2.944 ± 1.442*	7.879 ± 3.330*	18.90 ± 4.901*	3.579 ± 0.8825*	70.46 ± 11.50***	161.4 ± 30.20	219.7 ± 47.07***
CM	6.244 ± 0.8346#	3.606 ± 0.9045#	5.501 ± 1.315#	13.46 ± 3.650	28.43 ± 4.058#	7.799 ± 2.024#	159.7 ± 27.88##	171.8 ± 24.67	360.8 ± 62.24##
FI	4.996 ± 0.2512#	2.867 ± 0.8659	3.720 ± 0.7429	10.74 ± 2.316	25.10 ± 6.805	5.876 ± 2.133	95.48 ± 11.62***	166.2 ± 15.13	277.1 ± 47.04***
CM.FI	6.548 ± 0.9315#	3.829 ± 1.275#	6.099 ± 1.658#	15.17 ± 2.374#	33.75 ± 5.961#	8.770 ± 2.748#	235.6 ± 24.28#####	176.0 ± 30.28	564.5 ± 94.20#####
Fin	4.951 ± 0.5134#	2.659 ± 1.162	3.938 ± 1.254	12.19 ± 1.922	26.19 ± 3.139	5.526 ± 1.527	94.78 ± 12.36***	167.3 ± 19.57	253.8 ± 38.32***
CM.Fin	6.324 ± 0.9461#	3.614 ± 1.090#	6.233 ± 1.155#	14.05 ± 1.280#	31.93 ± 4.068#	8.184 ± 2.460#	223.8 ± 29.10##### &&&	175.9 ± 19.03	565.0 ± 84.49##### &&&

The mean and standard deviation of the numerical density of fibroblasts, basal cells, and spinous cells ($\times 10^3$ per mm^3) in the experimental groups (n=6). *, $P < 0.05$ vs. the PBS group, #; $P < 0.05$ vs. the P.T group. ***, $P < 0.001$ vs. the PBS group, ##; $P < 0.01$, ###; $P < 0.001$ vs. the P.T group, +; $P < 0.01$ vs. the CM group, \$\$\$; $P < 0.001$ vs. the FI group, and &&&; $P < 0.001$ vs. the Fin group.

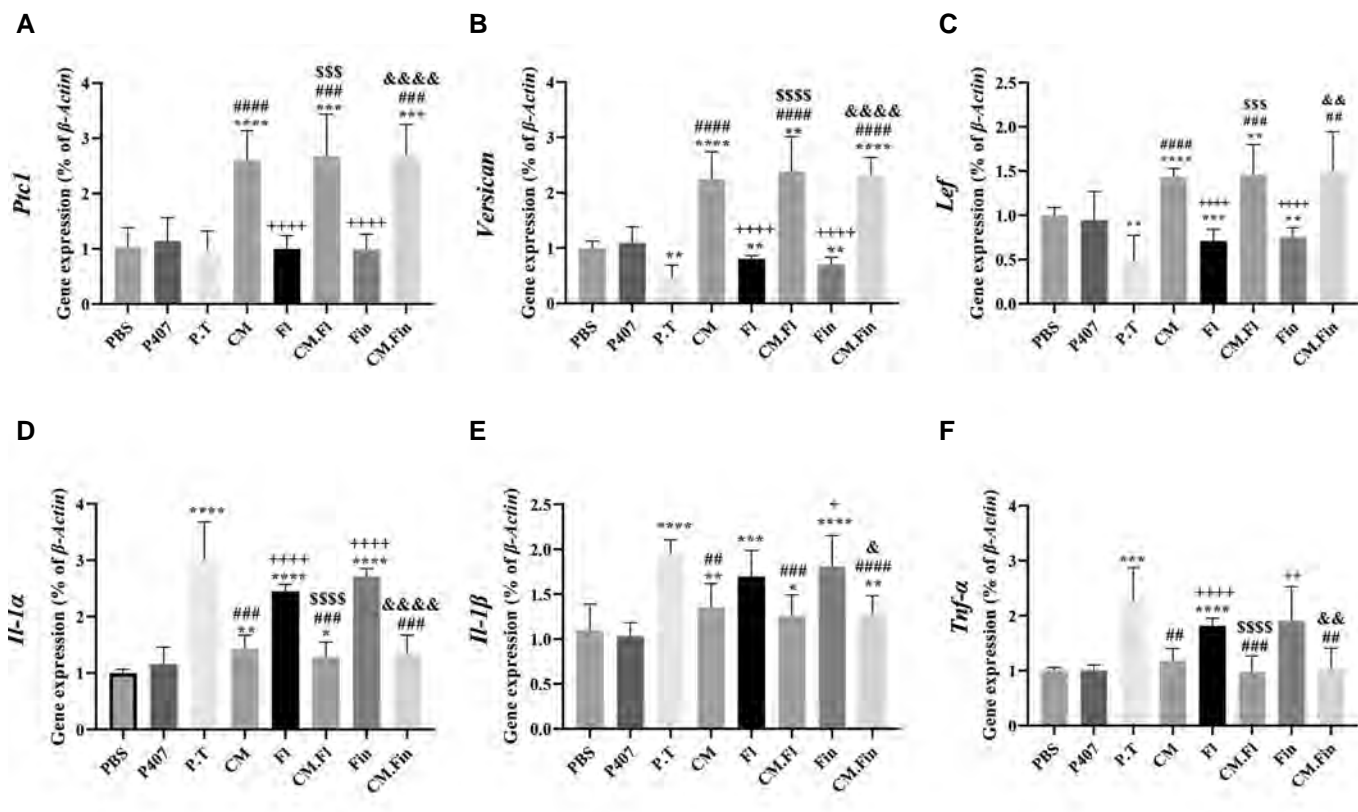


Fig.4: Expression of cytokine genes. **A.** *Il-1α*, **B.** *Il-1β*, and **C.** *Tnf-α* as well as growth and survival genes including, **D.** *Ptc1*, **E.** *Versican* and **F.** *Lef* in different studied groups. Expression level of genes related to in different studied groups. *: P<0.05, **: P<0.01, ***: P<0.001, ****: P<0.0001 vs. the PBS group, ###; P<0.01, ####; P<0.001, #####; P<0.0001 vs. the P.T group, +; P<0.05, +++; P<0.001, ++++; P<0.0001 vs. the CM group, \$\$\$; P<0.001, \$\$\$\$; P<0.0001 vs. the FI group, &; P<0.5, &&; P<0.01, &&&; P<0.001, &&&&; P<0.0001 vs. the Fin group, PBS; Phosphate-buffered saline, P407; Poloxamer 407, P.T; (Poloxamer 407+Testosterone), C.M; (Poloxamer 407+Testosterone)+(Poloxamer 407+conditioned media), F1; (Poloxamer 407+Testosterone)+(Oral flutamide), CM.F1; (Poloxamer 407+Testosterone)+(Oral flutamide)+(Poloxamer 407+conditioned media), Fin; (Poloxamer 407+Testosterone)+(Oral finasteride), and CM.Fin; (Poloxamer 407+Testosterone)+(Oral finasteride)+ (Poloxamer 407+conditioned media).

Discussion

CM derived from MSCs contains bioactive factors that are involved in a wide variety of physiological processes, including cellular proliferation, angiogenesis, and hair growth. In CM, the proangiogenic component consists of HIF-1α, hepatocyte growth factor (HGF), insulin-like growth factor-1 (IGF-1), fibroblast growth factor-2 (FGF-2), matrix metalloproteinase-2 (MMP-2) and CXCL5 (14).

A colony-stimulating factor, for example, may be capable of recruiting resident stem cells and/or PCs to facilitate hair regeneration. Overall, CM enhances angiogenesis and promotes hair regeneration in a complex and effective manner (14).

The present study evaluated the effects of CM-loaded hydrogel in combination with oral anti-androgen drugs on the histological and stereological changes in the mouse model of androgenetic alopecia. No side effects were observed in the control groups. We showed that CM-loaded hydrogel alone or combined with anti-androgen drugs improved hair regeneration by increasing HF, associated with increased densities of epidermis and hypodermis layers. An increased numerical density of fibroblasts with collagen bundles was also identified.

Furthermore, these treatments could promote hair growth by introducing HF in the anagen stage and shortening the telogen and catagen phases.

Hair growth can be induced by prolonged anagen and delayed catagen phases or by alternation from quiescent (telogen) to active (anagen) phases (26). It has been suggested that topical anti-androgenic compounds containing flutamide or finasteride could effectively stimulate hair growth in male-pattern baldness (27). Our result confirmed that flutamide and finasteride have been significantly successful in HF growth, and flutamide was more effective than finasteride. Other studies have shown flutamide to be effective in treating and preventing androgenic hair loss, especially in women (28), and the results obtained regarding the effectiveness of flutamide compared to finasteride in hair loss are in line with the results of this study. Moreover, localized supplementation of growth factors has been reported to promote hair regeneration and growth (29).

Previous studies have also shown that CM from Extracellular Matrix/Stromal Vascular Fraction Gel can promote hair growth by regulating the proliferation of DP cells and bulge cells, neovascularization and anagen induction in C57BL/6 mice (30). Lu et al. (31) stated

that an enriched culture medium contained effective proangiogenic elements and growth factors such as HIF-1 α , HGF, IGF-1, and FGF-2. Similarly, it has been reported that CM from vitamin D3 (Vd3) pre-activated preadipocytes have stimulatory effects on hair growth via the enhancement of angiogenesis in a hairless-induced C57BL/6 mouse model (32). Treatment of bone marrow MSCs with a Wnt1 α -conditioned medium accelerated the HF transition from the telogen to the anagen phase. Also, it activated DP cells and promoted mouse HF regrowth (33).

Oh et al. (22) showed that using an enriched culture medium obtained from UC stem cells pretreated with lithium chloride and TGF- β 1 significantly increased the thickness, growth rate, and number of HFs. In addition, HF-derived MSCs were able to decrease mouse hair loss and reduce inflammation around the HF(23). The concentrated conditioned medium-loaded hydrogel treatment accelerated wound closure, enhanced neovascularization, and promoted HF regeneration, which is in line with the results of this study (34). Nevertheless, to the best of our knowledge, the present study represents the first attempt to investigate the combination effects of CM-loaded hydrogel with flutamide or finasteride. The stereological analysis displayed that CM-loaded hydrogel alone or combined with oral intake of flutamide and finasteride could increase the numerical density of spinous cells, which may be the reason for the thickening of the epidermis. Our findings revealed that CM-loaded hydrogel alone or combined with flutamide and finasteride could also proliferate fibroblasts and improve collagen content. Fibroblasts are the main skin components that produce collagen and other matrix macromolecules for the structural support of connective tissues (35). Additionally, it has been reported that fibroblast proliferation could promote angiogenesis. Inconsistent with the findings here, Fong et al. (36) found that the enriched CM could significantly increase the cell life and total collagen, elastin, and fibronectin.

Liu et al. (37) determined that the enriched CM of stem cells increases collagen expression, activation, and migration of fibroblasts. Interestingly, combined treatment with CM significantly after exposure to testosterone reduced the volume density of sebaceous glands. It has been revealed that testosterone administration could increase the size of the sebaceous glands (38). Accordingly, despite the increase in fibroblasts and collagen content following combined treatment with CM, the lack of change in the dermis volume may be caused by a reduced sebaceous gland volume density. Medullation of the immune system with anti-inflammatory properties is another characteristic finding of stem cells and enriched CM (39). In this study, the enriched CM significantly reduced the expression of *interleukin 1 alpha*, *interleukin 1 beta*, and *Tnf alpha* genes. Accordingly, Deng et al. (23) showed that MSCs derived from HF can prevent hair loss by reducing inflammation. Also, Czarnecka et al. (40) stated that the immunoregulatory properties of

stem cells significantly increased hair growth. Expression of *ptc1*, *Versican*, and *lef1* genes activate the precocious anagen entry. Lef-1 plays an important role in regulating cell growth and differentiation through the Wnt signalling pathway. According to the results of this study, treatments with CM, CM.FI, and CM.Fin up regulates the expression of these genes and the Wnt/b-catenin signaling pathway promotes hair regeneration (33). Further investigations are needed to evaluate the protein profiles of the treated and control tissues and determine the effect of the treatment on the excessive or lessened expression of the proteins in the target tissue.

A significant advantage of this study is the identification of the therapeutic potential of regenerative medicine products in addition to conventional drugs for the treatment of androgenic hair loss. However, a genetic or animal model capable of accurately replicating AGA remains an area for further investigation. Future research should focus on the combination of CM with other drugs related to hair loss. Additionally, performing these experiments on other model animals may provide a better understanding of the quality of regenerative medicine treatments.

Conclusion

We have shown that the slow-release property of p407, which carries the therapeutic properties of CM at the injection site, provides a new treatment approach for male pattern hair loss. The injecting growth factors, anti-inflammatory and angiogenesis properties, in combination with oral anti-androgens, was found to be an optimal therapeutic strategy. Developing new effective treatments for this disease can be achieved by optimizing the injecting doses, type of cell therapy sources, and anti-androgen selections.

Acknowledgements

This study was funded by a grant from the Shiraz University of Medical Sciences [98-01-74-19509]. There is no conflicts of interest in this study.

Authors' Contributions

M.K.-D.A., N.A., M.D.; Conceptualization. M.K.-D.A., Gh.Y., F.D., A.A.A., M.A.M., G.N.; Methodology and Software. N.A., M.K.-D.A., A.J., S.P., M.N.; Data curation, Writing- Original draft preparation, and Supervision. M.K.-D.A., N.A., M.D., M.N.; Visualization and Investigation. N.A., M.D., M.N., F.D.; Software and Validation. M.K.-D.A., N.A., A.J., M.N., M.D.; Writing-Reviewing and Editing. All authors read and approved the final manuscript.

References

1. Devjani S, Ezemma O, Kelley KJ, Stratton E, Senna M. Androgenetic alopecia: therapy update. *Drugs*. 2023; 83(8): 701-715.
2. Ho CH, Sood T, Zito PM. Androgenetic alopecia. In: *StatPearls* [Internet]. Treasure Island (FL): StatPearls Publishing; 2023. Available from: <https://www.ncbi.nlm.nih.gov/books/NBK430924/> (16

- Oct 2022).
3. Lolli F, Pallotti F, Rossi A, Fortuna MC, Caro G, Lenzi A, et al. Androgenetic alopecia: a review. *Endocrine*. 2017; 57(1): 9-17.
 4. Anastassakis K. Flutamide. *Androgenetic alopecia from A to Z*. Springer; 2022; 193-197.
 5. Saceda-Corralo D, Domínguez-Santas M, Vañó-Galván S, Grimalt R. What's new in therapy for male androgenetic alopecia? *Am J Clin Dermatol*. 2023; 24(1): 15-24.
 6. Allam S, Elsakka EGE, Ismail A, Doghish AS, Yehia AM, Elkady MA, et al. Androgen receptor blockade by flutamide down-regulates renal fibrosis, inflammation, and apoptosis pathways in male rats. *Life Sci*. 2023; 323: 121697.
 7. Lei M, Yang L, Chuong CM. Getting to the core of the dermal papilla. *J Invest Dermatol*. 2017; 137(11): 2250-2253.
 8. Rahmani W, Abbasi S, Hagner A, Raharjo E, Kumar R, Hotta A, et al. Hair follicle dermal stem cells regenerate the dermal sheath, repopulate the dermal papilla, and modulate hair type. *Dev Cell*. 2014; 31(5): 543-558.
 9. Mohammadi P, Youssef KK, Abbasalizadeh S, Baharvand H, Aghdami N. Human hair reconstruction: close, but yet so far. *Stem Cells Dev*. 2016; 25(23): 1767-1779.
 10. Krefft-Trzcinińska K, Piętowska Z, Nowicka D, Szepletowski JC. Human stem cell use in androgenetic alopecia: a systematic review. *Cells*. 2023; 12(6): 951.
 11. Tabatabaei Qomi R, Sheykhasan M. Adipose-derived stromal cell in regenerative medicine: a review. *World J Stem Cells*. 2017; 9(8): 107-117.
 12. Giuliano E, Paolino D, Fresta M, Cosco D. Drug-loaded biocompatible nanocarriers embedded in poloxamer 407 hydrogels as therapeutic formulations. *Medicines (Basel)*. 2018; 6(1): 7.
 13. Kamishima T, Hirabe C, Ohnishi T, Taguchi J, Myint KZY, Koga S. Trichoscopic evaluation of dental pulp stem cell conditioned media for androgenic alopecia. *J Cosmet Dermatol*. 2023; 22(11): 3107-3117.
 14. Yuan A, Gu Y, Bian Q, Wang R, Xu Y, Ma X, et al. Conditioned media-integrated microneedles for hair regeneration through perifollicular angiogenesis. *J Control Release*. 2022; 350: 204-214.
 15. Asadi-Golshan R, Razban V, Mirzaei E, Rahmanian A, Khajeh S, Mostafavi-Pour Z, et al. Efficacy of dental pulp-derived stem cells conditioned medium loaded in collagen hydrogel in spinal cord injury in rats: Stereological evidence. *J Chem Neuroanat*. 2021; 116: 101978.
 16. Shaer A, Azarpira N, Aghdaie MH, Esfandiari E. Isolation and characterization of human mesenchymal stromal cells derived from placental decidua basalis; umbilical cord wharton's jelly and amniotic membrane. *Pak J Med Sci*. 2014; 30(5): 1022-1026.
 17. Nekoei SM, Azarpira N, Sadeghi L, Kamalifar S. In vitro differentiation of human umbilical cord Wharton's jelly mesenchymal stromal cells to insulin producing clusters. *World J Clin Cases*. 2015; 3(7): 640-649.
 18. Cespi M, Bonacucina G, Pucciarelli S, Cocci P, Perinelli DR, Cassetari L, et al. Evaluation of thermosensitive poloxamer 407 gel systems for the sustained release of estradiol in a fish model. *Eur J Pharm Biopharm*. 2014; 88(3): 954-961.
 19. Zhang Y, Wang X, Chen J, Qian D, Gao P, Qin T, et al. Exosomes derived from platelet-rich plasma administration in site mediate cartilage protection in subtalar osteoarthritis. *J Nanobiotechnology*. 2022; 20(1): 56.
 20. Yang C, Lei D, Ouyang W, Ren J, Li H, Hu J, et al. Conditioned media from human adipose tissue-derived mesenchymal stem cells and umbilical cord-derived mesenchymal stem cells efficiently induced the apoptosis and differentiation in human glioma cell lines in vitro. *Biomed Res Int*. 2014; 2014: 109389.
 21. Noorafshan A, Asadi-Golshan R, Erfanizadeh M, Karbalay-Doust S. Beneficial effects of olive oil on the rats' cerebellum: functional and structural evidence. *Folia Med (Plovdiv)*. 2018; 60(3): 454-463.
 22. Oh HA, Kwak J, Kim BJ, Jin HJ, Park WS, Choi SJ, et al. Migration inhibitory factor in conditioned medium from human umbilical cord blood-derived mesenchymal stromal cells stimulates hair growth. *Cells*. 2020; 9(6): 1344.
 23. Deng W, Zhang Y, Wang W, Song A, Mukama O, Huang J, et al. Hair follicle-derived mesenchymal stem cells decrease alopecia areata mouse hair loss and reduce inflammation around the hair follicle. *Stem Cell Res Ther*. 2021; 12(1): 548.
 24. Sperling LC, Cowper SE, Knopp EA. *An atlas of hair pathology with clinical correlations*. 2nd ed. New York & London: Informa Healthcare; 2012: 216.
 25. Galbraith GM, Thiers BH. In vitro suppression of human lymphocyte activity by minoxidil. *Int J Dermatol*. 1985; 24(4): 249-251.
 26. Choi M, Choi SJ, Jang S, Choi HI, Kang BM, Hwang ST, et al. Shikimic acid, a mannose bioisostere, promotes hair growth with the induction of anagen hair cycle. *Sci Rep*. 2019; 9(1): 17008.
 27. Sintov A, Serafimovich S, Gilhar A. New topical antiandrogenic formulations can stimulate hair growth in human bald scalp grafted onto mice. *Int J Pharm*. 2000; 194(1): 125-134.
 28. Johnson DB, Sonthalia S. FlutamideSeries. In: *StatPearls [Internet]*. StatPearls Publishing; 2021. Available from: <https://www.ncbi.nlm.nih.gov/books/NBK482215/> (1 May 2023).
 29. Ramdasi S, Tiwari SK. Human mesenchymal stem cell-derived conditioned media for hair regeneration applications. *J Stem Cells*. 2016; 11(4): 201-211.
 30. Anudeep TC, Jeyaraman M, Muthu S, Rajendran RL, Gangadaran P, Mishra PC, et al. Advancing Regenerative Cellular Therapies in Non-Scarring Alopecia. *Pharmaceutics*. 2022; 14(3): 612.
 31. Lu H, Poirier C, Cook T, Traktuev DO, Merfeld-Clauss S, Lease B, et al. Conditioned media from adipose stromal cells limit lipopolysaccharide-induced lung injury, endothelial hyperpermeability and apoptosis. *J Transl Med*. 2015; 13: 67.
 32. Jung MK, Ha S, Huh SY, Park SB, Kim S, Yang Y, et al. Hair-growth stimulation by conditioned medium from vitamin D3-activated preadipocytes in C57BL/6 mice. *Life Sci*. 2015; 128: 39-46.
 33. Dong L, Hao H, Xia L, Liu J, Ti D, Tong C, et al. Treatment of MSCs with Wnt1a-conditioned medium activates DP cells and promotes hair follicle regrowth. *Sci Rep*. 2014; 4: 5432.
 34. Li M, Zhong L, He W, Ding Z, Hou Q, Zhao Y, et al. Concentrated conditioned medium-loaded silk nanofiber hydrogels with sustained release of bioactive factors to improve skin regeneration. *ACS Appl Bio Mater*. 2019; 2(10): 4397-4407.
 35. Stortelers C, Kerkhoven R, Moolenaar WH. Multiple actions of lysophosphatidic acid on fibroblasts revealed by transcriptional profiling. *BMC Genomics*. 2008; 9: 387.
 36. Fong CY, Tam K, Cheyyatraivendran S, Gan SU, Gauthaman K, Armugam A, et al. Human Wharton's jelly stem cells and its conditioned medium enhance healing of excisional and diabetic wounds. *J Cell Biochem*. 2014; 115(2): 290-302.
 37. Liu C, Wang C, Yang F, Lu Y, Du P, Hu K, et al. The conditioned medium from mesenchymal stromal cells pretreated with proinflammatory cytokines promote fibroblasts migration and activation. *PLoS One*. 2022; 17(4): e0265049.
 38. Sauter LS, Weibel ER. Morphometric evaluation of skin structures by stereologic methods. Application to testosterone-treated rats. *Dermatologica*. 1971; 143(3): 174-183.
 39. Ban K, Bae S, Yoon YS. Current strategies and challenges for purification of cardiomyocytes derived from human pluripotent stem cells. *Theranostics*. 2017; 7(7): 2067-2077.
 40. Czarnańska A, Odziomek A, Murzyn M, Dubis J, Bałaj-Oleszczuk M, Hryniewicz-Gwóźdź A. Wharton's jelly-derived mesenchymal stem cells in the treatment of four patients with alopecia areata. *Adv Clin Exp Med*. 2021; 30(2): 211-218.

Annexin A7 and Its Related Protein Suppressor of Death Domains Regulates Migration and Proliferation of Hca-P Cells

Shaoqing Wang, Ph.D.¹, Qingyang Bai, M.M.¹, Xiuwen Yu, Ph.D.¹, Feng Gao, B.D.², Yurong Sun, M.M.¹,
Xianyan Wang, Ph.D.^{1*} 

1. School of Pathology, Qiqihar Medical University, Qiqihar, Heilongjiang, China

2. Anesthesia Surgery, The Third Affiliated Hospital of Qiqihar Medical University, Qiqihar, Heilongjiang, China

Abstract

Objective: This study was to investigate whether annexin A7 (AnnexinA7, ANXA7) and its co-related protein tumor cell death domain silencer [suppressor of death domains (SODD)] regulates the migratory phenotype of liver cancer cells.

Materials and Methods: In this experimental study, expression of ANXA7 in Hca-P cells, PANXA7 down-regulated cells and PANXA7 unrelated sequence cells was detected by real-time quantitative polymerase chain reaction (PCR) at mRNA level and western blotting at protein level. Transwell migration and invasion assays were performed to determine the migratory phenotype.

Results: After inhibition of ANXA7 expression, expression of SODD protein was also significantly decreased ($P < 0.05$). Transwell cell transfer experiments showed that number of tumor cells that penetrated into the cell membrane was significantly reduced after ANXA7 silencing ($P < 0.05$). Transwell cell invasion assay showed that number of tumor cells penetrating into Matrigel was significantly reduced after ANXA7 down-regulation ($P < 0.05$). The CCK8 assay was measured at 0, 24 and 48 hours, and proliferation rate of PANXA7 lower weir cells was slower than that of Hca-P cells and PANXA7 non-related sequence cells ($P < 0.05$).

Conclusion: SODD expression was decreased with the down-regulation of ANXA7. Down-regulating ANXA7 in Hca-P cells decreased proliferation, migration and invasion of tumor cells.

Keywords: ANXA7, Lymph Node Metastasis, Transfection

Citation: Wang Sh, Bai Q, Yu X, Gao F, Sun Y, Wang X. Annexin A7 and its related protein suppressor of death domains regulates migration and proliferation of Hca-P cells. Cell J. 2023; 25(11): 801-808. doi: 10.22074/CELLJ.2023.559724.1108

This open-access article has been published under the terms of the Creative Commons Attribution Non-Commercial 3.0 (CC BY-NC 3.0).

Introduction

Formation and development of tumors are caused by various genes, and they are also affected by external factors, such as physical and chemical factors. Transformation of normal into precancerous cells is the initial step leading to tumor formation. In this process, abnormal expression of the related genes and their product proteins is the key point. Level of tumor malignancy mainly depends on its ability to proliferate, invade and metastasize. Abilities of proliferation, invasion and metastasis are also the fundamental reason for high mortality and poor prognosis of patients' tumor. Primary liver cancer is a tumor derived from the liver epithelium, and one of its main risk factors is its early lymphatic metastasis (1). Therefore, studying occurrence and mechanism of lymphatic metastasis of liver cancer not only can help reduce mortality of liver cancer patients, but also lay a good foundation for preventing the early onset of the such diseases. In the recent years, several studies have been relatively performed on hematogenous metastasis of malignant tumors, but there are very few studies on lymphatic metastasis (2, 3). With the gradual deepening

of the research on function and mechanism of genes related to lymphatic metastasis of liver cancer, new gene therapy methods can be developed, and clinical application prospect is very broad. Annexin A7 (AnnexinA7, ANXA7) belongs to the annexin family, as one of the earliest discovered members. ANXA7 is involved in mediating the Ca^{2+} /GTP signaling pathway, and it is equivalent to the N-terminal tyrosine-, proline- and glycine-rich repeats of activated GTPase, providing a site for binding to the other proteins (4-7), due to the diversity of N-terminal amino acids of the annexin family, leading to the different properties of each annexin member (8-10). Proteins that bind or interact with ANXA7 have been discovered one after another. For example, suppressor of death domains (SODD) can assist ANXA7 to complete many biological functions. It binds to the TNF-R1 death domain and prevents TNF receptor 1 signaling activation (11). It was found that there was no relevant report on the mechanism of ANXA7 gene and its co-related protein SODD regulating lymphatic metastasis. Thus, we investigated whether ANXA7 and SODD are related to the migration phenotype of liver

Received: 05/August/2022, Revised: 09/April/2023, Accepted: 18/September/2023

*Corresponding Address: School of Pathology, Qiqihar Medical University, Qiqihar, Heilongjiang, China
Email: wxy200889@163.com



Royan Institute
Cell Journal (Yakhteh)

cancer cells in our study.

Materials and Methods

Materials

This is an experimental study, using hepatocarcinoma Hca-P cells as the *in vitro* model.

1. Cells: Hca-P cells with low lymphatic metastasis potential of mouse liver cancer, established and provided by the Department of Pathology, Dalian Medical University (Dalian, China).
2. Main instruments and reagents: CO₂ constant temperature incubator (ThermoFisher, USA), fluorescence inverted microscope from Olympus company (USA), microplate reader, UV-Vis spectrometer (both from ThermoFisher, USA), high-speed refrigerated centrifuge from Tomy kogyo company (Japan), ultra-low temperature refrigerator (Haier, China), gel imaging system (Shanfu Scientific Instrument, China), real-time polymerase chain reaction (PCR) instrument (Shanghai Fengling Biotechnology, China), fetal bovine serum (Wolcavi Biotech, Austria), RPMI-1640 medium (Gibco, USA), pGPU6/GFP/Neo (Shanghai Gema Pharmaceutical Technology, China), plasmid extraction kit (GE, USA), diethyl pyrocarbonate (DEPC, Invitrogen, USA), G418 (Gibco, USA), 24-wells cell plate and 96-wells cell plate (Corning, USA), the transfection reagent Sofast (Sunma Bioengineering, China), qRT-PCR kit (Qualit Yard, China), co-immunoprecipitation kit (ThermoFisher, USA), and ANXA7 antibody (Sigma, USA) and GAPDH antibodies (Beijing Quanshijin, China), SODD antibody (Abcam, USA), fluorescent secondary antibody (LI-COR, USA), BCA kit (Beijing Solarbio Life Sciences, China), and CCK8 kit was purchased from Tongjin Institute of Chemistry (Japan).

Methods

1. Synthesis of ANXA7 gene shRNA sequences and unrelated sequences

The ANXA7 gene sequence was searched in the gene bank (NM_009674.3), followed by analyzing the spatial accessibility and free energy properties of mRNA, while the off-target effects were excluded. Then, the RNA-interference efficiency prediction formulas were evaluated. shRNA and unrelated sequences were designed as negative controls.

TE buffer was used to dissolve DNA oligonucleotides in sense strand and antisense strand solutions at a concentration of 1000 μ M. The annealing experiment of the shRNA template was carried out according to the annealing reaction system using a PCR machine. Linearization experiment of the vector pGPU6/GFP/Neo was carried out according to the enzyme digestion reaction system, and constructing experiment of the expressing vector pGPU6/GFP/Neo-shRNA was carried out according to the ligation reaction system. ANXA7 and 0.6 μ g of irrelevant sequence plasmids were used to

dissolve them in 30 μ l of serum-free RPMI-1640 solution and they were mixed well for transfection. Fluorescence microscope was used to observe transfection efficiency. If the expression of green fluorescent protein was seen under the fluorescence microscope, G418 could be used for screening and culture, while the screening concentration was 400 μ g/ml. About 20 days, most of the cells died one after another, and after about 23 days, the cells began to gradually proliferate, expand, culture. They were then cryopreserved.

2. Quantitative reverse transcription PCR (qRT-PCR) was used to detect expression levels of PANXA7, ANXA7, and SODD in the cells.

After adding 0.2 ml chloroform to the cell samples and shaking slightly, they were centrifuged for 10 minutes at 4°C, 12000 rpm. The upper water phase was transferred to the eppendorf tube (EP) tube. Next, an equal volume of isopropanol was added to the samples and they were mixed. The samples were preserved at room temperature for 15 minutes, followed by centrifuging at 4°C and 12,000 rpm for 10 minutes.

Experiments were performed using a reverse transcription reaction system and a real-time quantitative PCR reaction system. Western blot was used to verify whether or not PAIIM7 down-regulated ANXA7, SODD and ALG in cells. Expression level of protein was collected by centrifugation to collect Hca-P cells, PANXA7 down-regulated cells, and PANXA7 unrelated sequence cells at density of 1×10^7 , and three times the volume of cell lysis buffer was added to the cell pellet, and lysed on ice for 15 minutes. Cells were disrupted by sonication, three cycles of 5 seconds each, a total of five times, with an interval of 8 minutes. Using refrigerated centrifuge 4°C, 12000 rpm, 10 minutes, the supernatant was aspirated and protein concentration was measured using a microplate reader.

3. Transwell chamber detected effect of down-regulation of ANXA7 gene expression in Hca-P cells on the migration ability of cells *in vitro*.

The cells were resuspended in serum-free RPMI-1640 culture media for starvation. The cells were collected and their density was adjusted to 1×10^4 cells/ml for 24 hours. The cell suspension was added to the chamber, and each group of cells was set to three duplicate wells, and 100 μ l of cell suspension was added to each well. They were incubated in a 37°C, 5% CO₂ incubator for 24 hours. The transwell chamber was taken out. The cells and a small amount of medium on the upper surface of the Transwell chamber were removed with a cotton swab and air-dried at room temperature for 30 minutes. Then, the cells were stained by adding 20 μ l of crystal violet solution to each hole of the 24-well plate and incubation for 20 minutes. After that, PBS was added to each well for washing the membrane, for 10 minutes. The lower chamber surface was observed with a microscope, and 10 fields of view were randomly selected for each Transwell chamber to take pictures, and number of the starved cultured

cells passing through the chamber was counted.

4. Transwell chamber detected effect of down-regulation of *ANXA7* gene expression in Hca-P cells on the invasion ability of cells cultured *in vitro*.

Extracellular matrix (ECM) gel was thawed at 4°C overnight, and the ECM gel and serum-free RPMI-1640 complete medium were mixed well at the ratio of 1. Next, 30 µl of the mixed ECM glue was added to each Transwell chamber, and the chamber was gently shaken; so that, the ECM glue was evenly and fully distributed on the surface of the upper chamber.

It was then incubated for 1 hour at 37°C. 10 µl of serum-free RPM-1640 medium was added to the lower chamber. Other steps were the same as the cell migration ability experiment.

5. Effect of down-regulating *ANXA7* gene expression in Hca-P cells on the proliferation ability of *in vitro* cultured cells was detected by CCK8 assay.

Cells were adjusted to a density of 1×10^4 cells/ml, and plated in four 96-well plates. Six duplicate wells were set for each group of cells, and 100 µl of cell suspension was added to each well. They were incubated for 24, 48 and 72 hours in a 37°C, 5% CO₂ incubator. Next, one of the 96-well plates was taken out, followed by adding 10 µl CCK8 solution to the cell suspension in each well, putting it back in the incubator and incubating it for 1 hour. Using a microplate reader, absorbance value of the cells was detected at 450 nm, and data of 5 replicate wells was recorded in each group. At different time-points of 0, 24, 48 and 72 hours, the numerical changes were observed. The experimental values analyzed by the microplate reader were statistically processed by repeated measures analysis of variance.

Ethics approval

This study was approved by Ethics Committee of

Animal Ethical Care Committee of Qiqihar Medical University (Heilongjiang Province, China, No. QMU-AECC-2021-243).

Statistical analysis

The experimental data were processed with SPSS 23.0 statistical software (IBM, USA) Two-sample t test was used for analysis and comparison. LSD method was used for pairwise comparison of means. Chi-square test and Spearman rank correlation method were used for rate comparison and correlation analysis. $P < 0.05$ indicated that the difference was statistically significant.

Results

Manipulating *ANXA7* using shRNA mediated gene silencing

pGPU6/GFP/Neo-shRNA-*ANXA7* and pGPU6/GFP/Neo-shRNA-NC plasmids were transfected into Hca-P cells for 48 hours, and most of the cells showed green light under an inverted fluorescence microscope (Fig.1A). G418 was used to screen the cells, in terms of generating cells with stable *PANXA7* down-regulation.

qRT-PCR method was used to detect the down-regulation of *ANXA7* in Hca-P cells. Compared with Hca-P group and *PANXA7* unrelated sequence group, mRNA expression levels of SODD and *ANXA7* in the *PANXA7* down-regulated group were decreased, by silencing *ANXA7* gene expression; there was no statistical difference between the normal Hca-P cells and the *PANXA7* unrelated sequence group (Fig.1B, Table 1). These results fully indicated that expression of SODD gene was also significantly reduced after inhibiting *ANXA7* expression.

Table 1: Expression levels of *ANXA7* and SODD mRNA in each experimental group ($X \pm S$)

Group	GAPDH OD value	Target gene OD value	IOD value (GAPDH OD value/target gene OD value)	Set irrelevant sequences to 1, normalize
<i>ANXA7</i>				
<i>PANXA7</i> unrelated sequence group	70.24	65.45	0.93	
Hca-P group	76.18	61.79	0.81	0.87
<i>PANXA7</i> down-regulated group	69.31	14.85	0.21*	0.23
SODD				
<i>PANXA7</i> unrelated sequence group	70.24	76.32	1.09	
Hca-P group	76.18	80.84	1.06	0.98
<i>PANXA7</i> down-regulated group	69.31	21.34	0.31*	0.28

SODD; Suppressor of death domains, OD; Optical density, IOD; Integrated optical density, and *; $P < 0.05$, compared to the unrelated sequence group.

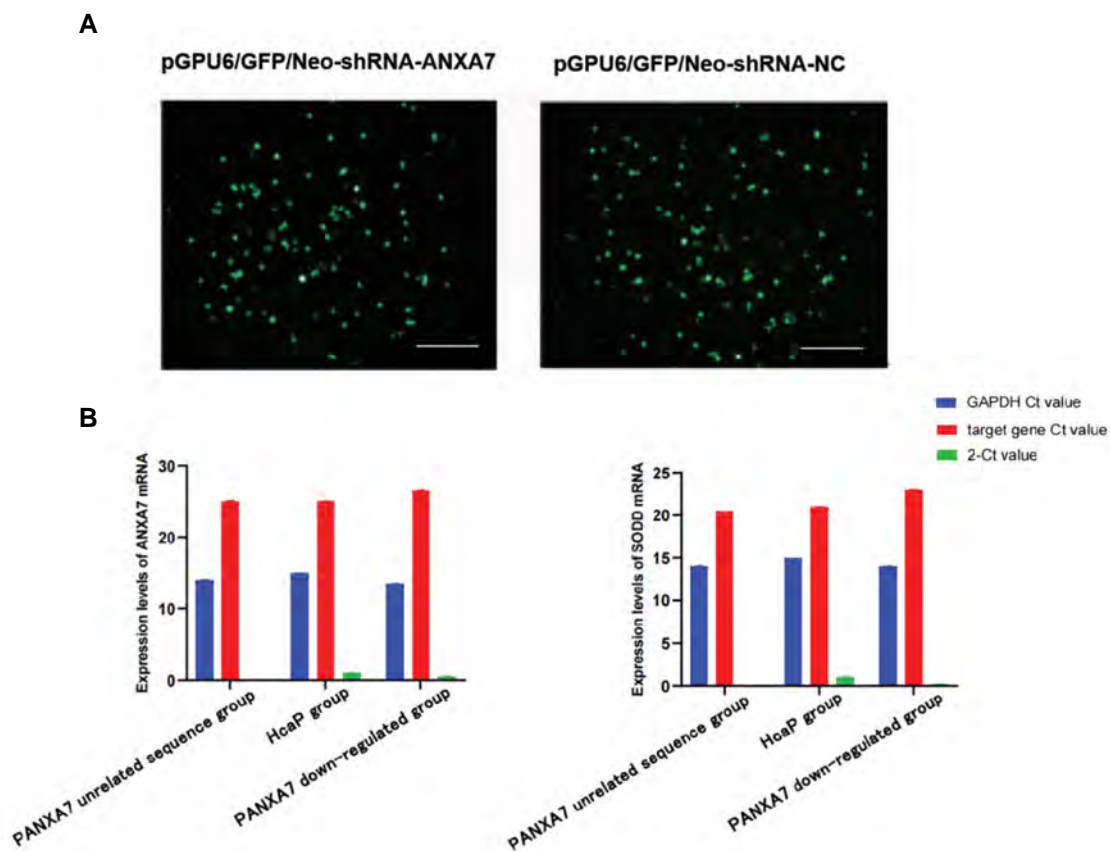


Fig.1: Silencing *ANXA7* gene by using shRNA. **A.** Hca-P cells were transfected with expressing vectors pGPU6/GFP/Neo-shRNA and pGPU6/GFP/Neo-shRNA-*ANXA7* (scale bar: 100 μ m). **B.** Expression levels of *ANXA7* and SODD mRNA in Hca-P cells, Hca-P cells transfected with pGPU6/GFP/Neo-shRNA or Hca-P cells transfected with pGPU6/GFP/Neo-shRNA-*ANXA7*.

Protein levels of *ANXA7* and SODD in *PANXA7* down-regulated cells

Protein levels of *ANXA7* and SODD in Hca-P cells were determined by western blot. Findings showed that SODD level in the *PANXA7* down-regulated group was lower than the Hca-P group and the *PANXA7* unrelated sequence group. There was no significant difference between normal Hca-P cells and *PANXA7* unrelated sequence group (Fig.2). These results fully indicated that expression of SODD protein was also significantly reduced after inhibiting *ANXA7* expression.

Transwell assay to detect effect of down-regulation of *ANXA7* on cell migration and invasion ability

Experiments showed that number of the cells penetrated into the membrane of the Transwell chamber was significantly reduced in the *PANXA7* down-regulated group after 24 hours of starvation, compared to the Hca-P group and the *PANXA7* unrelated sequence group (Fig.3A, B). This indicated that cell migration ability was decreased after down-regulation of *ANXA7* gene expression. Transwell invasion assay showed that number of cells that penetrated into the membrane of the Transwell chamber was significantly

reduced in the *PANXA7* down-regulated group after 24 hours of starvation, compared to the cells of the Hca-P group and the *PANXA7* unrelated sequence group. Additionally, invading cell number remained the same between the Hca-P group and the *PANXA7* unrelated sequence group (Fig.4A, B). This indicated that the cell invasion ability was decreased after down-regulation of *ANXA7* gene expression.

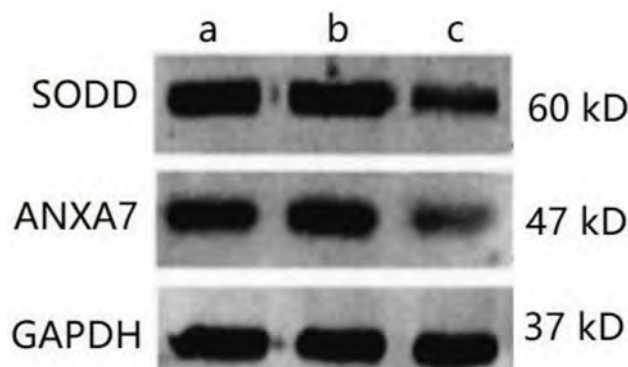


Fig.2: Western blot analysis of *ANXA7* and SODD proteins in the indicated groups. Hca-P cells (a), Hca-P cells transfected with pGPU6/GFP/NeoshRNA (b), and Hca-P cells transfected with pGPU6/GFP/NeoshRNA-*ANXA7* (c). SODD; Suppressor of death domains.

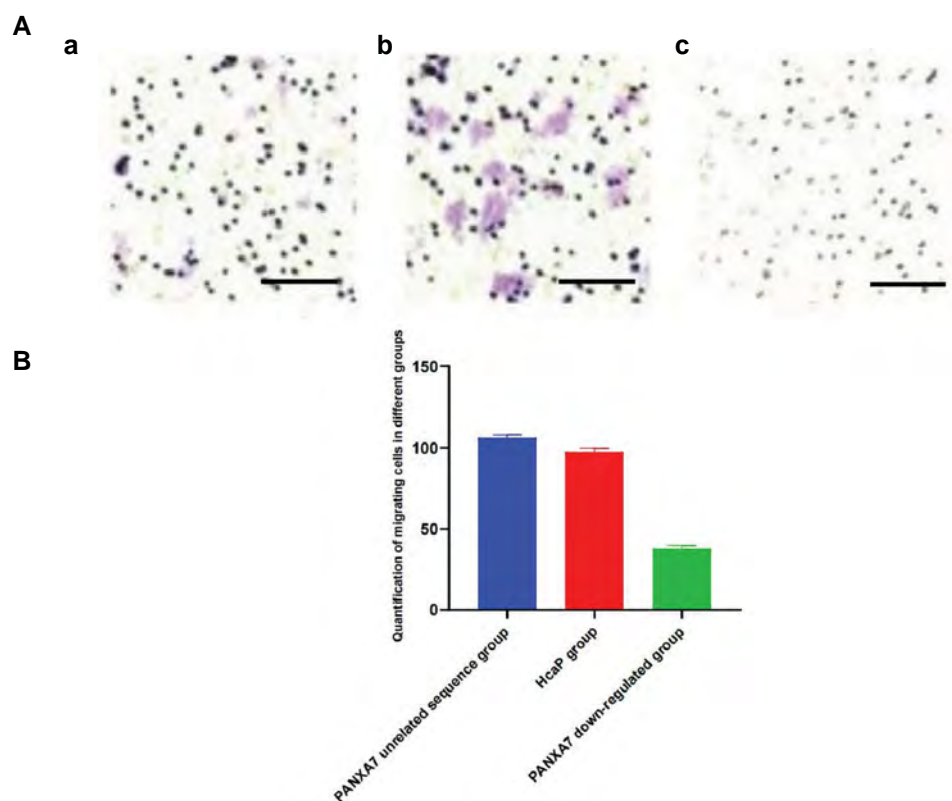


Fig.3: The down-regulation effect of *ANXA7* on cell migration was detected by Transwell assay. **A.** Representative images of transwell migration assay in Hca-P cells (a), Hca-P cells transfected with pGPU6/GFP/Neo-shRNA (b), and Hca-P cells transfected with pGPU6/GFP/Neo-shRNA-*ANXA7* (c) (scale bar: 100 μ m). **B.** Quantification of migrating cells in the above groups.

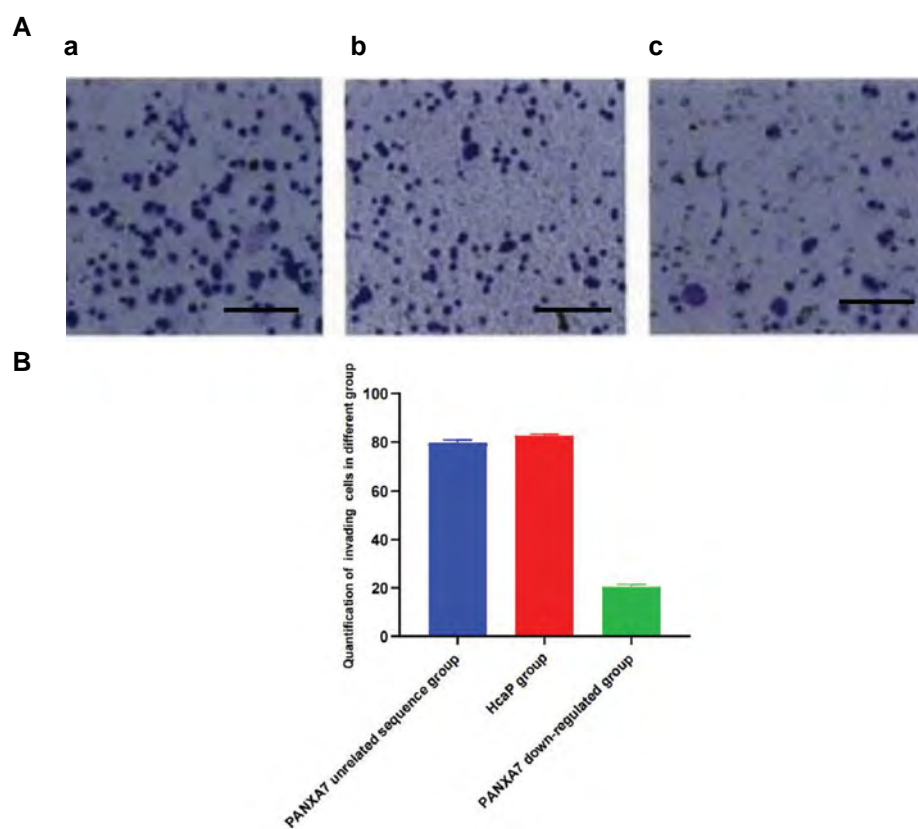


Fig.4: The effect of silencing *ANXA7* on cell invasion. **A.** Representative images of transwell invasion assay in Hca-P cells (a), Hca-P cells transfected with pGPU6/GFP/Neo-shRNA (b), and Hca-P cells transfected with pGPU6/GFP/Neo-shRNA-*ANXA7* (c) (scale bar: 100 μ m). **B.** Quantification of invading cells in the above groups.

Down-regulation of ANXA7 impaired cell proliferation of Hca-P cells

CCK-8 proliferation assay showed that after 0, 24, 48, 72 hour(s) of incubation, number of the Hca-P cells, *PANXA7* unrelated sequence cells, and *PANXA7* down-regulated cells increased significantly at 24 hours, while numbers of *PANXA7* down-regulated cells' proliferation ability was always lower than Hca-P and *PANXA7* irrelevant sequence cells. There was no significant difference between Hca-P and *PANXA7* irrelevant sequence cells (Fig.5). These data suggested that down-regulation of *ANXA7* would impair cell proliferation of Hca-P cells.

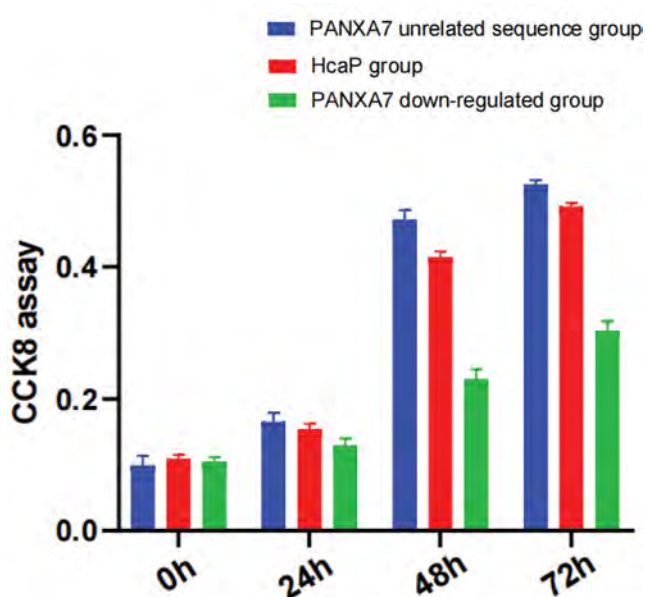


Fig.5: Inhibition of *ANXA7* impairs the cell proliferation of Hca-P cells. CCK8 proliferation assay in Hca-P cells (blue group), Hca-P cells transfected with pGPU6/GFP/Neo-shRNA (yellow group), Hca-P cells transfected with pGPU6/GFP/Neo-shRNA-*ANXA7* (grey group). h, Hour.

Discussion

Terminus of the *ANXA7* contain four repeat sequences consisting of about 70 amino acids, each of which has phospholipid, Ca^{2+} and insulin sites. It can be phosphorylated by protein kinase C to become a substrate of protein kinase C (12). *ANXA7* has also Ca^{2+} -dependent membrane fusion activity and it is a Ca^{2+} -dependent phospholipid-binding protein involved in mediating the Ca^{2+} /GTP signaling pathway, equivalent to an activated GTPase. In the annexin family, *ANXA7* has the longest N-terminus and it is rich of tyrosine, proline and glycine, providing binding sites for the other proteins. Experiments showed while *ANXA7* and the N-terminus of *ANXA7* were truncated, they did not bind to any protein (13). In terms of biological characteristics, *ANXA7* gene is involved in many biological behaviors of cells. It can promote membrane binding, regulate function of membrane receptors, inhibit activity of phospholipase A in cells, promote cell

secretion and exocytosis, and participate in interventional interventions. Activity of the cytoskeleton plays a significant role in the signal transduction process of cells. Numerous reports confirmed that expression of *ANXA7* was various in different tumor tissues. For example, Srivastava et al. (14) found that *ANXA7* had stably high expression in prostate cell lines, while expression of *ANXA7* was significantly reduced in prostate cancer; when *ANXA7* gene was transfected into prostate cancer cell lines, LNCaP and DU145 cells, colony formation and cell proliferation were observed.

In this study, proliferation was significantly reduced, leading to the conclusion that *ANXA7* gene might belong to a tumor suppressor gene, which was consistent to the other study (15). However, the other study (16) found that expression of *ANXA7* was significantly increased in 525 breast cancer tissues collected clinically. In this study, they demonstrated lower survival rate of patients in those who carried higher the expression of *ANXA7*. Ultimately, it was concluded that *ANXA7* may be a tumor-promoting gene. There are also some related reports (17) that in gastric cancer, metastatic melanoma, cervical cancer and other tissue cells, while their conclusions on the role of *ANXA7* as a tumor-promoting or a tumor-suppressing gene are controversial. In our previous transwell experiments of liver cancer Hca-P cells with *ANXA7* down-regulation, migration ability of tumor cells was significantly decreased in comparison with the control cells. The *PANXA7* unrelated sequence cells and *PANXA7* down-regulated cells were injected into mouse footpads, respectively. After that, the metastasis rate of lymph nodes was counted. Therefore, we believe that *ANXA7* mechanism of action in tumors may be very complex, and it may be involved in regulation of different gene and protein pathways. So it may play different roles in different types or different stages of tumor.

Suppressor of death domains (SODD), also known as BAG4, is an apoptosis-regulating gene discovered by Jiang et al. (18), using yeast two-hybrid technology. Its molecular weight is 60 kD. SODD can specifically recognize and bind to cytoplasmic death domains (DD) such as TNF-R1 and Bcl-2 under physiological conditions, preventing activation of TNF apoptotic pathway. The DD protein sequence is an essential structure for generation of the intracellular toxicity signals and exerting TNF-R1 effects, providing a binding site for DD-binding proteins. Only when DD-containing proteins are involved, different death receptors (DRs) can be activated and play a role in inducing apoptosis. TNF-receptor (TNF-R) is divided into TNF-R1 and TNF-R2. TNF-R1 contains DD, activating NF- κ B transcription factor after binding to the ligand and initiating apoptosis program. So TNF-R1 is also called DR. The emergence of SODD rationally explained mechanism of action of the TNF-R1 signal transduction pathway. The yeast two-hybrid assay showed that SODD could specifically recognize and combine with TNF-R1 and DR3 to form a complex, thereby preventing TNF-R1 from binding to the other proteins. SODD can combine

with the DD structure of the TNF-R1 cytoplasmic segment to form a complex SODD. Once the TNF-R1 complex is formed, it can no longer interact with the other proteins of DD. Thus, the TNF-R1 signaling pathway was blocked and cell apoptosis was inhibited.

Upon stimulating by TNF receptors, SODD sheds the TNFR-I-TRADD-FADD-caspase-8 death-inducing signaling complex (DISC) from the SODD-TNF-R1 complex, resulting in apoptosis (19). Studies showed that SODD was stably and highly expressed in cervical cancer, liver cancer and the other cell lines (20).

It was also seen in our experiments that by reduction of *ANXA7* expression level, SODD expression, proliferation, migration and invasion ability of tumor cells cultured in vitro was also decreased. We speculated that the possible mechanisms are as follows: First, *ANXA7* gene participates in or regulates transcription and translation of SODD. At the transcriptional level, when *ANXA7* was down-regulated, expression level of *SODD* gene was decreased, resulting in the down-regulation of SODD protein expression, which in turn affected cell function; at the translational level, *ANXA7* may be a cis-translation agent of SODD. Part of the acting element, either *ANXA7* positively regulates the cis-acting element of SODD or negatively regulates its trans-acting element, participates in regulating the translation level of SODD. The second possible mechanism is that *ANXA7* protein can act as a regulatory factor and participate in its own signal transduction pathway by binding to SODD. In the third possible mechanism, after *ANXA7* forms a complex with SODD, the latter can no longer bind to the receptors in the original signal transduction pathway. So, it can no longer participate in its signal transduction pathway, resulting in destruction of the apoptosis mechanism of cells.

This study confirmed that SODD was stably expressed in Hca-P cells. In addition, we determined that SODD and *ANXA7* were co-associated proteins in tumor cytoplasm. When *ANXA7* was decreased, protein expression and mRNA level of SODD were decreased, indicating that *ANXA7* gene was involved in or regulated transcription and translation of SODD. At the transcriptional level, when *ANXA7* was down-regulated, expression level of *SODD* gene was decreased, and reduction of mRNA template resulted in down-regulation of cellular SODD protein expression, thus affecting the function of cells. The results of CCK8 showed that proliferative ability of tumor cells was decreased by down-regulation of *ANXA7*. High expression of SODD can also inhibit TNFR1-mediated apoptosis, resulting in decreased sensitivity of tumor cells to DR-mediated apoptosis; if the expression of intracellular SODD protein is inhibited, the sensitivity to apoptosis can be restored (21-28). Our experiments also demonstrated that down-regulating *ANXA7* expression inhibited migration and metastasis of the Hca-P cell. Therefore, it can be considered that *ANXA7* and SODD proteins are not only related to cell apoptosis, but also to cell migration. The limitation of this study was lack of

the prospective studies. In addition, results of the animal experiments may have errors and contingencies. So it needs to be confirmed by repeated experiments.

Conclusion

Both mRNA and protein levels of SODD were decreased after *ANXA7* knockdown. *ANXA7* silencing suppressed proliferation, migration and the invasion of hepatocarcinoma Hca-P cells. These data suggest that *ANXA7* and SODD may be implicated in the invasiveness of hepatocarcinoma cells.

Acknowledgements

This study was supported by Item of Scientific Research Fund for Doctor of Qiqihar Medical University (No. QMSI2017B-12). The authors declare that they have no competing interest.

Authors' Contributions


X.W.; Was dedicated to the integrity of the entire study, study concepts, study design, literature research, and manuscript review. Y.S.; Review and editing the manuscript and statistical analysis. S.W.; Was dedicated to the experimental studies, manuscript preparation and manuscript editing. X.Y.; Was involved in the definition of intellectual content and data analysis. F.G.; Original draft preparation and clinical studies. Q.B.; Methodology. All authors read and approved the final manuscript.

References

- Zanetto A, Campello E, Pelizzaro F, Farinati F, Burra P, Simioni P, et al. Haemostatic alterations in patients with cirrhosis and hepatocellular carcinoma: laboratory evidence and clinical implications. *Liver Int.* 2022; 42(6): 1229-1240.
- Haschemi R, Kobelt D, Steinwarz E, Schlesinger M, Stein U, Bendas G. Insulin-like growth factor binding protein-2 (IGFBP2) is a key molecule in the MACC1-mediated platelet communication and metastasis of colorectal cancer cells. *Int J Mol Sci.* 2021; 22(22): 12195.
- Yang WJ, Zhang GL, Cao KX, Yang GW. A hypercoagulable hematological metastasis breast cancer model. *Biomed Res Int.* 2021; 2021: 5473959.
- Leighton X, Eidelman O, Jozwik C, Pollard HB, Srivastava M. *ANXA7*-GTPase as tumor suppressor: mechanisms and therapeutic opportunities. *Methods Mol Biol.* 2017; 1513: 23-35.
- Manke MC, Geue S, Coman C, Peng B, Kollotzek F, Münzer P, et al. *ANXA7* regulates platelet lipid metabolism and Ca²⁺ release in arterial thrombosis. *Circ Res.* 2021; 129(4): 494-507.
- Voelkl J, Alesutan I, Pakladok T, Viereck R, Feger M, Mia S, et al. Annexin A7 deficiency potentiates cardiac NFAT activity promoting hypertrophic signaling. *Biochem Biophys Res Commun.* 2014; 445(1): 244-249.
- Monastyrskaya K, Babychuk EB, Draeger A. The annexins: spatial and temporal coordination of signaling events during cellular stress. *Cell Mol Life Sci.* 2009; 66(16): 2623-2642.
- Simpkins B, Donohue MP, Li Y. Molecular dynamic studies on the impact of mutations on the structure, stability, and N-terminal orientation of annexin A1: implications for membrane aggregation. *Proteins.* 2014; 82(12): 3327-3334.
- Stuqui B, de Paula-Silva M, Carlos CP, Ullah A, Arni RK, Gil CD, et al. Ac2-26 mimetic peptide of annexin A1 inhibits local and systemic inflammatory processes induced by bothrops moojeni venom and the Lys-49 phospholipase A2 in a rat model. *PLoS One.* 2015; 10(7): e0130803.
- Vago JP, Tavares LP, Sugimoto MA, Lima GL, Galvão I, de Caux TR, et al. Proresolving actions of synthetic and natural protease

- inhibitors are mediated by annexin A1. *J Immunol.* 2016; 196(4): 1922-1932.
11. Singh PR, Priya ES, Balakrishnan S, Arunkumar R, Sharmila G, Rajalakshmi M, et al. Nimbolide inhibits androgen independent prostate cancer cells survival and proliferation by modulating multiple pro-survival signaling pathways. *Biomed Pharmacother.* 2016; 84: 1623-1634.
 12. Caohuy H, Pollard HB. Activation of annexin 7 by protein kinase C in vitro and in vivo. *J Biol Chem.* 2001; 276(16): 12813-12821.
 13. Liu S, Li X, Lin Z, Su L, Yan S, Zhao B, et al. SEC-induced activation of ANXA7 GTPase suppresses prostate cancer metastasis. *Cancer Lett.* 2018; 416: 11-23.
 14. Srivastava M, Torosyan Y, Raffeld M, Eidelman O, Pollard HB, Bubendorf L. ANXA7 expression represents hormone-relevant tumor suppression in different cancers. *Int J Cancer.* 2007; 121(12): 2628-2636.
 15. Leighton X, Bera A, Eidelman O, Eklund M, Puthillathu N, Pollard HB, Srivastava M. High ANXA7 potentiates eucalyptol toxicity in hormone-refractory prostate cancer. *Anticancer Res.* 2018; 38(7): 3831-3842.
 16. Huang Y, Wang H, Yang Y. Annexin A7 is correlated with better clinical outcomes of patients with breast cancer. *J Cell Biochem.* 2018; 119(9): 7577-7584.
 17. Guo C, Liu S, Greenaway F, Sun MZ. Potential role of annexin A7 in cancers. *Clin Chim Acta.* 2013; 423: 83-89.
 18. Jiang Y, Woronicz JD, Liu W, Goeddel DV. Prevention of constitutive TNF receptor 1 signaling by silencer of death domains. *Science.* 1999; 283(5401): 543-546.
 19. Cisterne A, Baraz R, Khan NI, Welschinger R, Basnett J, Fung C, et al. Silencer of death domains controls cell death through tumour necrosis factor-receptor 1 and caspase-10 in acute lymphoblastic leukemia. *PLoS One.* 2014; 9(7): e103383.
 20. Lv W, Wu C, Lin S, Wang X, Wang Y. Integrated utilization strategy for soybean oil deodorizer distillate: synergically synthesizing biodiesel and recovering bioactive compounds by a combined enzymatic process and molecular distillation. *ACS Omega.* 2021; 6(13): 9141-9152.
 21. Duell ER, D'Agostino PM, Shapiro N, Woyke T, Fuchs TM, Gulder TAM. Direct pathway cloning of the *sodorifen* biosynthetic gene cluster and recombinant generation of its product in *E. coli*. *Microb Cell Fact.* 2019; 18(1): 32.
 22. Nielsen KO, Jacobsen KS, Mirza AH, Winther TN, Størling J, Glebe D, et al. Hepatitis B virus upregulates host microRNAs that target apoptosis-regulatory genes in an in vitro cell model. *Exp Cell Res.* 2018; 371(1): 92-103.
 23. Zhang M, Yao F, Qin T, Hou L, Zou X. Identification, expression pattern and functional characterization of *As-kip2* in diapause embryo restarting process of *Artemia sinica*. *Gene.* 2017; 608: 28-40.
 24. Li D, Hong J, Cao W. Silencer-of-death domain mediates acid-induced decrease in cell apoptosis in barrett's associated esophageal adenocarcinoma cells. *J Pharmacol Exp Ther.* 2017; 360(1): 14-22.
 25. Davidson B, Valborg Reinertsen K, Trinh D, Reed W, Bøhler PJ. BAG-1/SODD, HSP70, and HSP90 are potential prognostic markers of poor survival in node-negative breast carcinoma. *Hum Pathol.* 2016; 54: 64-73.
 26. Tao H, Hu Q, Fang J, Liu A, Liu S, Zhang L, et al. Expression of SODD and P65 in ALL of children and its relationship with chemotherapeutic drugs. *J Huazhong Univ Sci Technolog Med Sci.* 2007; 27(3): 326-329.
 27. Tao HF, Hu Q, Liu SY, Liu AG, Hu Y, Jiang Y, et al. The significance and correlation of SODD and Bcl-2 protein expression in acute leukemia of children. *Chinese Journal of Clinical Oncology* 2006; 3(5): 332-336.
 28. Reuland SN, Smith SM, Bemis LT, Goldstein NB, Almeida AR, Parityka KA, et al. MicroRNA-26a is strongly downregulated in melanoma and induces cell death through repression of silencer of death domains (SODD). *J Invest Dermatol.* 2013; 133(5): 1286-1293.
-

Royan Institute First Attempts: Autotransplantation of Vitrified Human Ovarian Tissue in Cancer Patients

Naeimeh Sadat Abtahi, M.Sc.¹, Bita Ebrahimi, Ph.D.^{1*} , Firouzeh Ghaffari, M.D.², Rouhollah Fathi, Ph.D.¹,
Mojtaba Rezazadeh Valojerdi, Ph.D.^{1,3}, Abolfazl Mehdizadehkashi, M.D.⁴, Sepideh Khodaverdi, M.D.⁴,
Azar Yahyaei, M.Sc.², Maziar Faridi, M.D.⁵

1. Department of Embryology, Reproductive Biomedicine Research Center, Royan Institute for Reproductive Biomedicine, ACECR, Tehran, Iran

2. Department of Endocrinology and Female Infertility, Reproductive Biomedicine Research Center, Royan Institute for Reproductive Biomedicine, ACECR, Tehran, Iran

3. Department of Anatomy, Faculty of Medical Science, Tarbiat Modares University, Tehran, Iran

4. Endometriosis Research Center, Iran University of Medical Sciences, Tehran, Iran

5. Department of Surgery, Iranmehr Hospital, Tehran, Iran

Abstract

Today, timely diagnosis and therapeutic progress open a road of hope for survival in cancerous patients. Increased knowledge about the various cytotoxic treatment's impacts on ovarian function and fertility has resulted in a surge in the number of patients seeking to preserve their fertility before starting the anti-cancer treatment process. In this regard, embryo cryopreservation can be recommended for fertility preservation when the woman is married and has adequate time for ovarian stimulation. If patients are prepubertal girls or not married women, oocytes or ovarian tissue can be frozen instead to be used in the future. In this regard, the first attempts for ovarian tissue transplantations were conducted in 2016 and in 2019 for two cancerous patients whose ovarian tissue was cryopreserved in the Royan Human Ovarian Tissue Bank (Tehran, Iran). Unfortunately, the transplantations did not result in a live birth.

Keywords: Fertility Preservation, Human, Oncofertility, Ovarian Tissue, Transplantation

Citation: Abtahi NS, Ebrahimi B, Ghaffari F, Fathi R, Valojerdi MR, Mehdizadehkashi A, Khodaverdi S, Yahyaei A, Faridi M. Royan institute first attempts: autotransplantation of vitrified human ovarian tissue in cancer patients. Cell J. 2023; 25(11): 809-812. doi: 10.22074/CELLJ.2023.2000360.1289

This open-access article has been published under the terms of the Creative Commons Attribution Non-Commercial 3.0 (CC BY-NC 3.0).

Introduction

Because of timely diagnosis and new treatments, we encounter an increase in the survival rate for cancer. Increased knowledge about the various cytotoxic treatment impacts on the ovary has resulted in a surge in the number of patients seeking to preserve their fertility before starting treatments. If there is time for ovarian stimulation, embryo, and oocyte cryopreservation are standard techniques for fertility preservation. At present, ovarian cryopreservation is the only fertility preservation option that can be offered to women who have ovary stimulation limitations (such as inadequate time for stimulation or the impossibility of stimulating) and prepubertal girls. A transplantation of cryopreserved ovarian tissue after cancer treatment is a promising fertility restoration strategy that has already led to more than 200 live births worldwide (1-3).

After a decade of investigations, the Royan Human Ovarian Tissue Bank (OTB, ACECR, Tehran, Iran)

was established in 2010 and started patient reception (4). In 2015, Royan Institute obtained international certificate, ISO 9001:2015, for this bank. From that time, consultations for approximately 1000 patients between 7- 47 years have been directed and ovarian tissues of more than 100 patients who had our criteria, have been cryopreserved.

In recent years, the Royan OTB has been requested for only three cases of ovarian tissue transplantation following cancer survival, that we will report two of them here. Before transplantation, a general consultation was conducted about the ovary transplantation and its outcomes in Iran and other countries. Consultation with an oncologist was conducted to declare the complete remission of the underlying disease and a consultation with the surgical team was carried out to manage possible adhesions during surgery for both patients. The informed consents were obtained from both patients (4).



Case report

First case: She was a 22 years old girl with a history of colon cancer. She was affected by rectal bleeding when she was 17. The diagnosis of hyperplastic adenomatous polyps with focal high-grade dysplasia was established by colonoscopy biopsy. The pathological examination of the colon identified an invasive adenocarcinoma that its serosal surface and margin was tumor free, and also four reactive hyperplasia pericolic lymph nodes were detected. Her right ovary was resected and vitrified in 28 strips in the Royan OTB after one course of chemotherapy. Thereafter, she received five courses of chemotherapy and 40 sessions of radiotherapy. Hormone-replacement therapy (HRT), including 0.625 mg of conjugated estrogens (Aburaihan Pharma.Co., Tehran, Iran) plus 10 mg of medroxyprogesterone acetate (Aburaihan Pharma.Co., Tehran, Iran), was administered for the relief of menopausal symptoms monthly for 5 years. At the 5th year, she asked for the ovary transplantation. Serum concentrations of follicle-stimulating hormone (FSH), luteinizing hormone (LH), and Estradiol (E₂) levels were measured before ovary transplantation (Table 1).

Second case: She was a 37-year old married woman who experienced a radical abdominal hysterectomy and bilateral salpingoophorectomy and pelvic lymph node dissection because of stage IA well-differentiated adenocarcinoma. She did not receive any chemotherapy or radiotherapy before ovariectomy. Both ovaries were resected, and 40 strips were vitrified and stored in the Royan OTB. Four years later,

she asked for ovary transplantation. Serum concentrations of FSH, LH, and E₂ levels were measured before ovary transplantation (Table 2).

Ovarian tissue preservation procedure

In each case, after ovarian tissue resection, ovaries were quickly transferred to the Royan OTB (during approximately 1 hour) with a transfer medium at 4°C with ice packs. This medium consisted of Medium 199+Heppes (HTCM, Gibco, Paisley, UK) that was supplemented with 20% human serum albumin (HSA, Biotest, Germany). The transferred ovary was washed in the HTCM+20% HSA medium. The medullary part was removed and the thinnest cortical part was cut into 10×5×1 mm strips. Finally, the strips were vitrified in a two-step procedure as following:

First, each strip was transferred to an equilibration medium composed of HTCM, 7.5% ethylene glycol (EG, Sigma, St. Louis, MO, USA), 7.5% dimethyl sulfoxide (DMSO, Sigma, St. Louis, MO, USA), and 20% HSA for 15 minutes, and then the strips were washed in the vitrification medium [HTCM, 15% DMSO, 15% EG, 0.25 M sucrose, and 20% HSA] for 10 minutes. After the removal of the extra medium, the strips were directly transferred into liquid nitrogen. All steps were performed at 4°C (4).

Of note, one strip was randomly selected and fixed for histological and pathological evaluation via hematoxylin and eosin staining before cryopreservation (5).

Table 1: The hormonal profile of the first patient

Evaluation time according to transplantation day	FSH (mIU/mL)	LH (mIU/mL)	Estradiol (pg/mL)
Before transplantation	75.62	25.48	12
2 months after transplantation day	54	24.6	<5
4 months after transplantation day	64.8	27.8	37.2
5 months after transplantation day	57.3	30.9	52.3
7 months after transplantation day	92.6	32.7	13.7
9 months after transplantation day	159.6	71.7	<5

FSH; Follicle-stimulating hormone and LH; Luteinizing hormone.

Table 2: The hormonal profile of the second patient

Evaluation time according to transplantation day	FSH (mIU/mL)	LH (mIU/mL)	Estradiol (pg/mL)
Before transplantation	200	77	7
2 months after transplantation day	200	61	7
4 months after transplantation day	199	65	11
5 months after transplantation day	200	65	11
7 months after transplantation day	200	65	9.7
9 months after transplantation day	200	76	10

FSH; Follicle-stimulating hormone and LH; Luteinizing hormone.

Auto-transplantation

Both patients underwent the laparoscopic autologous orthotopic transplantation. The surgery and postoperative period were uneventful.

Before transplantation, the patient's ovarian cryopreserved strips were warmed and incubated at 37°C.

Warming procedure was performed in four steps in a descending sucrose concentration (1, 0.5, 0.25, and 0.125 M). The base medium was composed of HTCM and 20% HSA. To make sure tumor cells free, a histopathological examination of the storage tissue were performed before transplantation.

For the first case, 15 strips were warmed and prepared in two forms, including separate (7 strips) and ribbon-shaped (containing 8 strips). For preparing the ribbon-shaped, the strips were sutured under the surgical microscope by 8/0 "Coated VICRYL® (polyglactin 910) Suture - Ethicon" and a 1.5×2 cm ribbon was made. For transplantation, first, the pelvic area was evaluated well; no adhesion was observed, and the uterus was completely healthy and free from any pathology. Because the patient's right ovary had been removed and her left ovary was very small, a peritoneal pouch in the left broad ligament, under the fallopian tube was created. The ribbon-shaped strip was transplanted into the pouch, the medullary side facing the pelvic floor. Likewise, a peritoneal pouch was formed in the right broad ligament below the uterosacral ligament and the separate strips were transplanted inside it. Peritoneal pouch was sutured using a Vicryl suture. The patient was discharged 24 hours after surgery without any complications. The transplantation procedure for the first patient was conducted in the gynecology and obstetrics department of the Rasool_e_Akram University General Hospital, Tehran, Iran.

For the second patient, 17 strips were warmed. Nine separate strips were transplanted in the right ovarian fossa, and 8 separate strips in the left ovarian fossa. Under general anesthesia, her pelvic area was evaluated, and then an incision (1 cm) was made in the parietal peritoneum between the infundibular pelvic and uterosacral ligament on both sides. The sub-peritoneal pocket was bluntly dissected, and the ovarian strips were placed separately with their medullary side facing the pelvic floor. Finally, the peritoneal closure was performed with an interrupted suture (Monocryl suture 3-0, W3326, ETHICON surgical technology, USA). The transplantation procedure for the second patient was conducted in the gynecology and obstetrics department of the Royan Institute, Tehran, Iran.

Patients follow-up

Both patients' follow-up was carried out until 9 months after transplantation. Menstrual monitoring, ultrasonography, and measurement of the hormonal profile were conducted after the transplantation for the first patient. Her hormonal profile was reported in Table 1. Monthly sonography examinations revealed no follicular

development and she didn't report menstruation during a year.

For the second patient, according to her hysterectomy and bilateral salpingoophorectomy, only hormonal profiles could be followed up which was reported in Table 2. Same as our first patient, no decrease in FSH levels and no increase in estradiol was observed, and as a result the transplanted ovarian strips are considered to be non-functional.

Discussion

If a transplantation is successful and its related transplanted ovarian tissue is functional, we must observe a decrease in the FSH level and an increase in the E2 level. Hormonal fluctuations are current after an ovarian tissue transplantation, in such a way that the FSH level will be decreased after 4-5 months of transplantation, and then will be returned to its premenopausal level (6). In the first patient, although 2-6 months after transplantation, the FSH hormone decreased to 50-60 mIU/mL, suddenly, an increasing trend was observed in the following months. Unfortunately, in the second patient, no decrease in the FSH level was observed after 9 months following transplantation.

As mentioned earlier, 200 live births have been reported worldwide but unfortunately we have not. It might be due to various reasons such as cryopreservation method, pre-cryopreservation ovarian tissue quality, follicle loss prior to the freezing process, size of the tissue, tissue revascularisation, and re-transplantation performance. Although, ovarian tissue integrity was well preserved by the vitrification method, only 2 live births have been reported after transplantation of vitrified tissue (7). Most live births were reported after a slow-freezing procedure (8-10). It seems that multiple transplantations, double or triple, may be successful in some patients (9). Although, we suggested a re-transplantation plan to both of our patients, they did not accept because of their personal desire. As there are no standard protocols for ovarian tissue cryopreservation and transplantation worldwide, differences in acquired results are predictable (11).

Conclusion

It is very encouraging that ovarian tissue cryopreservation and transplantation have resulted in a live birth. We acquired ovary cryopreservation knowledge in 2010 and tried transplantation 6 years later, but unfortunately did not result in a live birth. Continued research efforts are required to optimize our approach, and we hope to report successful transplantation soon.

Acknowledgments

We are thankful of financial support of the Royan Institute, Tehran, Iran. We are grateful of our participants and their kind collaboration. The authors declare that they have no conflict of interests.

Authors' Contributions

N.S.A., B.E., R.F.; Conducted ovarian tissue cryopreservation procedures. M.R.V.; Supervisor. F.G., A.M.K., S.K., M.F.; Autotransplantation surgery. F.G., N.S.A.; Patients follow up. A.Y.; Data collection. N.S.A., F.G., S.K.; Writing original draft of the manuscript. B.E.; Manuscript reviewer. All authors read and approved the final manuscript.

References

1. Donnez J, Dolmans MM, Demylle D, Jadoul P, Pirard C, Squifflet J, et al. Livebirth after orthotopic transplantation of cryopreserved ovarian tissue. *Lancet*. 2004; 364(9443): 1405-1410.
 2. Fraison E, Huberlant S, Labrune E, Cavalieri M, Montagut M, Brugnon F, et al. Live birth rate after female fertility preservation for cancer or haematopoietic stem cell transplantation: a systematic review and meta-analysis of the three main techniques; embryo, oocyte and ovarian tissue cryopreservation. *Hum Reprod*. 2023; 38(3): 489-502.
 3. Segers I, Bardhi E, Mateizel I, Van Moer E, Schots R, Verheyen G, et al. Live births following fertility preservation using in-vitro maturation of ovarian tissue oocytes. *Hum Reprod*. 2020; 35(9): 2026-2036.
 4. Abtahi NS, Ebrahimi B, Fathi R, Khodaverdi S, Mehdizadeh Kashi A, Valojerdi MR. An introduction to the royan human ovarian tissue bank. *Int J Fertil Steril*. 2016; 10(2): 261-263.
 5. Ghezelayagh Z, Abtahi NS, Khodaverdi S, Rezazadeh Valojerdi M, Mehdizadeh A, Ebrahimi B. The effect of agar substrate on growth and development of cryopreserved-thawed human ovarian cortical follicles in organ culture. *Eur J Obstet Gynecol Reprod Biol*. 2020; 258(2): 139-145.
 6. Hornshøj Greve V, Dueholm M, Mamsen LS, Kristensen SG, Ernst E, Andersen CY. Hormonal characteristics of women receiving ovarian tissue transplantation with or without endogenous ovarian activity. *J Clin Med*. 2021; 10(22): 5217.
 7. Donnez J, Dolmans MM. Ovarian cortex transplantation: 60 reported live births brings the success and worldwide expansion of the technique towards routine clinical practice. *J Assist Reprod Genet*. 2015; 32(8): 1167-1170.
 8. Dolmans MM, von Wolff M, Poirot C, Diaz-Garcia C, Cacciottola L, Boissel N, et al. Transplantation of cryopreserved ovarian tissue in a series of 285 women: a review of five leading European centers. *Fertil Steril*. 2021; 115(5): 1102-1115.
 9. Gellert SE, Pors SE, Kristensen SG, Bay-Björn AM, Ernst E, Yding Andersen C. Transplantation of frozen-thawed ovarian tissue: an update on worldwide activity published in peer-reviewed papers and on the Danish cohort. *J Assist Reprod Genet*. 2018; 35(4): 561-570.
 10. Khattak H, Malhas R, Craciunas L, Afifi Y, Amorim CA, Fishel S, et al. Fresh and cryopreserved ovarian tissue transplantation for preserving reproductive and endocrine function: a systematic review and individual patient data meta-analysis. *Hum Reprod Update*. 2022; 28(3): 400-416.
 11. Amorim CA, Leonel ECR, Afifi Y, Coomarasamy A, Fishel S. Cryostorage and retransplantation of ovarian tissue as an infertility treatment. *Best Pract Res Clin Endocrinol Metab*. 2019; 33(1): 89-102.
-